

# **Electrokinetic Barriers to Contaminant Transport: Numerical Modelling and Laboratory Scale Experimentation**

By

**BALAJI NARASIMHAN**

A thesis  
submitted to the Faculty of Graduate Studies  
in Partial Fulfilment of the Requirements  
for the Degree of

**MASTER OF SCIENCE**

Department of Biosystems Engineering  
University of Manitoba  
Winnipeg, MB, CANADA.

© August 1999



**National Library  
of Canada**

**Acquisitions and  
Bibliographic Services**

**395 Wellington Street  
Ottawa ON K1A 0N4  
Canada**

**Bibliothèque nationale  
du Canada**

**Acquisitions et  
services bibliographiques**

**395, rue Wellington  
Ottawa ON K1A 0N4  
Canada**

*Your file Votre référence*

*Our file Notre référence*

**The author has granted a non-exclusive licence allowing the National Library of Canada to reproduce, loan, distribute or sell copies of this thesis in microform, paper or electronic formats.**

**The author retains ownership of the copyright in this thesis. Neither the thesis nor substantial extracts from it may be printed or otherwise reproduced without the author's permission.**

**L'auteur a accordé une licence non exclusive permettant à la Bibliothèque nationale du Canada de reproduire, prêter, distribuer ou vendre des copies de cette thèse sous la forme de microfiche/film, de reproduction sur papier ou sur format électronique.**

**L'auteur conserve la propriété du droit d'auteur qui protège cette thèse. Ni la thèse ni des extraits substantiels de celle-ci ne doivent être imprimés ou autrement reproduits sans son autorisation.**

**0-612-45103-8**

**Canada**

**THE UNIVERSITY OF MANITOBA**  
**FACULTY OF GRADUATE STUDIES**  
**\*\*\*\*\***  
**COPYRIGHT PERMISSION PAGE**

**Electrokinetic Barriers to Contaminant Transport:  
Numerical Modelling and Laboratory Scale Experimentation**

**BY**

**Balaji Narasimhan**

**A Thesis/Practicum submitted to the Faculty of Graduate Studies of The University  
of Manitoba in partial fulfillment of the requirements of the degree  
of  
Master of Science**

**BALAJI NARASIMHAN©1999**

**Permission has been granted to the Library of The University of Manitoba to lend or sell copies of this thesis/practicum, to the National Library of Canada to microfilm this thesis and to lend or sell copies of the film, and to Dissertations Abstracts International to publish an abstract of this thesis/practicum.**

**The author reserves other publication rights, and neither this thesis/practicum nor extensive extracts from it may be printed or otherwise reproduced without the author's written permission.**

## ABSTRACT

Vertical barriers such as cutoff walls, grout curtains or sheet piles are frequently used for containing the contaminants in place during remediation of contaminated soil and groundwater. The electrokinetic barrier is an emerging technique which can be used as a low-cost alternative for containing the spread of contaminants. An electrical potential gradient applied across the electrodes inserted in the subsurface could create an electro-osmotic counter gradient high enough to stop the flow of water due to the hydraulic gradient. A laboratory scale experiment was conducted to study the effectiveness of electrokinetic barriers in containing the spread of contaminants. Potassium chloride was used as a tracer to find the effectiveness of electrokinetic barriers.

Laboratory experiments in sandy clay soils showed that without electrokinetic barriers the  $K^+$  ions migrated at a rate of  $2 \text{ mm} \cdot \text{d}^{-1}$  whereas, with the electrokinetic barriers the  $K^+$  ions migrated at a rate of  $0.1 \text{ mm} \cdot \text{d}^{-1}$ . Hence, electrokinetic barriers could be used as an effective system for preventing the spread of the contaminants in the subsurface. A two-dimensional finite element model was developed to investigate the contaminant migration under hydraulic, electrical, and chemical gradients. Migration of a pH front due to the electrolysis reactions at the anode and the cathode and development of non-linear hydraulic and electrical potential gradients brought about by the changes in the electrical properties of the soil could be simulated by the model developed in this thesis. The model results compared well with the experimental results. The numerical model developed in this thesis was also used to evaluate the effectiveness of different electrode configurations for possible field applications.

## **ACKNOWLEDGEMENTS**

I would like to express my sincere thanks to my advisor Dr. R. Sri Ranjan for his excellent guidance and support during my Masters program and for his counsel in my professional development activities. I would also like to appreciate Dr. Qiang Zhang for his counsel in my professional development activities and for his service as member of my thesis committee. Many thanks to Dr. Allan Woodbury for teaching me the principles of contaminant transport and for his service as member of my thesis committee.

Special thanks to Mrs. Rehana Mirza and Mr. Peter Haluschak of Manitoba Soil Survey for the use their lab facilities and for their excellent support for conducting the chemical analysis of the soil samples. Thanks to Dr. T. B. Goh, Department of Soil Science for his constructive suggestions. Special thanks to Dr. A. Chow, Department of Chemistry and Dr. G. Racz, Department of Soil Science for the use of their lab facilities. Thanks to NSERC for their financial support of this innovative project. Thanks to Messrs. Dale Bourns, Matt McDonald, and Jack Putnam for their technical support during various phases of the experiments.

My sincere thanks to Dr. K. Alagusundaram, Tamil Nadu Agricultural University, India for serving as a mentor in my career development. Thanks to my friends, Jeyamkondan, Seshadri, and Sajan for making my stay in Canada memorable.

I am indebted to my family and would like to express my deepest gratitude for their love, encouragement, and support during my Masters program.

# TABLE OF CONTENTS

ABSTRACT .....	i
ACKNOWLEDGEMENT .....	ii
TABLE OF CONTENTS .....	iii
LIST OF TABLES .....	vii
LIST OF FIGURES .....	viii
LIST OF SYMBOLS .....	xi
1.0 INTRODUCTION .....	1
1.1 Problem statement .....	1
1.2 Physical containment techniques .....	2
1.3 Electrokinetic barrier .....	3
1.4 Objectives .....	6
1.5 Organization .....	6
2.0 LITERATURE REVIEW .....	8
2.1 Introduction .....	8
2.2 Electrokinetic phenomena .....	8
2.2.1 Electrical double layer .....	8
2.2.2 Electrolysis of water .....	9
2.2.3 Electro-osmosis .....	12
2.2.4 Electro-migration .....	17
2.2.5 Electrophoresis .....	18
2.2.6 Streaming potential .....	18
2.2.7 Migration potential .....	19
2.3 Applications of electrokinetic phenomena .....	19

2.3.1	Electrokinetic remediation	19
2.3.2	Electrokinetic barriers	20
2.3.3	Electrokinetic consolidation	23
2.3.4	De-watering and concentration	23
2.4	Theoretical model studies	23
2.5	Summary	28
3.0	MODEL DEVELOPMENT	30
3.1	Introduction	30
3.2	Contaminant transport mechanisms in electrokinetic processes	30
3.2.1	Advection due to hydraulic and electrical gradients	30
3.2.2	Hydrodynamic dispersion	32
3.2.3	Ionic migration	34
3.3	Solute transport	36
3.4	Transient saturated flow	39
3.5	Charge flux	40
4.0	NUMERICAL MODELLING	41
4.1	Introduction	41
4.2	Weighted residual method	42
4.2.1	Formulation of the residual	43
4.2.2	Formulation of element matrices	45
4.2.3	Finite difference solution in time	48
4.2.4	LU decomposition	49
4.3	Computer coding of the mathematical model	51
4.4	Verification of computer code	54
4.4.1	Verification with Ogata-Banks analytical solution	54
4.4.2	Verification with Esrig's analytical solution	55
4.4.3	Mass balance and charge balance calculations	58

<b>5.0 LABORATORY SCALE EXPERIMENTATION</b> .....	<b>61</b>
5.1 Objectives .....	61
5.2 Experimental setup .....	61
5.2.1 Plexiglass soil columns .....	62
5.2.2 Constant head and Flow rate measuring devices .....	62
5.2.3 Constant voltage source and data acquisition .....	64
5.2.4 Mini tensiometer and pore water pressure measurement .....	64
5.3 Experimental soil .....	66
5.4 Physical properties of the soil .....	66
5.4.1 Particle size distribution .....	66
5.4.2 Particle density .....	68
5.5 Chemical properties of the experimental soil .....	68
5.5.1 Soil pH .....	68
5.5.2 Electrical conductivity .....	69
5.5.3 Soluble cations .....	69
5.5.4 Soluble anions .....	71
5.6 Experimental procedure .....	71
5.6.1 Soil column preparation .....	71
5.6.2 Saturation of the soil columns .....	72
5.6.3 Hydraulic conductivity measurements .....	74
5.6.4 Electro-osmotic conductivity measurements .....	74
5.6.5 Pore water pressure measurements .....	76
5.6.6 Voltage drop measurements .....	77
5.6.7 Contaminant simulation .....	78
5.6.8 Soil column sectioning and sampling .....	78
5.6.9 Chemical analysis for potassium .....	80
5.6.10 Chemical analysis for chloride .....	81

<b>6.0 RESULTS AND DISCUSSION</b> .....	<b>83</b>
6.1 Introduction .....	83
6.2 Hydraulic and electro-osmotic conductivities .....	83
6.3 Electrical conductivity .....	85
6.4 Experimental results and model predictions .....	87
6.4.1 pH distribution .....	87
6.4.2 Voltage distribution .....	92
6.4.3 Hydraulic head distribution .....	92
6.4.4 Distribution of potassium .....	94
6.4.5 Distribution of chloride .....	98
<b>7.0 FIELD APPLICATION SCENARIOS</b> .....	<b>100</b>
7.1 Introduction .....	100
7.2 Electrokinetic barriers for vapour-extraction system .....	100
7.3 Electrokinetic barriers for pump-and-treat system .....	105
<b>8.0 CONCLUSIONS AND RECOMMENDATIONS</b> .....	<b>110</b>
<b>REFERENCES</b> .....	<b>114</b>

## **LIST OF TABLES**

<b>Table 2.1</b>	<b>Differential Equations developed by previous researchers . . . . .</b>	<b>24</b>
<b>Table 5.1</b>	<b>Concentrations of cations and anions present in the experimental soil . .</b>	<b>70</b>
<b>Table 5.2</b>	<b>Bulk density and porosity of the soil columns . . . . .</b>	<b>73</b>
<b>Table 6.1</b>	<b>Modelling parameters used in the computer model . . . . .</b>	<b>89</b>

## LIST OF FIGURES

Figure 1.1	Schematic field arrangement of electrokinetic barrier . . . . .	5
Figure 2.1	Diffuse double layer of ions adjacent to the surface of clay particle . . . . .	10
Figure 2.2	Charge distribution adjacent to the clay surface (Mitchell 1993) . . . . .	11
Figure 2.3	Electrokinetic phenomena. (a) Electro-osmosis (b) Electrophoresis (c) Streaming potential (d) Migration or sedimentation potential (Mitchell 1993) . . . . .	13
Figure 2.4	Relationship between pH and zeta potential for Kaolinite soil (Eykholt and Daniel 1991) . . . . .	16
Figure 2.5	Cost estimate of electrokinetic fencing as a function of groundwater flow velocity (Lageman <i>et al.</i> , 1989) . . . . .	22
Figure 3.1	Schematic diagram representing the two dimensional domain with boundary conditions (Huyakorn and Pinder, 1983) . . . . .	37
Figure 4.1	Interpolation functions for the linear triangular element . . . . .	46
Figure 4.2	Flow chart for the computer code FENCE . . . . .	52
Figure 4.3	Verification of the FEM solution with Ogata-Banks analytical solution for Advection-Dispersion equation . . . . .	56
Figure 4.4	Finite element model verification with the analytical solution derived by Esrig(1968) . . . . .	59
Figure 5.1	Schematic of the electrical column packed with soil used in the experiment . . . . .	63
Figure 5.2	Schematic diagram of the experimental set-up. Columns E1,E2, and E3 are electrical columns and columns H1,H2, and H3 are the hydraulic columns . . . . .	65
Figure 5.3	Particle size distribution of Red River clay . . . . .	67
Figure 6.1	Hydraulic conductivity of hydraulic columns . . . . .	84

Figure 6.2	Hydraulic and electro-osmotic conductivity of electrical columns . . . . .	84
Figure 6.3	Electrical conductivity distribution of hydraulic columns . . . . .	86
Figure 6.4	Electrical conductivity distribution of electrical columns . . . . .	86
Figure 6.5	Finite element discretization of the soil column used in the experiment .	88
Figure 6.6	pH distribution in the electrical columns . . . . .	91
Figure 6.7	Voltage distribution of electrical columns . . . . .	93
Figure 6.8	Hydraulic head distribution of electrical columns . . . . .	93
Figure 6.9	Distribution of potassium ion after 8 days . . . . .	95
Figure 6.10	Distribution of chloride ion after 8 days . . . . .	95
Figure 6.11	Distribution of potassium ion after 20 days . . . . .	96
Figure 6.12	Distribution of chloride ion after 20 days . . . . .	96
Figure 6.13	Distribution of potassium ion after 32 days . . . . .	97
Figure 6.14	Distribution of chloride ion after 32 days . . . . .	97
Figure 7.1	Hydrodynamic control of water table using electro-kinetic barriers for increasing the efficiency of vacuum extraction technique in removing volatile contaminants . . . . .	102
Figure 7.2	Simulation results of constant hydraulic head lines for a proposed electrokinetic barrier arrangement with the vapour-extraction system (a) plan view (b) side view . . . . .	103
Figure 7.3	Simulation results of constant voltage lines for a proposed electrokinetic barrier arrangement with the vapour-extraction system (a) plan view (b) side view . . . . .	104
Figure 7.4	Control of contaminant plume by electro-osmotic flow using electro-kinetic barriers. This setup can also improve the contaminant flushing using pump-and-treat technique . . . . .	106

<b>Figure 7.5</b>	<b>Simulation results of constant hydraulic head lines for a proposed electrokinetic barrier arrangement with the pump-and-treat system (a) plan view (b) side view</b> .....	<b>107</b>
<b>Figure 7.6</b>	<b>Simulation results of constant voltage lines for a proposed electrokinetic barrier arrangement with the pump-and-treat system (a) plan view (b) side view</b> .....	<b>108</b>

## LIST OF SYMBOLS

$a$	=	area of cross-section of the glass tube ( $\text{cm}^2$ )
$A$	=	area of cross-section of the soil column ( $\text{cm}^2$ )
$C$	=	concentration of the contaminant ( $\text{moles}\cdot\text{m}^{-3}$ )
$C_i$	=	unknown nodal values of concentration
$C_p$	=	electrical capacitance per unit volume ( $\text{Farad}\cdot\text{m}^{-3}$ )
$C_v$	=	Terzaghi coefficient of consolidation
$D_o$	=	diffusion coefficient in dilute solution ( $\text{m}^2\cdot\text{s}^{-1}$ )
$D^*$	=	effective diffusion coefficient in the porous medium ( $\text{m}^2\cdot\text{s}^{-1}$ )
$D_d$	=	dispersion coefficient ( $\text{m}^2\cdot\text{s}^{-1}$ )
$DF$	=	dilution factor
$F$	=	Faraday's constant ( $96487 \text{ C mol}^{-1}$ )
$I$	=	current density ( $\text{A}\cdot\text{m}^{-2}$ )
$J_{ai}$	=	contaminant flux of $i^{\text{th}}$ ion due to advection ( $\text{moles}\cdot\text{s}^{-1}\cdot\text{m}^{-2}$ )
$J_{di}$	=	contaminant flux of $i^{\text{th}}$ ion due to dispersion ( $\text{moles}\cdot\text{s}^{-1}\cdot\text{m}^{-2}$ )
$J_{ioni}$	=	contaminant flux of $i^{\text{th}}$ due to ionic migration ( $\text{moles}\cdot\text{s}^{-1}\cdot\text{m}^{-2}$ )
$K_e$	=	electro-osmotic conductivity ( $\text{m}^2\cdot\text{V}^{-1}\cdot\text{s}^{-1}$ )
$K_{ex}$ & $K_{ey}$	=	electro-osmotic conductivities of the porous medium in x and y directions respectively ( $\text{m}^2\cdot\text{V}^{-1}\cdot\text{s}^{-1}$ )
$K_h$	=	hydraulic conductivity ( $\text{m}\cdot\text{s}^{-1}$ )
$K_{hx}$ & $K_{hy}$	=	hydraulic conductivities of the porous medium in x and y directions respectively ( $\text{m}\cdot\text{s}^{-1}$ )
$m_v$	=	coefficient of volume compressibility

$n_e$	=	effective porosity of the porous media
$N_i, N_j, N_k$	=	interpolation functions or element shape functions
$q_h$	=	hydraulic flux ( $m \cdot s^{-1}$ )
$q_e$	=	electro-osmotic flux ( $m \cdot s^{-1}$ )
$R_d$	=	retardation coefficient
$R_g$	=	universal gas constant ( $8.314 \text{ J} \cdot \text{K}^{-1} \cdot \text{K}^{-1}$ )
$S_s$	=	specific storage of the porous medium ( $m^{-1}$ )
$t$	=	time
$T$	=	absolute temperature (K)
$u_{ion}^*$	=	effective ionic mobility in a porous medium ( $m^2 \cdot V^{-1} \cdot s^{-1}$ )
$u_{ion}$	=	ionic mobility in free solution ( $m^2 \cdot V^{-1} \cdot s^{-1}$ )
$V_h$ & $V_e$	=	velocity of flow due to hydraulic gradient and electrical gradient respectively ( $m \cdot s^{-1}$ )
$V_{ion}$	=	velocity of migration of ions ( $m \cdot s^{-1}$ )
$V_p$	=	volume of pore fluid present in the soil
$V_t$	=	total velocity of the contaminant ( $m \cdot s^{-1}$ ) = $V_h + V_e + V_{ion}$
$V_w$	=	volume of water added
$Z_i$	=	charge of the $i^{th}$ ion
$\alpha_L$	=	longitudinal dispersivity (m)
$\alpha_T$	=	transverse dispersivity (m)
$\delta$	=	dielectric constant of the fluid (unitless)
$\delta_{ij}$	=	Kronecker delta

$\epsilon$	=	permittivity of the vacuum ( $8.854 \times 10^{-12} \text{ F}\cdot\text{m}^{-1}$ )
$\zeta$	=	zeta potential (V)
$\eta$	=	viscosity of the fluid ( $1 \times 10^{-3} \text{ N}\cdot\text{s}\cdot\text{m}^{-2}$ )
$\rho_w$	=	density of water
$\sigma$	=	electrical conductivity of the soil medium ( $\text{S}\cdot\text{m}^{-1}$ )
$\tau$	=	tortuosity of the porous medium
$\theta_m$	=	dry basis moisture content of the soil
[C]	=	global capacitance matrix
{C} <sup>(e)</sup>	=	nodal concentration of element (e)
{F}	=	global force matrix
[K]	=	global stiffness matrix
$\nabla C$	=	concentration gradient
$\nabla E$	=	electrical potential gradient
$\nabla h$	=	hydraulic potential gradient
$\Delta t$	=	time step

## **1.0 INTRODUCTION**

### **1.1 Problem statement**

Increased use of chemicals by modern industrial societies has led to frequent occurrences of soil and groundwater contamination. Transportation systems that rely on petroleum-based energy sources and widespread uses of chemicals in agricultural production have also increased the risk of groundwater contamination. According to the National Pollutant Release Inventory of Canada (1996) about 207,239 tonnes of contaminants were released to the environment, of which 26,800 tonnes (about 13%) were released to the subsurface. This estimate does not include pollutants released due to accidental spills. According to the National Round Table on the Environment and the Economy report (1997) “there may be over 20,000 sites in Canada contaminated by gasoline storage, industrial operations, or accidental spills, as well as an estimated 10,000 active and inactive waste disposal sites.” The National Science Academy (1994) has estimated that, during the next three decades US\$750 billion will be spent for remediating 300,000 to 400,000 hazardous waste sites in the United States (Hannesin and Gillham, 1998). With over 50% of the population in the United States and over 26% of the population in Canada depending on the groundwater as a source for drinking water, the problem of groundwater contamination is gaining importance (Hess, 1986; Putnam, 1988).

Several remediation techniques are developed to deal with various kinds of contaminants and site conditions. Techniques like soil washing, bio-remediation, air-sparging and vacuum extraction are being used to remediate the contaminated sites.

Several options might exist to clean-up a contaminated site, however, tradeoffs between the level of clean-up and the cost of remediation determine the selection of remediation technique. There is not a single technology that can be used for all types of contaminants and site conditions. Every contaminated site requires site specific management practices. When planning to remove the contaminants, containing the contaminants in place is also equally important for effective and economic restoration of contaminated soil and groundwater. Otherwise, the contaminants will spread making the remediation difficult and expensive.

## **1.2 Physical containment techniques**

“Remediation of a waste disposal site frequently requires the use of vertical barriers to minimize the influx of uncontaminated groundwater into the site, minimize the migration of contaminated groundwater out of the site, and/or minimize groundwater pumpage and treatment rates (Evans *et al.*, 1987).” Slurry trench walls, grout curtains, and sheet piling are some of the vertical subsurface barriers used to contain the lateral spread of the contaminants. However, there are limitations associated with each of these containment techniques. Slurry walls are limited by the availability of bentonite clay and the patents associated with several aspects of construction procedures (Rogoshewski *et al.*, 1983). Research has identified some uncertainties associated with bentonite slurry trench due to their potential for construction defects, long-term performance in terms of waste compatibility, hydraulic fracturing, and chemical effects of contaminant on the slurry trench (Ryan, 1987). Similar problems exist with grout curtains. Sheet piling is subject to corrosion depending on the type of contaminants, concentrations, and the site conditions.

The availability of suitable access for the machinery and large equipment to the contaminated site is a major limitation of the conventional techniques. A new technique based on the principles of electrokinetic phenomena has been proposed to create an electrokinetic barrier for preventing contaminant migration in the subsurface.

### 1.3 Electrokinetic barrier

Applying a low DC electrical potential difference through inert electrodes buried in the soil induces flow of water due to electro-osmosis. During electro-osmosis, water moves from the anode towards the cathode. In fine grained soils, the movement of water due to electro-osmosis is highly significant when compared to the flow of water under a hydraulic gradient. The values of hydraulic conductivity can differ by orders of magnitude but, the coefficient of electro-osmotic conductivity is generally in the range of  $1 \times 10^{-9}$  to  $1 \times 10^{-10} \text{ m}^2 \cdot \text{V}^{-1} \cdot \text{s}^{-1}$  (Mitchell, 1993).

A simple numerical example can illustrate the effectiveness of electro-osmosis over the flow caused by the hydraulic gradient. Consider a clayey soil with a hydraulic conductivity of  $1 \times 10^{-9} \text{ m} \cdot \text{s}^{-1}$  and an electro-osmotic conductivity of  $5 \times 10^{-9} \text{ m}^2 \cdot \text{V}^{-1} \cdot \text{s}^{-1}$ . For equal volume flow rates per unit cross-sectional area:

$$K_h \nabla h = K_e \nabla E \quad (1.1)$$

where:

$K_h$  = hydraulic conductivity tensor ( $\text{m} \cdot \text{s}^{-1}$ ),

$\nabla h$  = hydraulic gradient,

$K_e$  = electro-osmotic conductivity scalar ( $m^2 \cdot V^{-1} s^{-1}$ ),

$\nabla E$  = electrical gradient ( $V \cdot m^{-1}$ ).

If an electrical potential gradient of  $25 V \cdot m^{-1}$  is applied then:

$$\nabla h = \frac{5 \times 10^{-9}}{1 \times 10^{-9}} \times 25 = 125 \quad (1.2)$$

Thus, the electro-osmotic flow created by an electrical potential gradient of  $25 V \cdot m^{-1}$  can oppose the flow of water caused by a hydraulic gradient of 125. This principle has been used by Civil and Geotechnical engineers to stabilize slopes and to de-water construction sites. During the past decade, the ability of this technique to clean-up the contaminated sites has been studied. Bench scale and field studies showed encouraging results (Acar, 1992; Eykholt and Daniel, 1991; Lageman *et al.*, 1989). Laboratory scale experiments also demonstrated the potential application for using electrokinetic phenomena to reclaim saline and alkaline soils for crop production (Ahmad *et al.*, 1997; Elsawaby, 1981).

The movement of water due to electrical gradients (electro-osmosis) can also be used to create a counter gradient, to the existing hydraulic gradient, for preventing the migration of contaminants. The viability of using an electrokinetic barrier to prevent the contaminant migration has not been investigated in detail. Figure 1.1 shows the principle of the electrokinetic barrier. Series of anode and cathode electrodes are installed perpendicular to the direction of contaminant migration. The electrodes are oriented in such a way that, the electro-osmotic flow occurs in a direction opposite to the direction of contaminant migration under natural groundwater gradients. As illustrated by the example, a sustained electro-osmotic flow can effectively contain the migration of contaminants. The counter-flow created due to electro-osmosis should be well above the regional groundwater



velocity in order to mitigate the contaminant migration due to hydrodynamic dispersion in addition to advection.

#### **1.4 Objectives**

The objectives of this study are to:

1. Conduct laboratory scale experiments to investigate the feasibility of using electrokinetic principles in creating subsurface barriers for contaminant migration.
2. Monitor and investigate the changes in chemical concentration, electrical and hydraulic potential gradients during the creation of electrokinetic barriers.
3. Develop a two-dimensional numerical model for the transport of contaminants under hydraulic, electrical and chemical gradients. The model should take into account the electrolysis reactions that occur at the anode and the cathode and the non-linear hydraulic and electrical gradients that develop due to contaminant migration.
4. Validate the numerical model, by comparing the model results with the measurements made in the experimental study.

#### **1.5 Organization**

This thesis consists of eight chapters. Chapter 1 briefly described the problem of groundwater contamination and the scope for using electrokinetic barriers in preventing contaminant migration. Chapter 2 discusses the electrokinetic phenomena, different applications of electrokinetic phenomena and modelling studies done by previous researchers. A mathematical model is proposed in chapter 3 to model the solute transport

through electrokinetic barriers. Chapter 4 discusses the finite element solution for the partial differential equations described in chapter 3. It also explains the organization of the computer code and the model verification with analytical solutions. The experimental procedures adopted in this study to assess the effectiveness of the electrokinetic barrier are explained in Chapter 5. In Chapter 6, the results obtained from the experiments are discussed and compared with the modelling results. Chapter 7 describes different applications of electrokinetic barriers in real world situations. Conclusions and recommendations for future research are given in chapter 8.

## **2.0 LITERATURE REVIEW**

### **2.1 Introduction**

During the past two decades the problem of groundwater contamination has gained prominence. New techniques have been developed for restoring contaminated soils and groundwater. As the knowledge and understanding of the principles of electrokinetics increased during the past decade, its potential uses in remediation engineering have been explored. Studies conducted so far on the potential use of this technique in remediating contaminated soils have shown encouraging results. One of the potential applications of electrokinetic phenomena is creating a subsurface barrier for contaminant migration. Only limited studies have been done until now to investigate its feasibility for possible field-scale applications. A detailed review of the theory underlying the electrokinetic phenomena is presented in this chapter. Literatures concerning different applications of electrokinetic phenomena have been reviewed and presented. A detailed review of different modelling studies has been done for subsequent development of a two-dimensional model for contaminant transport through electrokinetic barriers.

### **2.2 Electrokinetic phenomena**

#### **2.2.1 Electrical double layer**

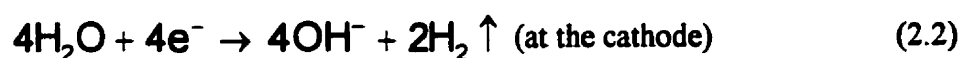
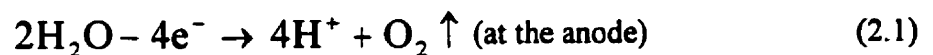
Clay particles are negatively charged due to the presence of broken bonds and the isomorphous substitution of aluminum ( $\text{Al}^{3+}$ ) instead of silica ( $\text{Si}^{4+}$ ) in the structure of clay minerals (Mitchell, 1993). The negative charge on the clay surface is neutralized by the

cations present in the pore fluid. These neutralizing cations together with the negatively charged particle surface form an electrostatic double layer (Hillel, 1982; Mitchell, 1993). Figures 2.1 and 2.2 explain the formation of diffuse double layer adjacent to the negatively charged clay surface. Several theories have been proposed on the formation of the diffuse electrostatic double layer. The Stern-Gouy-Chapman theory of diffuse double layer has been widely accepted. Detailed description of this theory has been given by Mitchell (1993). The quantity of the exchangeable cations required to neutralize the negative surface charge of clay is termed the cation exchange capacity (CEC), and is expressed in milliequivalent per gram (mEq/g) of dry soil. Montmorillonite has a CEC of about 0.95 mEq/g and kaolinite has a CEC of about 0.09 mEq/g (Hillel, 1982).

When an electrical potential gradient is applied across a column of soil, five different electrokinetic phenomena arise due to the presence of electrical double-layer and the movement of charged ions in the pore fluid. They are electro-osmosis, electro-migration, electrophoresis, streaming potential and migration potential. In addition to the different electrokinetic processes, electrolysis reactions occur at the anode and the cathode.

### 2.2.2 Electrolysis of water

When an electrical potential gradient is applied along a column of soil, electrolysis reactions take place at the anode and the cathode. Electrolysis of water releases  $H^+$  ions at the anode and the  $OH^-$  ions at the cathode. The electrolysis of water is given by the Eqs. 2.1 and 2.2:



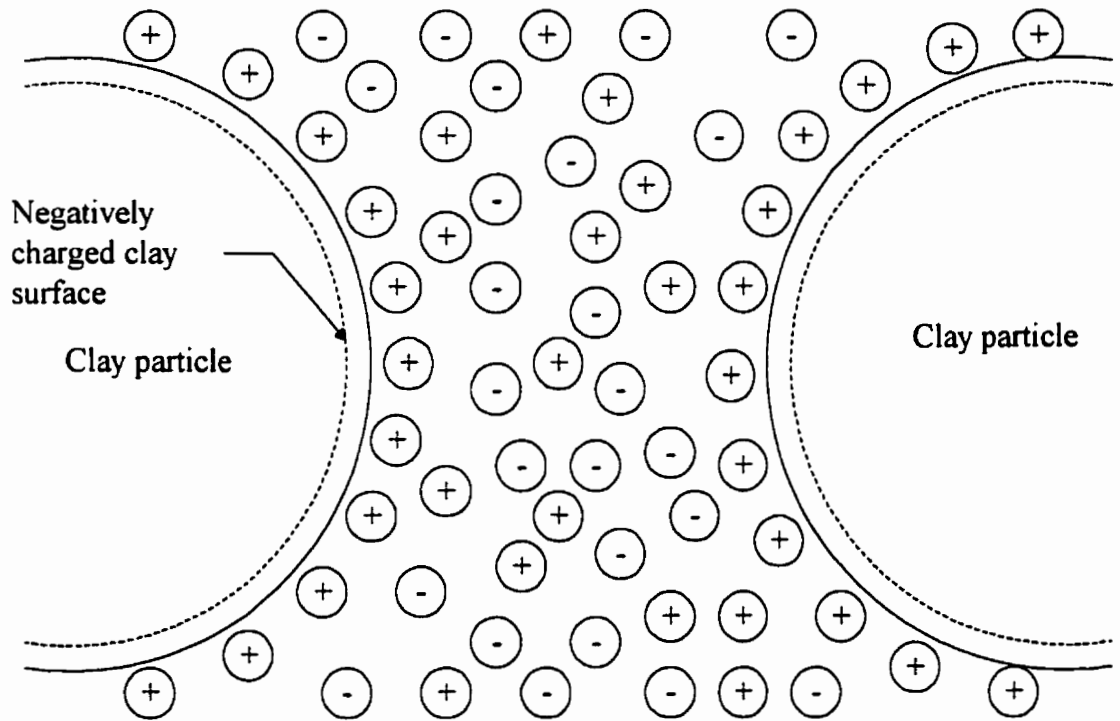


**Figure 2.1** Diffuse double layer of ions adjacent to the surface of clay particle.

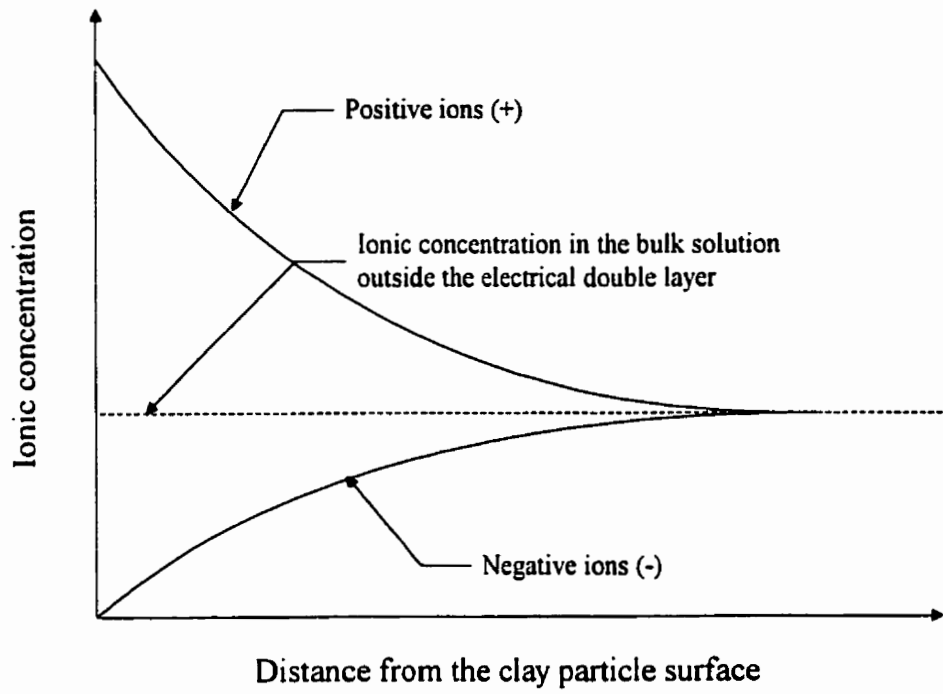
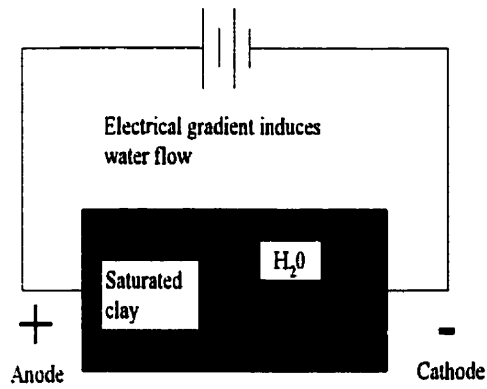


**Figure 2.2** Charge distribution adjacent to the clay surface (Mitchell, 1993).

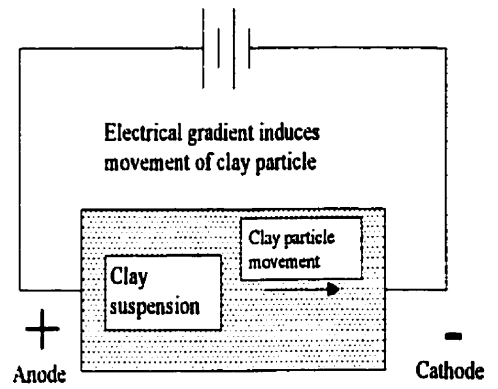
A sharp acid-base front develops due to the electrolysis of water (Acar *et al.*, 1993; Eykholt and Daniel, 1994; Mise, 1961). The acid front moves towards the cathode by advection (due to electro-osmosis), diffusion (due to chemical gradients) and ionic-migration (due to electrical potential gradients). The base front migrates in the opposite direction towards the anode. Since, the ionic mobility of  $H^+$  ions is 1.75 times that of the  $OH^-$  ions, the  $H^+$  ions dominate the system chemistry (Acar and Alshawabkeh, 1993). As a result, the migration of the acid front from the anode and the base front from the cathode takes place at different rates. The migration of the acid front and the base front considerably impacts the electrochemical properties of the soil and the removal of contaminants (Alshawabkeh and Acar, 1996; Eykholt and Daniel, 1994). Therefore, the migration of the acid and base fronts should be taken into account in modelling the contaminant migration through the electrokinetic barriers.

### **2.2.3 Electro-osmosis**

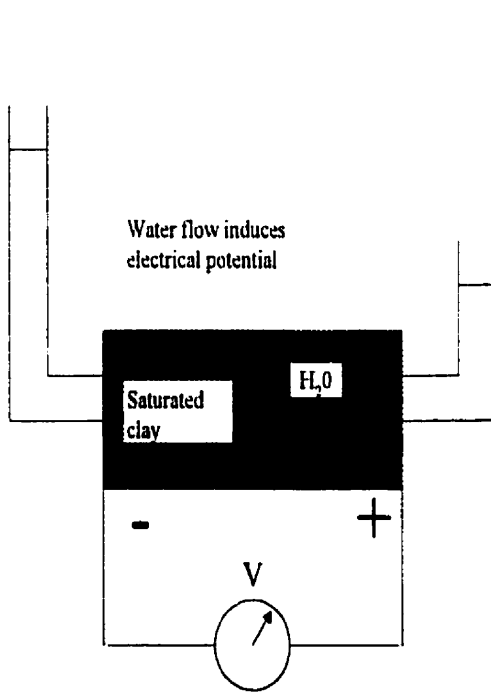
When an electrical potential gradient is maintained along a column of soil, water moves from the anode towards the cathode because of the electrical potential difference between the negatively charged soil surface and the solution (Kitahara and Watanabe, 1984). This phenomenon is called as electro-osmosis (Fig.2.3.). The movement of water under the influence of an electrical potential gradient is due to the viscous drag created by the mobile counter ions in the electrical double layer (Yeung, 1994). The cations in the pore fluid drag the water towards the cathode and the anions drag the water towards the anode. However, due to the presence of a net excess amount of cations (positively charged ions) in the clay-water-electrolyte system the net movement of water is more towards the cathode (Mitchell, 1991; Yeung, 1994). Electro-osmotic flow rate can be given by the relation:



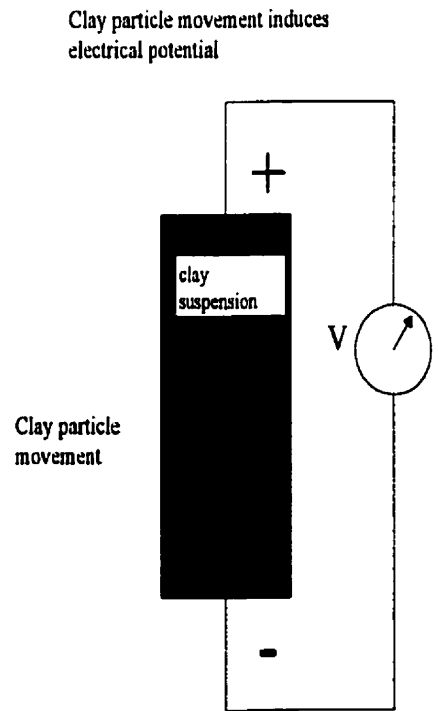
(a)



(b)



(c)



(d)

**Figure 2.3** Electrokinetic phenomena. (a) Electro-osmosis (b) Electrophoresis (c) Streaming potential (d) Migration or sedimentation potential (Mitchell, 1993).

$$\bar{q}_e = -K_e \nabla E \quad (2.3)$$

where:

$\bar{q}_e$  = electro-osmotic flux ( $m \cdot s^{-1}$ ),

$\nabla E$  = electrical potential gradient ( $V \cdot m^{-1}$ ),

$K_e$  = electro-osmotic conductivity scalar ( $m^2 \cdot V^{-1} \cdot s^{-1}$ ).

The values of hydraulic conductivity can differ by orders of magnitude but, the coefficient of electro-osmotic conductivity is generally in the range of  $1 \times 10^{-9}$  to  $1 \times 10^{-10} m^2 \cdot V^{-1} \cdot s^{-1}$  (Mitchell, 1993).

Electro-osmotic conductivity depends on several variables. Based on Helmholtz-Smoluchowski model, Casagrande (1949) derived an equation for electro-osmotic conductivity as follows:

$$K_e = \frac{-\zeta \delta \varepsilon n_e}{\eta \tau} \quad (2.4)$$

where:

$\zeta$  = zeta potential (V),

$\delta$  = dielectric constant of the fluid (unitless),

$\varepsilon$  = permittivity of the vacuum ( $8.854 \times 10^{-12} F \cdot m^{-1}$ ),

$n_e$  = effective porosity,

$\tau$  = tortuosity,

$\eta$  = viscosity of the fluid ( $1 \times 10^{-3} N \cdot s \cdot m^{-2}$ ).

The negative sign in the Eq.2.4 suggests that, the water will flow towards the cathode if the concentration of cations in the pore fluid exceeds that of anions (positive zeta potential).

Zeta potential is defined as the potential difference between the shearing surface in the diffuse double layer and the liquid. According to Yeung (1994) values of  $\zeta$  is in the range of +50mV to -50 mV. The pH of the soil determines the zeta potential. For most clayey soils, zeta potential is in the range of 0 to -50 mV (Yeung, 1994). A value above 0 mV can occur in highly acidic soils where, the electro-osmotic flow will be towards the anode instead of towards the cathode (Eykholt and Daniel, 1994) . With electro-osmotic flow, there is a pH front that moves along the length of the soil column, due to the electrolysis reaction at the electrodes as explained in Sec.2.2.2, and as a result the zeta potential also changes. Therefore, the electro-osmotic conductivity is not a constant.

Kruyt (1952) showed that, the zeta potential changes linearly with the logarithm of ionic concentration of the pore fluid:

$$\zeta = A - B \log_e C \quad (2.5)$$

where:

A&B = constants,

C = the total concentration of the electrolyte.

A graph (Fig.2.4) was plotted between  $\zeta$  and pH for kaolinite by Lorenz (1969) by measuring the streaming potential (Sec.2.2.6). An equation similar in the form of Eq.2.5 was fitted to this graph by Eykholt and Daniel (1994) and is given below:

$$\zeta = -38.6 + 281e^{-0.48\text{pH}} \quad (2.6)$$

According to this equation, when the pH is low, very little electro-osmotic flow occurs. The

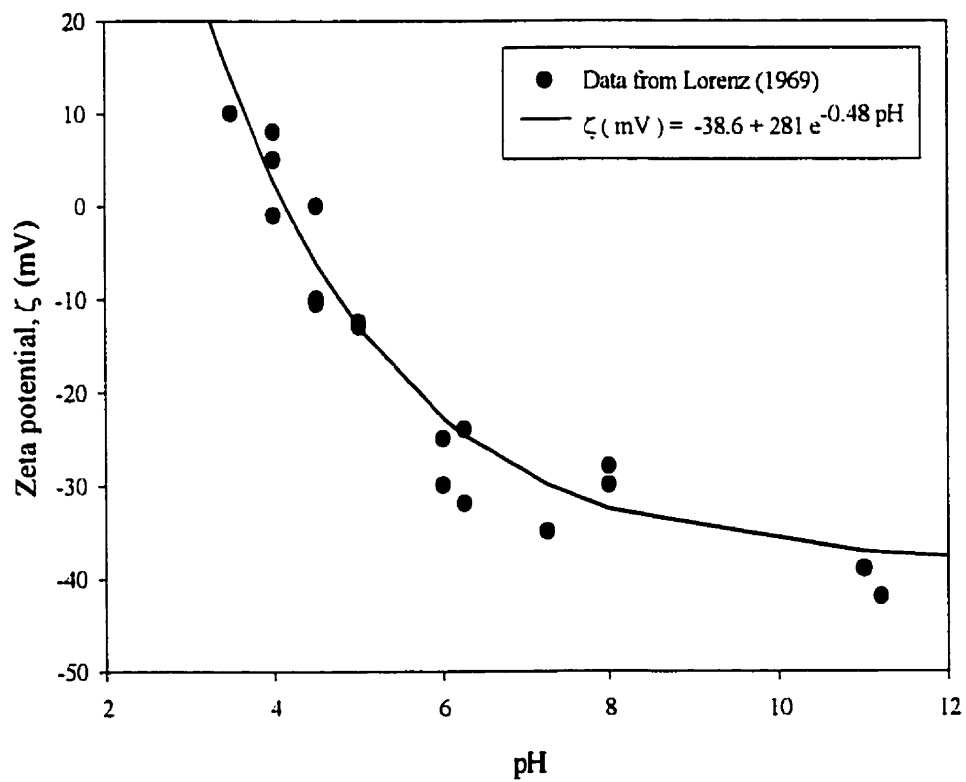


**Figure 2.4** Relationship between pH and zeta potential for Kaolinite soil (Eykholt and Daniel 1991).

electro-osmotic flow will be zero at the iso-electric point, occurring near a pH of 4 and can reverse when the pH is reduced below the iso-electric point. The iso-electric point is the pH where, the molecule bears no net charge so that, the zeta potential is zero (Probstein and Hicks, 1993).

From Eq.2.4, it is important to note that unlike the hydraulic conductivity the electro-osmotic conductivity depends mainly on the zeta potential and the porosity and not on the pore size or pore size distribution (Probstein and Hicks, 1993). Hence, the electro-osmotic flow will be significant in fine-grained soils and the flow distribution will be uniform even in heterogenous soils (Acar and Alshawabkeh, 1993). Electro-osmotic flow occurs both in saturated and unsaturated soils, but increases with increasing water content (Pamucku and Wittle, 1992).

#### **2.2.4 Electro-migration**

Electro-migration is the migration of charged ions towards oppositely charged electrodes under an applied electrical potential gradient. Positively charged cations move towards the cathode and the negatively charged anions move towards the anode. The rate of migration of ions under an applied electrical potential gradient can be given by:

$$q_{ion} = -u_i \nabla E \quad (2.7)$$

where:

$q_{ion}$  = rate of migration of ions ( $m \cdot s^{-1}$ ),

$\nabla E$  = electrical potential gradient ( $V \cdot m^{-1}$ ),

$u_i$  = ionic mobility in free solution ( $m^2 \cdot V^{-1} \cdot s^{-1}$ ).

Ionic mobility can be defined as the velocity of the ion in the soil under the influence of a

unit electrical potential gradient. The ionic mobility and the diffusion coefficient of an ion in dilute solution are related by the Nernst-Einstein equation (Koryta, 1982):

$$u_i = \frac{D_{oi} z_i F}{R_g T} \quad (2.8)$$

where:

$D_{oi}$  = diffusion coefficient of species  $i$  in dilute solution ( $m^2 \cdot s^{-1}$ ),

$z_i$  = charge of the chemical species,

$F$  = Faraday's constant ( $96487 \text{ C mol}^{-1}$ ),

$R_g$  = universal gas constant ( $8.314 \text{ J} \cdot \text{mol}^{-1} \cdot \text{K}^{-1}$ ),

$T$  = absolute temperature (K).

According to Acar and Alshawabkeh (1993), the mass transport rate due to electro-migration is 10 times more than that due to electro-osmosis.

### **2.2.5 Electrophoresis**

When an electrical potential gradient is applied to a suspension of clay particles, the negatively charged clay particles move towards the anode and positively charged colloidal particles present in the suspension move towards the cathode. This phenomena is called electrophoresis (Mitchell, 1993).

### **2.2.6 Streaming potential**

Streaming potential is the reverse process of electro-osmosis. When a liquid flows through a column of soil, an electrical potential difference is created between the upstream and downstream ends of the soil column. This electrical potential difference is created due to the

transport of mobile ions in the diffuse double layer towards the downstream end of the liquid. This phenomenon is called as streaming potential (Mitchell, 1993).

### **2.2.7 Migration potential**

Migration potential is the reverse process of electrophoresis. When a charged clay particle or colloidal particle settles down in a soil suspension, an electrical potential difference is created between the top and the bottom of the soil suspension. This electrical potential difference created due to the settlement of charged particles in one end of the suspension is called as migration potential (Mitchell, 1993).

## **2.3 Applications of electrokinetic phenomena**

### **2.3.1 Electrokinetic remediation**

The concept of remediating contaminated soils using electrical fields evolved from several studies conducted during the past decade (Hamed *et al.*, 1991; Lageman *et al.*, 1989; Probstein and Hicks, 1993; Qian, 1998; Segall and Bruell, 1992; Thomas, 1996; Yeung, 1990). Electrokinetic remediation involves the application of an electrical potential gradient between electrodes installed in a contaminated zone. Applying an electrical potential gradient causes the movement of water by electro-osmosis and ions by electro-migration. Non-ionic contaminants like gasoline can be effectively removed by flushing the water through the contaminated zone by electro-osmosis. Studies conducted by Bruell *et al.* (1992) showed that, hydrocarbon contaminants like gasoline and TCE could be effectively removed from fine-grained soils using electrokinetic remediation. Within 3 days of treatment, 15% of TCE and 15% of benzene were removed. Phenol has a very high retardation coefficient

and is less volatile. Hence, remediation techniques like air sparging or vapour extraction to remediate phenol contaminated soil are least effective. Studies conducted by Acar *et al.* (1992) showed a removal of 85-95% of phenol from contaminated soil using electrokinetic remediation. Electrokinetic remediation can also be combined with remediation techniques like surfactant flushing and bio-remediation for effective removal of hydrocarbon contaminants. Studies conducted by Thomas (1996) and Qian (1998) showed effective removal of gasoline contaminants from fine-grained soils by this technique. Acar *et al.* (1996) showed that, bio-remediation of hydrocarbon contaminants can be enhanced by injecting microorganisms and nutrients into the soil using electrical fields.

Heavy metal contaminants like lead can also be removed efficiently using this technique. Using electrokinetic remediation, Lagemen *et al.* (1989) removed more than 80% of lead and copper from an abandoned paint factory site. About 75-95% of absorbed lead was removed in a laboratory scale study conducted by Hamed (1991).

### **2.3.2 Electrokinetic barriers**

The movement of water due to an applied electrical potential gradient (electro-osmosis) and the migration of ions towards oppositely charged electrodes (electro-migration) can be effectively used to prevent the migration of contaminants. Electrokinetic barriers can be used at refuse sites or abandoned factory sites where the contamination of soil and water has been already detected or in places where the contamination is likely to occur. The idea of using electrical fields to prevent the contaminant migration was conceived by Lageman *et al.* (1989). They used this technique successfully to prevent the migration of heavy metal contaminants like lead, copper, zinc and cadmium during electrokinetic remediation of an

abandoned paint factory site. Studies conducted by Lageman *et al.* (1989) showed that, in fine-grained soils like clay, the yearly energy costs of an electrokinetic fence are insignificant. Figure 2.5 shows the energy costs of an electrokinetic fence as a function of groundwater velocity and soil resistivity. From the graph, it can be inferred that the electrokinetic barriers can be used effectively in fine-grained soils to prevent the migration of contaminants.

Yeung (1993) conducted lab scale experiments to study the feasibility of using electrical fields to control the migration of contaminants across a compacted clay liner. Clay liners used in hazardous waste sites are subject to cracking due to wetting and drying cycles (Ryan, 1987). The cracks developed during this process will allow the contaminants present in the clay liner to migrate, and cause soil and groundwater contamination. Installing electrodes across this clay liner will prevent the contaminants from spreading. Yeung (1993) found that, the electrokinetic barriers can effectively prevent the cationic contaminants from migration, but it increased the migration of anions. This is because of the effectiveness of electro-migration in moving the charged ions over electro-osmosis (Sec.2.2.4). Proper configuration of electrodes should be used depending on the type of contaminants and the field conditions. It can be inferred from this study that, the migration of non-ionic contaminants such as gasoline, could be effectively controlled by using this technique. Renaud and Probst (1987) suggested the use of electro-osmosis for diverting the water flowing through hazardous waste facilities. A steady state model developed by them showed that, using electro-osmosis, the ground water flow due to the existing hydraulic gradient can be diverted from flowing through hazardous waste facilities.

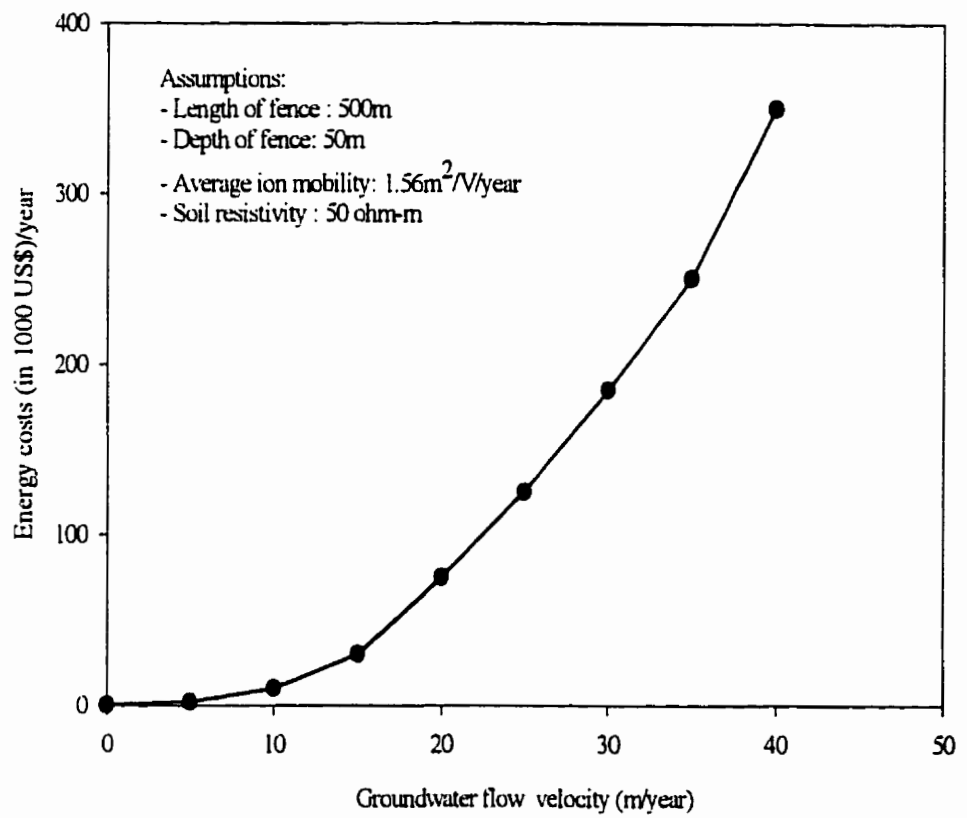


**Figure 2.5** Cost estimate of electrokinetic fencing as a function of groundwater flow velocity (Lageman *et al.*, 1989).

### **2.3.3 Electrokinetic consolidation**

Casagrande(1949) reported the efficiency of electro-osmosis in moving water in fine grained soils. Since then, Civil and Geotechnical engineers used this technique primarily for consolidation of soil and stabilization of the slope. In the field, electrokinetic consolidation is carried out by driving two parallel rows of closely spaced anode and cathode electrodes (Esrig, 1968). Applying an electrical potential difference between electrodes causes water movement from the anode towards the cathode. The water collected at the cathode compartment is pumped out. As no water is supplied at the anode, the electro-osmotic flow towards the cathode causes consolidation of the soil between the electrodes.

### **2.3.4 De-watering and concentration**

Wastewater sludges, coal washings and mine tailings have high water content. As the suspended particles in these materials are of colloidal size, it might take a longer time for these particles to settle (Yeung, 1994). Electrophoresis and electro-osmosis can be effectively used for concentration and de-watering. If an electrical potential gradient is applied on a slurry containing negatively charged colloidal particles, the suspended particles will migrate towards the anode. After sufficient densification has been achieved, further de-watering and consolidation of the sludge can be achieved by electro-osmosis.

## **2.4 Theoretical model studies**

Many theoretical models have been developed by researchers to investigate the movement of water and the migration of contaminants under the influence of electrical potential gradients. The differential equations developed thus far by researchers are tabulated in Table 2.1 and are discussed in this section.

**Table 2.1** Differential Equations developed by previous researchers

Reference	Modelling equations
<p>Lewis and Garner (1972)</p>	$K_{hx} \frac{\partial^2 h}{\partial x^2} + K_{ex} \frac{\partial^2 E}{\partial x^2} + K_{hy} \frac{\partial^2 h}{\partial y^2} + K_{ey} \frac{\partial^2 E}{\partial y^2} = x_{11} \frac{\partial h}{\partial t} + x_{12} \frac{\partial E}{\partial t}$ $G_x \frac{\partial h}{\partial x} + \frac{1}{\rho_x} \frac{\partial E}{\partial x} + G_y \frac{\partial h}{\partial y} + \frac{1}{\rho_y} \frac{\partial E}{\partial y} = x_{21} \frac{\partial h}{\partial t} + x_{22} \frac{\partial E}{\partial t}$ <p>where:</p> <p><math>K_{hx}</math> and <math>K_{hy}</math> = hydraulic conductivities in x and y directions,</p> <p><math>K_{ex}</math> and <math>K_{ey}</math> = electro-osmotic conductivities in x and y directions,</p> <p><math>X_{11}, X_{12}, X_{21}</math> and <math>X_{22}</math> = coupling coefficients,</p> <p><math>G_x</math> and <math>G_y</math> = streaming current coefficient,</p> <p><math>\rho_x</math> and <math>\rho_y</math> = electrical resistivity of the soil.</p>
<p>Renaud and Probst (1987)</p>	$q = q_h + q_e = -\frac{K_h}{\mu} \frac{\partial P}{\partial x} - \frac{K_e}{\mu} \frac{\partial \phi}{\partial x}$ $i = i_h + i_e = -\sigma_h \frac{\partial P}{\partial x} - \sigma_e \frac{\partial \phi}{\partial x}$ <p>where:</p> <p><math>q</math> = water flux,</p> <p><math>i</math> = current flux,</p> <p><math>P</math> = hydraulic pressure,</p> <p><math>\phi</math> = electrical potential,</p> <p><math>\mu</math> = viscosity of water,</p> <p><math>\sigma_h</math> = streaming current coefficient,</p> <p><math>\sigma_e</math> = electrical conductivity.</p>

**Table 2.1** Differential Equations developed by previous researchers (contd.)

<p>Yeung (1993)</p>	$J_c = (L_{31} + C_c L_{11}) \gamma_w \nabla(-h) + (L_{32} + C_c L_{12}) \nabla(-E)$ $+ (L_{33} + C_c L_{13}) \frac{RT}{C_c} \nabla(-C_c) + (L_{34} + C_c L_{14}) \frac{RT}{C_a} \nabla(-C_a)$ $J_a = (L_{41} + C_a L_{11}) \gamma_w \nabla(-h) + (L_{42} + C_a L_{12}) \nabla(-E)$ $+ (L_{43} + C_a L_{13}) \frac{RT}{C_c} \nabla(-C_c) + (L_{44} + C_a L_{14}) \frac{RT}{C_a} \nabla(-C_a)$ <p>where:</p> <p><math>J_c</math> = concentration flux of cation,  <math>J_a</math> = concentration flux of anion,  <math>L_{ij}</math> = phenomenological coupling coefficients,  <math>C_c</math> = concentration of cation,  <math>C_a</math> = concentration of anion,  <math>R</math> = universal gas constant,  <math>T</math> = temperature.</p>
<p>Acar <i>et al.</i> (1990)</p>	$q_c = \left[ -D_j \left( \frac{\partial C_j}{\partial x} \right) + V_x C_j - \frac{zF}{RT} D_j C_j \left( \frac{\partial \phi}{\partial x} \right) \right] n \, dA$ <p>where:</p> <p><math>q_c</math> = chemical flux,  <math>D_i</math> = diffusion coefficient,  <math>n</math> = porosity,  <math>dA</math> = cross-sectional area,  <math>V_x</math> = average seepage velocity,  <math>F</math> = faradays constant.</p>
<p>Corapcioglu (1991)</p>	$q_r = -\frac{k}{\mu_f} \nabla p - k_{hc} \nabla C_s - k_e \nabla \phi$ $q_e = -\frac{\sigma_h}{g \rho_f} \nabla p - k_{ec} \nabla C_s - \sigma_e \nabla \phi$ <p>where:</p> <p><math>q_r</math> = specific discharge of the water phase relative to the moving solid matrix,  <math>q_e</math> = constant current density applied at a boundary,  <math>k</math> = permeability tensor of the porous medium,  <math>\mu_f</math> = viscosity of the water phase,  <math>k_{hc}</math> = chemico-osmotic coupling coefficient,  <math>k_{ec}</math> = coefficient of migration potential.</p>

**Table 2.1** Differential Equations developed by previous researchers (contd.)

<p>Bruell <i>et al.</i> (1992)</p>	$\frac{\partial C}{\partial t} = D_i \frac{\partial^2 C}{\partial x^2} - v \frac{\partial C}{\partial x} + \frac{\rho_b}{n} \frac{\partial S}{\partial t}$ <p>where:  <math>S</math> = mass of contaminant adsorbed per unit mass of solid porous material,  <math>\rho_b</math> = dry bulk density of porous material.</p>
<p>Alshawabkeh <i>et al.</i> (1992)</p>	$J_w = k_h \nabla(-h) + k_e \nabla(-E)$ $J_j = D_j^* \nabla(-C_j) + C_j \left( \frac{ Z_j }{Z_j} \right) u_j^* + k_e \nabla(-E) + C_j K_h \nabla(-h)$ $I = F \sum_{j=1}^N Z_j D_j^* \nabla(-C_j) + \sigma \nabla(-E)$ <p>where:  <math>J_w</math> = fluid flux,  <math>J_j</math> = chemical flux,  <math>I</math> = current flux,  <math>\sigma</math> = bulk electrical conductivity of the pore fluid.</p>
<p>Shapiro and Probstein (1993)</p>	$\frac{\partial \bar{c}_i}{\partial t} = \frac{D_i}{\tau^2} \frac{\partial^2 \bar{c}_i}{\partial z^2} - \frac{\partial}{\partial z} [\bar{c}_i (u_{e,i} + \bar{u}_c)] + \bar{R}_i$ $i = -\sigma \nabla \phi - F \sum_{i=1}^m z_i D_i \nabla c_i + Fu \sum_{i=1}^m z_i c_i$ $\sigma = F^2 \sum z_i^2 u_i c_i$ <p>where:  <math>\tau</math> = tortuosity,  <math>u_{e,i}</math> = electro-migration velocity,  <math>\bar{u}_c</math> = bulk electro-osmotic velocity,  <math>u</math> = mass average velocity,  <math>u_i</math> = ionic mobility,  <math>\sigma</math> = electrical conductivity.</p>

The earliest finite element model for coupled electro-osmotic and hydrodynamic flow was developed by Lewis and Garner (1972). The model predicted the changes in pore water pressure created by the electro-osmotic flow. Finite element modelling of electro-osmotic flow process applied to the control of hazardous waste was developed by Renaud and Probst (1987). The effect of electro-osmotic flow to divert the groundwater from passing through a hypothetical hazardous waste land fill was simulated. Their model predicted the voltage gradients, electro-osmotic flow and the hydrodynamic pressure distribution around the land fill. The migration of contaminants was not considered in these models.

Research done by Acar *et al.* (1990) suggested that, the changes in pH along the column of soil due to electrolysis of water will affect the electrokinetic remediation of soil. A numerical model was developed to simulate the migration of hydrogen and hydroxyl ions using a modified advection-dispersion equation. Yeung (1990) developed a set of coupled flow equations based on irreversible thermodynamics. The migration of contaminants under the coupled hydraulic, electrical and chemical gradients was modelled. The phenomenological coefficients used in the model are related to the conductivity coefficients for the flow of water, chemicals and current. Yeung (1990) assumed that, the voltage and hydraulic gradient were linearly distributed in the soil column. Migration of hydrocarbon contaminants like gasoline and TCE under the influence of linear electrical potential gradient was modelled by Bruell *et al.* (1992). As time proceeds, non-linear hydraulic and electrical potential gradients arise. This non-linearity developed in the voltage and the hydraulic gradients were not considered in these models.

Corapcioglu (1991) proposed a model based on macroscopic conservation of mass and charge. The movement of water, migration of the contaminant and the electrical current flux in a compressible porous media were modelled. However, the coefficients used in this model cannot be measured readily. Eykholt and Daniel (1994) attempted to simulate the migration of acid and base front from the anode and the cathode respectively during electrokinetic process. The developed model simulated the migration of hydrogen and hydroxyl ion and the non-linearity in electrical and hydraulic potential gradients brought about by the pH gradients. The changes in the electro-osmotic conductivity brought about due to the changes in the zeta potential and pH were related by an empirical relation. However, the contaminant migration was not included in their model.

Alshawabkeh and Acar (1992) proposed a comprehensive model to simulate the migration of contaminants, development of acid front and the non-linear changes in electrical and hydraulic potential gradients, brought about by the changes in the electrical conductivity of the soil. The model reasonably predicted the migration of contaminants and the associated changes in pH, electrical gradients and the hydraulic gradients.

## **2.5 Summary**

Research done, until now, have demonstrated several applications of electrokinetic phenomena in the field of Geotechnical and Environmental Engineering. Only few studies have been done to investigate the feasibility of using electrokinetic phenomena in creating subsurface barriers to prevent the contaminant migration. The present study investigated the effectiveness of electrokinetic barriers in preventing contaminant migration, the effect of pH

migration on the effectiveness of the barrier and the development of non-linear electrical and hydraulic gradients. A two-dimensional finite element model for contaminant migration was developed using the partial differential equations developed by various researchers. The numerical model simulated the effect of different electrokinetic phenomena on the contaminant transport. The procedures adopted for the model development and the experimental validation are explained in the subsequent chapters.

## **3.0 MODEL DEVELOPMENT**

### **3.1 Introduction**

An electrokinetic barrier can be created by applying an electrical potential gradient counter to the existing hydraulic gradient. However, applying the electrical potential gradient continuously over a long period of time generates  $H^+$  ions at the anode and  $OH^-$  ions at the cathode due to electrolysis (Chapter 2). Migration of these species into the soil could affect the transport of contaminants and the distribution of hydraulic and electrical potential gradients in the soil. Hence, in order to develop a realistic model for contaminant migration under the influence of hydraulic, electrical and chemical gradients, mathematical formulations have to be done to account for the electrolysis reactions at the electrodes. This chapter discusses the mechanisms of contaminant transport and presents the governing equations for the numerical model.

### **3.2 Contaminant transport mechanisms in electrokinetic processes**

During the electrokinetic process the contaminants can migrate by 1) advection - due to the movement of water under hydraulic and electrical potential gradient 2) dispersion - due to the concentration gradients and 3) electro-migration - due to the ionic mobilities of charged ions towards oppositely charged electrodes.

#### **3.2.1 Advection due to hydraulic and electrical gradients**

The advection is an important solute transport process in which the dissolved solids are carried along with the flowing pore water. The amount of solute that is being transported is

a function of its concentration and the quantity of the pore water flowing. In the electrokinetic process water flows due to the applied electrical potential gradient and the existing hydraulic gradient. The flow of water due to a hydraulic gradient is given by Darcy's law:

$$\bar{q}_h = -K_h \cdot \nabla h \quad (3.1)$$

where:

$\bar{q}_h$  = flux due to hydraulic gradient ( $m \cdot s^{-1}$ ),

$\nabla h$  = hydraulic gradient,

$K_h$  = hydraulic conductivity tensor ( $m \cdot s^{-1}$ ).

The fluid flux due to electro-osmosis is given by:

$$\bar{q}_e = -K_e \nabla E \quad (3.2)$$

where:

$\bar{q}_e$  = electro-osmotic flux ( $m \cdot s^{-1}$ ),

$\nabla E$  = electrical potential gradient ( $V \cdot m^{-1}$ ),

$K_e$  = electro-osmotic conductivity scalar ( $m^2 \cdot V^{-1} \cdot s^{-1}$ ).

Previous studies have proved that, the water flux due to a hydraulic gradient and an electrical potential gradient are numerically additive (Esrig, 1968; Esrig and Majtenyi, 1965; Lewis, 1973). Therefore, the total advective flux of the contaminant due to a hydraulic gradient and an electrical gradient is given by:

$$\bar{J}_a = (\bar{V}_h + \bar{V}_e) n_e C \quad (3.3)$$

where:

$\bar{J}_a$  = contaminant flux due to advection ( $moles \cdot s^{-1} \cdot m^{-2}$ ),

- $C$  = concentration of the contaminant ( $\text{moles}\cdot\text{m}^{-3}$ ),
- $\bar{V}_h$  = velocity of water due to a hydraulic gradient ( $\text{m}\cdot\text{s}^{-1}$ ) =  $\bar{q}_h / n_e$ ,
- $\bar{V}_e$  = velocity of water due to an electrical gradient ( $\text{m}\cdot\text{s}^{-1}$ ) =  $\bar{q}_e / n_e$ ,
- $n_e$  = effective porosity (taken as being equal to the total porosity in this thesis).

### 3.2.2 Hydrodynamic dispersion

Dispersion is a process by which the dissolved solids in the flowing groundwater spread beyond the region it would normally occupy due to advection alone (Domenico and Schwartz, 1990). Hydrodynamic dispersion consists of two components, mechanical dispersion and molecular diffusion.

Mechanical dispersion occurs due to variation of velocity within the pores in a microscopic scale. As the solute-containing water is not travelling at the same velocity, mixing occurs along the flow-path. This results in dilution of the solute at the advancing front of flow (Fetter, 1992). The contaminant flux due to mechanical dispersion is given by:

$$\bar{J}_m = -D_m \cdot \nabla C n_e \quad (3.4)$$

where:

- $\bar{J}_m$  = contaminant flux due to mechanical dispersion ( $\text{moles}\cdot\text{s}^{-1}\cdot\text{m}^{-2}$ ),
- $D_m$  = coefficient of mechanical dispersion ( $\text{m}^2\cdot\text{s}^{-1}$ ) =  $\alpha_T |V| \delta_{ij} + (\alpha_T - \alpha_L) \frac{V_i V_j}{|V|}$
- $\alpha_L, \alpha_T$  = Longitudinal and transverse dispersivities, respectively (m),
- $\delta_{ij}$  = Kronecker delta (with  $\delta_{ij} = 0$  for  $i \neq j$  and  $\delta_{ij} = 1$  for  $i = j$ )
- (Bear and Verruijt, 1987)

$V$  = velocity of water due to hydraulic and electrical gradients ( $m \cdot s^{-1}$ ),

$\nabla C$  = concentration gradient.

Molecular diffusion occurs due to the concentration gradient of the contaminant in the flowing pore fluid. The diffusion component is very important in heavy soils like clay where, the groundwater flow velocity is very low. The mass of the diffusing fluid is proportional to the concentration gradient, which can be expressed by Fick's law. For a nonporous, simple, aqueous system, Fick's law is expressed as:

$$J_d = -D_o \nabla C \quad (3.5)$$

where:

$J_d$  = contaminant flux due to diffusion ( $moles \cdot s^{-1} \cdot m^{-2}$ ),

$D_o$  = diffusion coefficient in a free solution ( $m^2 \cdot s^{-1}$ ).

The diffusion coefficient in a porous medium is smaller than in free solution primarily because collision with the solids of the medium hinders diffusion (Domenico and Schwartz, 1990). Hence, the diffusion coefficient in free solution must be modified with porosity and tortuosity factors to account for the hindering of free diffusion by collision with the pore walls. The modified diffusion coefficient is called effective diffusion coefficient (Domenico and Schwartz, 1990):

$$D^* = \frac{n_e}{\tau} D_o \quad (3.6)$$

where:

$D^*$  = effective diffusion coefficient ( $m^2 \cdot s^{-1}$ ),

$n_e$  = effective porosity,

$\tau$  = tortuosity.

The ratio of the length of the actual flow path for a fluid particle ( $L_e$ ) to the length of a porous medium of the sample ( $L$ ) is defined as tortuosity ( $L_e/L$ ). A personal communication with Dr. K. R. Rowe (Professor, University of Western Ontario, Canada) suggested that the tortuosity factor is not affected by electrical potential gradients. Studies conducted suggest that, the ratio ( $n_e/\tau$ ) varies between 0.13 and 0.49 (Acar *et al.*, 1990). Therefore, the flux of the contaminant due to hydrodynamic dispersion is given by:

$$\bar{J}_{hd} = -D_d \cdot \nabla Cn_e \quad (3.7)$$

where:

$\bar{J}_{hd}$  = contaminant flux due to hydrodynamic dispersion ( $\text{moles} \cdot \text{s}^{-1} \cdot \text{m}^{-2}$ ),

$D_d$  = hydrodynamic dispersion coefficient ( $\text{m}^2 \cdot \text{s}^{-1}$ ) =  $D_m + D^*$ .

### 3.2.3 Ionic migration

Ionic migration is the movement of the charged particles dissolved in water towards oppositely charged electrodes under the influence of an electrical field. Particles with zero charge will not have this component of contaminant migration. Ionic mobility can be defined as the velocity of the ion in the soil under the influence of a unit electrical potential gradient.

The ionic mobility and the diffusion coefficient of an ion in dilute solution are related by the Nernst-Einstein equation (Koryta, 1982):

$$u_{ion} = \frac{D_o zF}{R_g T} \quad (3.8)$$

where:

$u_{ion}$  = ionic mobility in free solution ( $\text{m}^2 \cdot \text{V}^{-1} \cdot \text{s}^{-1}$ ),

$D_o$  = diffusion coefficient in dilute solution ( $\text{m}^2 \cdot \text{s}^{-1}$ ),

- $z$  = charge of the chemical species (unitless),  
 $F$  = Faraday's constant (96487 C mol<sup>-1</sup>),  
 $R_g$  = universal gas constant (8.314 J•mol<sup>-1</sup>•K<sup>-1</sup>),  
 $T$  = absolute temperature (K).

As represented by Eq.3.6, the effective diffusion coefficient has to be used in finding the effective ionic mobilities of the charged particles in a porous medium (Alshawabkeh and Acar, 1996).

$$u_{ion}^* = \frac{D^* zF}{R_g T} \quad (3.9)$$

where:

$u_{ion}^*$  = effective ionic mobility in a porous medium (m<sup>2</sup>•V<sup>-1</sup>•s<sup>-1</sup>).

The rate of ion migration under an applied electrical potential gradient can then be given by:

$$\vec{V}_{ion} = -u_{ion}^* \nabla E \quad (3.10)$$

where:

$\vec{V}_{ion}$  = rate of migration of ions (m•s<sup>-1</sup>),

$\nabla E$  = electrical potential gradient (V•m<sup>-1</sup>).

Hence, the contaminant flux due to ionic migration can be given by:

$$\vec{J}_{ion} = \vec{V}_{ion} C n_e \quad (3.11)$$

Therefore, the total velocity of the ion due to hydraulic flow, electro-osmotic flow and electro-migration is given by (Alshawabkeh and Acar, 1996):

$$\vec{V}_t = \vec{V}_h + \vec{V}_e + \vec{V}_{ion} \quad (3.12)$$

Therefore, the total ionic flux from Eq.3.12 is:

$$\bar{J}_a = \bar{V}_t C n_e \quad (3.13)$$

where:

$$\bar{V}_t = \text{the total velocity of the contaminant (m}\cdot\text{s}^{-1}) = \bar{V}_h + \bar{V}_e + \bar{V}_{ion}.$$

### 3.3 Solute transport

The general advection-dispersion equation for a two-dimensional flow system is given by

(Domenico and Schwartz, 1990):

$$D_{dx_i} \frac{\partial^2 C}{\partial x^2} + D_{dy_i} \frac{\partial^2 C}{\partial y^2} - V_{rx_i} \frac{\partial C}{\partial x} - V_{ry_i} \frac{\partial C}{\partial y} = R_{di} \frac{\partial C}{\partial t} \quad (3.14)$$

where:

$D_{dx_i}$  &  $D_{dy_i}$  = hydrodynamic dispersion in x and y directions respectively for the ionic species  $i$  ( $\text{m}^2\cdot\text{s}^{-1}$ ),

$V_{rx_i}$  &  $V_{ry_i}$  = total velocity of the ionic species  $i$  in the x and y directions respectively ( $\text{m}\cdot\text{s}^{-1}$ ),

$R_{di}$  = retardation coefficient of the ionic species  $i$ .

Since the flow processes are coupled, a single retardation coefficient is used to account for the combined effect of the different driving gradients. A Similar approach has been used by other researchers (Acar *et al.*, 1990; Alshwabkeh *et al.*, 1992; Shapiro and Probstein, 1993; Yeung, 1993).

Constant and flux boundary conditions for the solute transport can be defined as:

$$C_i(\beta_1, t) = C_{0i} \quad t > 0 \quad \text{at} \quad \beta_1 \quad (3.15a)$$

and ,

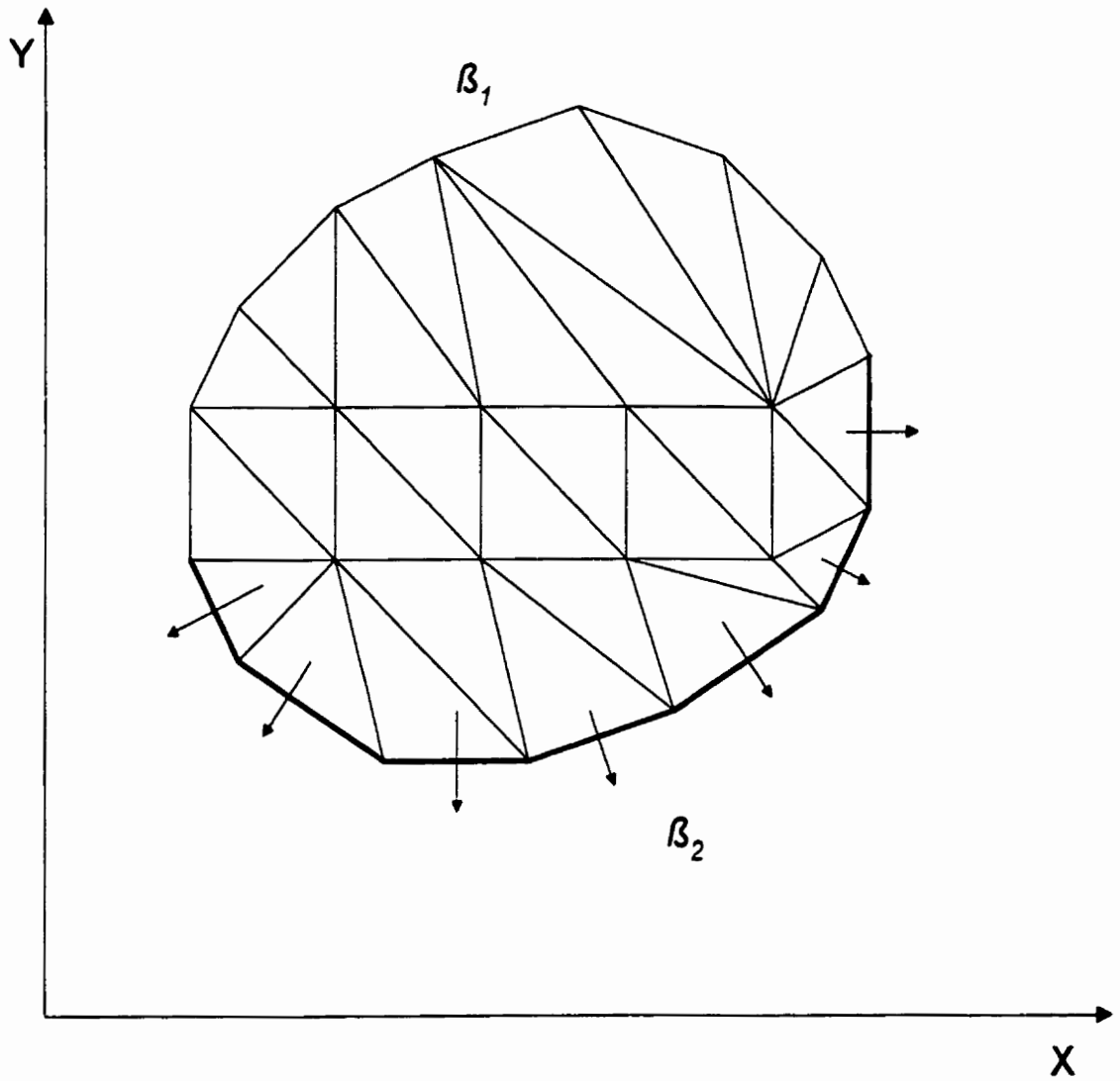


**Figure 3.1** Schematic diagram representing the two dimensional domain with boundary conditions (Huyakorn and Pinder, 1983).

$$-D_{dx_i} \frac{\partial C_i}{\partial x} - D_{dy_i} \frac{\partial C_i}{\partial y} + V_{vx_i} C_i + V_{vy_i} C_i = q_{ci} \quad \text{at} \quad \beta_2 \quad (3.15b)$$

where  $q_{ci}$  is the mass flux of species  $i$  at the boundary  $\beta_2$ .

The velocity of the solute in the Eq.3.14 is the total velocity of the contaminant due to the hydraulic and electrical gradients as given by Eq.3.12. In the present study potassium chloride salt is used as a tracer to simulate the contaminant transport. Potassium chloride is chosen as a tracer because it does not readily react with other chemicals present in the pore fluid and gives a conservative estimate of contaminant migration. Hence, there are two solute transport equations, one for the migration of  $K^+$ , and the other for the migration of  $Cl^-$ . The application of the electrical potential gradient along the soil sample leads to electrolysis reaction at the electrodes, resulting in the release of  $H^+$  and  $OH^-$  ions at the anode and the cathode, respectively (Eqs.2.1 and 2.2). Migration of the  $H^+$  and  $OH^-$  ions should also be considered because, this will affect the electrical potential gradient distribution which will in turn affect the rate of the contaminant ( $K^+$  and  $Cl^-$ ) migration. Hence, migration of four ions  $H^+$ ,  $OH^-$ , and  $K^+$ ,  $Cl^-$  is considered for modelling. The four solute transport equations are:

$$D_{H^+x} \frac{\partial^2 C_{H^+}}{\partial x^2} + D_{H^+y} \frac{\partial^2 C_{H^+}}{\partial y^2} - V_{H^+x} \frac{\partial C_{H^+}}{\partial x} - V_{H^+y} \frac{\partial C_{H^+}}{\partial y} = R_{H^+} \frac{\partial C_{H^+}}{\partial t} \quad (3.16a)$$

$$D_{OH^-x} \frac{\partial^2 C_{OH^-}}{\partial x^2} + D_{OH^-y} \frac{\partial^2 C_{OH^-}}{\partial y^2} - V_{OH^-x} \frac{\partial C_{OH^-}}{\partial x} - V_{OH^-y} \frac{\partial C_{OH^-}}{\partial y} = R_{OH^-} \frac{\partial C_{OH^-}}{\partial t} \quad (3.16b)$$

$$D_{K^+x} \frac{\partial^2 C_{K^+}}{\partial x^2} + D_{K^+y} \frac{\partial^2 C_{K^+}}{\partial y^2} - V_{K^+x} \frac{\partial C_{K^+}}{\partial x} - V_{K^+y} \frac{\partial C_{K^+}}{\partial y} = R_{K^+} \frac{\partial C_{K^+}}{\partial t} \quad (3.16c)$$

$$D_{Cl^-x} \frac{\partial^2 C_{Cl^-}}{\partial x^2} + D_{Cl^-y} \frac{\partial^2 C_{Cl^-}}{\partial y^2} - V_{Cl^-x} \frac{\partial C_{Cl^-}}{\partial x} - V_{Cl^-y} \frac{\partial C_{Cl^-}}{\partial y} = R_{Cl^-} \frac{\partial C_{Cl^-}}{\partial t} \quad (3.16d)$$

where  $R_{H^+}$ ,  $R_{OH^-}$ ,  $R_{K^+}$  and  $R_{Cl^-}$  are the retardation coefficients of the ions. The retardation coefficients are represented by a single value as discussed before.

### 3.4 Transient saturated flow

The velocity of water flowing due to a hydraulic gradient and an electrical potential gradient (electro-osmotic flow) is given by Eqs.3.1 and 3.2. Previous studies proved that, the water flux due to a hydraulic gradient and an electrical gradient are numerically additive (Esrig, 1968; Esrig and Majtenyi, 1965; Lewis, 1973). Applying the law of conservation of mass for the fluid flux:

$$\frac{\partial q_{hx}}{\partial x} + \frac{\partial q_{ex}}{\partial x} + \frac{\partial q_{hy}}{\partial y} + \frac{\partial q_{ey}}{\partial y} = S_s \frac{\partial h}{\partial t} \quad (3.17)$$

Expanding Eq.3.17

$$K_{hx} \frac{\partial^2 h}{\partial x^2} + K_{ex} \frac{\partial^2 E}{\partial x^2} + K_{hy} \frac{\partial^2 h}{\partial y^2} + K_{ey} \frac{\partial^2 E}{\partial y^2} = S_s \frac{\partial h}{\partial t} \quad (3.18)$$

where:

$K_{hx}$  and  $K_{hy}$  = hydraulic conductivities of the porous medium in x and y directions respectively ( $m \cdot s^{-1}$ ),

$K_{ex}$  and  $K_{ey}$  = electro-osmotic conductivities of the porous medium in x and y directions respectively ( $m^2 \cdot V^{-1} \cdot s^{-1}$ ),

$S_s$  = specific storage of the porous medium ( $m^{-1}$ ).

Equation 3.17 is for a two-dimensional fluid flow system due to hydraulic and electrical potential gradients (Esrig, 1968; Esrig and Majtenyi, 1965; Lewis, 1973).

### 3.5 Charge flux

The governing equation for the two-dimensional charge flux is given by (Alshwabkeh and Acar, 1996):

$$F \sum_{i=1}^N Z_i D_{dx_i} \frac{\partial^2 C_i}{\partial x^2} + F \sum_{i=1}^N Z_i D_{dy_i} \frac{\partial^2 C_i}{\partial y^2} + \sigma_x \frac{\partial^2 E}{\partial x^2} + \sigma_y \frac{\partial^2 E}{\partial y^2} = C_p \frac{\partial E}{\partial t} \quad (3.19)$$

where:

F = Faraday's constant (96487 coulombs),

$Z_i$  = charge of the ionic species  $i$  (unitless),

$D_{dx_i}$  &  $D_{dy_i}$  = hydrodynamic dispersion in  $x$  and  $y$  directions respectively of the ionic species  $i$  ( $m^2 \cdot s^{-1}$ ),

N = Number of ionic species present in the system,

$\sigma_x$  &  $\sigma_y$  = electrical conductivity of the soil ( $S \cdot m^{-1}$ ) =  $F \sum_{i=1}^N Z_i u_{ion_i}^* C_i$

$C_p$  = electrical capacitance per unit volume ( $farad \cdot m^{-3}$ ).

The first two terms in this equation are present to preserve the electrical neutrality of the system. Depending on the concentration gradients of the charged species, the electrical potential gradient undergoes a change in its distribution to preserve electrical neutrality (Alshwabkeh and Acar, 1996). The last two terms in Eq.3.19 is the Ohm's law.

Based on the theory of electrokinetic phenomena reported in the literature, two-dimensional modelling equations for contaminant transport under the hydraulic, electrical and chemical gradients have been developed. The finite element method was used to solve these partial differential equations. Chapter 4 explains in detail the finite element formulation of the equation describing contaminant transport through electrokinetic barriers.

## **4.0 NUMERICAL MODELLING**

### **4.1 Introduction**

Numerical methods are indispensable tools to solve complex equations describing coupled processes in heterogeneous and anisotropic formations under various initial and boundary conditions. Finite element and finite difference methods are widely used to solve the partial difference equations for solute transport in the subsurface for various initial and boundary conditions. In the finite element method (FEM) complex differential equations are solved by means of piecewise approximation. The FEM is more flexible and lends itself to modular computer programming, where in, many types of problems can be solved using a small set of identical computer procedures. Hence, FEM method is widely adopted to solve the partial differential equations for simulating solute transport .

Using FEM, a two dimensional numerical model was developed, to simulate the migration of charged or uncharged chemical species under hydraulic, electrical and chemical gradients and the changes brought about by different electrokinetic phenomena.

The numerical model development involves:

1. Finite element solution using Galerkin's formulation for the partial difference equations developed in chapter 3 .
2. Formation of element matrices from the integrals obtained using Galerkin's formulation.
3. Finite difference formulation for the time derivative.
4. Solving the system of equations using LU decomposition

5. Development of a computer code based on the developed model
6. Verification of the model results with the analytical solutions.

#### 4.2 Weighted residual method

The element matrix can be formulated either using the variational approach or weighted residual approach. In recent years the Galerkin's weighted residual method has gained popularity owing to its generality in application (Huyakorn and Pinder, 1983; Istok, 1989; Javandel *et al.*, 1995; Segerlind, 1984; Wang and Anderson, 1982). In the weighted residual method an approximate solution is substituted into the governing differential equation. Since, the approximate solution does not satisfy the equation, a residual or error term results (Segerlind, 1984). A one-dimensional advection-dispersion equation is solved in this section to explain the weighted residual method:

$$D_x \frac{d^2C}{dx^2} - V_x \frac{dC}{dx} = 0 \quad (4.1)$$

In the Galerkin's formulation, the domain is subdivided into finite elements and the approximate trial function is represented over an element subregion. The trial function is of the form:

$$C'(x) = \sum_{i=1}^n N_i C_i \quad (4.2)$$

where:

- $N_i$  = basis functions or shape functions,
- $C_i$  = unknown nodal values of concentration,
- $n$  = number of nodes on the element.

Since this is only an approximate solution, substitution of this approximate function results in a residual  $r(x)$ :

$$D_x \frac{d^2 C'(x)}{dx^2} - V_x \frac{dC'(x)}{dx} = r(x) \neq 0 \quad (4.3)$$

The weighted residual method requires that, the unknown values of  $C_i$  are determined in such a way that, the error is minimized. This is done by setting the weighted integral of the error term over the entire domain to zero:

$$\int W_i r(x) dx = 0 \quad (4.4)$$

where,  $W_i$  is the weighting function. There are three commonly used weighted residual method: 1) The point collocation method, 2) The sub domain collocation method, and 3) The Galerkin's method.

The Galerkin's method uses the same shape function or the basis functions as the weighting function (Huyakorn and Pinder, 1983), i.e.,  $W_i = N_i$ . Therefore, Eq. 4.4 becomes:

$$\int N_i r(x) dx = 0 \quad (4.5)$$

Finite element equations formed as explained by the given procedure are assembled into a global matrix equation and the boundary conditions are incorporated. Finally decomposition methods like Gauss elimination or LU decomposition methods are used to solve the system of equations during every time step to get the unknown nodal values.

#### **4.2.1 Formulation of the residual**

The partial differential equations (Eqs.3.16, 3.18 and 3.19) developed in chapter 3 were solved by finite element method. The solution procedure for solving Eq.3.16 is given in this

chapter. Adopting a similar procedure, the other two equations (Eqs.3.18 and 3.19) were solved by the finite element method.

The governing equation for solute transport under hydraulic, electrical and chemical gradients is given as:

$$D_{dx_i} \frac{\partial^2 C_i}{\partial X^2} + D_{dy_i} \frac{\partial^2 C_i}{\partial Y^2} - V_{vx_i} \frac{\partial C_i}{\partial X} - V_{vy_i} \frac{\partial C_i}{\partial Y} = R_{di} \frac{\partial C_i}{\partial t} \quad (4.6)$$

where:

$D_{dx_i}$  &  $D_{dy_i}$  = hydrodynamic dispersion in x and y directions respectively,

$V_{vx_i}$  &  $V_{vy_i}$  = total velocity of the contaminant due to hydraulic flow, electro-osmotic flow and ionic migration in the x and y directions respectively,

$R_{di}$  = retardation coefficient.

Galerkin's weighted residual method is used to solve the above partial differential equation. The approximate solution is given by Eq.4.2. Linear triangular elements are used for domain discretization. Then Eq.4.2 becomes:

$$C^{(e)} = N_i C_i^{(e)} + N_j C_j^{(e)} + N_k C_k^{(e)} \quad (4.7)$$

where:

$N_i, N_j, N_k$  = interpolation functions or element shape functions,

$C_i^{(e)}, C_j^{(e)}, C_k^{(e)}$  = nodal concentration of ions for a triangular element.

Figure 4.1 shows the linear triangular element. Shape functions of linear triangular element are derived by Segerlind (1984).

Applying Galerkin's method to the two-dimensional solute transport equation Eq.4.6 gives:

$$\{r^{(e)}\} = - \int_A [N]^T \left( D_{dx_i} \frac{\partial^2 C_i}{\partial x^2} + D_{dy_i} \frac{\partial^2 C_i}{\partial y^2} - V_{\alpha_i} \frac{\partial C_i}{\partial x} - V_{\gamma_i} \frac{\partial C_i}{\partial y} - R_{d_i} \frac{\partial C_i}{\partial t} \right) dA \quad (4.8)$$

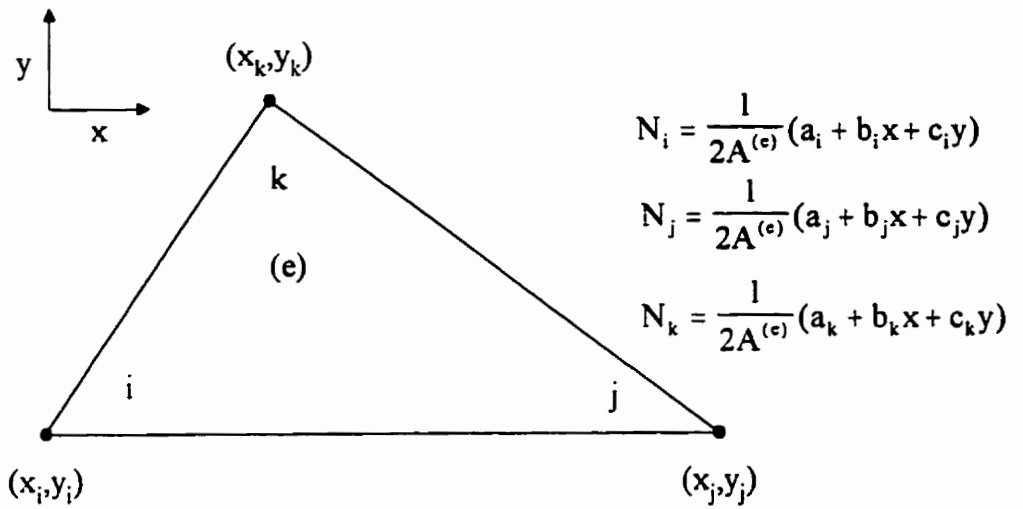
#### 4.2.2 Formulation of element matrices

Solution to the equation of this form is given by Segerlind (1984):

$$\begin{aligned} \{r^{(e)}\} = & \int_A \left( D_{dx_i} \frac{\partial [N]^T}{\partial x} \frac{\partial C_i}{\partial x} + D_{dy_i} \frac{\partial [N]^T}{\partial y} \frac{\partial C_i}{\partial y} \right) dA \\ & + \int_A [N]^T \left( V_{\alpha_i} \frac{\partial C_i}{\partial x} + V_{\gamma_i} \frac{\partial C_i}{\partial y} \right) dA \\ & + \int_A [N]^T R_{d_i} \frac{\partial C_i}{\partial t} dA \\ & - \int_{\beta} [N]^T \left( D_{dx_i} \frac{\partial C_i}{\partial x} \cos \phi + D_{dy_i} \frac{\partial C_i}{\partial y} \sin \phi \right) d\beta \end{aligned} \quad (4.9)$$

Substituting Eqs.4.7 in 4.9 gives:

$$\begin{aligned} \{r^{(e)}\} = & \int_A \left( D_{dx_i} \frac{\partial [N]^T}{\partial x} \frac{\partial [N]}{\partial x} + D_{dy_i} \frac{\partial [N]^T}{\partial y} \frac{\partial [N]}{\partial y} \right) dA \{C_i\}^e \\ & + \int_A [N]^T \left( V_{\alpha_i} \frac{\partial [N]}{\partial x} + V_{\gamma_i} \frac{\partial [N]}{\partial y} \right) dA \{C_i\}^e \\ & + \int_A R_{d_i} [N]^T \frac{\partial [N]}{\partial t} dA \{C_i\}^e \\ & - \int_{\beta} [N]^T \left( D_{dx_i} \frac{\partial C_i}{\partial x} \cos \phi + D_{dy_i} \frac{\partial C_i}{\partial y} \sin \phi \right) d\beta \end{aligned} \quad (4.10)$$



where:

$$\begin{aligned}
 a_i &= x_j^{(e)} y_k^{(e)} - x_k^{(e)} y_j^{(e)} & a_j &= x_k^{(e)} y_i^{(e)} - x_i^{(e)} y_k^{(e)} & a_k &= x_i^{(e)} y_j^{(e)} - x_j^{(e)} y_i^{(e)} \\
 b_i &= y_j^{(e)} - y_k^{(e)} & b_j &= y_k^{(e)} - y_i^{(e)} & b_k &= y_i^{(e)} - y_j^{(e)} \\
 c_i &= x_k^{(e)} - x_j^{(e)} & c_j &= x_i^{(e)} - x_k^{(e)} & c_k &= x_j^{(e)} - x_i^{(e)}
 \end{aligned}$$

$A^{(e)}$  = Area of element

$$A^{(e)} = \frac{1}{2} \begin{vmatrix} 1 & x_i^{(e)} & y_i^{(e)} \\ 1 & x_j^{(e)} & y_j^{(e)} \\ 1 & x_k^{(e)} & y_k^{(e)} \end{vmatrix}$$

**Figure 4.1** Interpolation functions for the linear triangular element

The first two integrals in Eq.4.10 will form the element stiffness matrix for the two-dimensional solute transport equation. The third integral involves the time derivative and forms the element capacitance matrix. The final integral in Eq.4.10 accounts for the derivative boundary condition. In the case of a constant boundary this becomes zero. This integral constitutes the element force matrix.

Linear triangular elements are widely used for subsurface solute transport modelling. Element matrices using linear triangular elements are derived from Eq.4.10. The element stiffness matrix for the two-dimensional solute transport is given by:

$$[K^{(e)}] = \int_A \left( D_{dx} \frac{\partial [N]^T}{\partial x} \frac{\partial [N]}{\partial x} + D_{dy} \frac{\partial [N]^T}{\partial y} \frac{\partial [N]}{\partial y} \right) dA + \int_A [N]^T \left( V_{vx} \frac{\partial [N]}{\partial x} + V_{vy} \frac{\partial [N]}{\partial y} \right) dA \quad (4.11)$$

Solving Eq.4.11 using triangular elements gives:

$$[K^{(e)}] = \frac{D_{dx}^*}{4A^{(e)}} \begin{bmatrix} b_i^2 & b_i b_j & b_i b_k \\ b_j b_i & b_j^2 & b_j b_k \\ b_k b_i & b_k b_j & b_k^2 \end{bmatrix} + \frac{D_{dy}^*}{4A^{(e)}} \begin{bmatrix} c_i^2 & c_i c_j & c_i c_k \\ c_j c_i & c_j^2 & c_j c_k \\ c_k c_i & c_k c_j & c_k^2 \end{bmatrix} + \frac{V_{vx}}{6} \begin{bmatrix} b_i & b_j & b_k \\ b_i & b_j & b_k \\ b_i & b_j & b_k \end{bmatrix} + \frac{V_{vy}}{6} \begin{bmatrix} c_i & c_j & c_k \\ c_i & c_j & c_k \\ c_i & c_j & c_k \end{bmatrix} \quad (4.12)$$

The velocities in the x and y directions are given by:

$$V_{vx} = \frac{1}{2A^{(e)}} K_{hx} [b_i h_i + b_j h_j + b_k h_k] + \frac{1}{2A^{(e)}} K_{ex} [b_i E_i + b_j E_j + b_k E_k] + \frac{1}{2A^{(e)}} u_{ion}^* [b_i E_i + b_j E_j + b_k E_k] \quad (4.13)$$

$$\begin{aligned}
V_{ty} = & \frac{1}{2A^{(e)}} K_{hy} [c_i h_i + c_j h_j + c_k h_k] \\
& + \frac{1}{2A^{(e)}} K_{ey} [c_i E_i + c_j E_j + c_k E_k] \\
& + \frac{1}{2A^{(e)}} u_{ion}^* [c_i E_i + c_j E_j + c_k E_k]
\end{aligned} \tag{4.14}$$

The lumped formulation is being used to derive the element capacitance matrix. In the lumped formulation, the rate of change of the parameter within a given element is assumed to remain constant. Using the lumped formulation, the element capacitance matrix is given by:

$$[C^{(e)}] = \int_A R_d [N]^T [N] dA \tag{4.15}$$

Solving Eq.4.15 using lumped formulation for triangular elements gives:

$$[C^{(e)}] = \frac{A^{(e)}}{3} R_{di} \begin{bmatrix} 1 & 0 & 0 \\ 0 & 1 & 0 \\ 0 & 0 & 1 \end{bmatrix} \tag{4.16}$$

### 4.2.3 Finite difference solution in time

Several techniques such as Euler's forward difference, Euler's Backward difference, Crank-Nicholson central difference, Galerkin's residual approach and least squares approach could be used to discretize in the time domain. The general form of the finite element equation as derived by Segerlind (1984):

$$\begin{aligned}
([C] + \theta \Delta t [K]) \{C\}_{t+\Delta t}^{(e)} = & ([C] - (1-\theta) \Delta t [K]) \{C\}_t^{(e)} \\
& + \Delta t ((1-\theta) \{F\}_t + \theta \{F\}_{t+1})
\end{aligned} \tag{4.17}$$

where:

- [C] = global capacitance matrix,
- [K] = global stiffness matrix,
- {C}<sup>(e)</sup> = nodal concentration of element (e),
- Δt = time step,
- {F} = global force matrix.

Euler's Backward Difference technique was selected over others because of its inherent stability. For Euler's backward difference method,  $\theta = 1$ . Substituting for  $\theta$  in Eq.4.17 and rearranging gives:

$$\left( [K] + \frac{[C]}{\Delta t} \right) \{C\}_{t+1}^{(e)} = \frac{[C]}{\Delta t} \{C\}_t^{(e)} + \{F\}_{t+1} \quad (4.18)$$

The partial differential equations for two-dimensional fluid flow and charge flux were similarly solved by adopting the procedure explained above. Equations similar to Eq.4.18 were developed from partial differential equations involving transient saturated flow and charge flux (Eqs.3.18 and 3.19).

#### 4.2.4 LU decomposition

Application of Galerkin's method for solute transport results in systems of equation that can be written in matrix form:

$$[A]\{C\} = [F] \quad (4.19)$$

LU decomposition method was used to solve equations similar to Eq.4.19 to obtain the values of hydraulic head, solute concentrations, and electrical potential at each node in the mesh. The matrix [A] is first decomposed into lower and upper triangular matrix:

$$[L][U] = [A] \quad (4.20)$$

Where, [L] is the lower triangular matrix and [U] is the upper triangular matrix. The components of the lower and the upper triangular matrices are found by:

$$L_{ij} = A_{ij} - \sum_{k=1}^{j-1} L_{ik} U_{kj} \quad j \leq i \quad i = 1, 2, 3, \dots, n \quad (4.21a)$$

$$U_{ij} = \frac{A_{ij} - \sum_{k=1}^{i-1} L_{ik} U_{kj}}{L_{ii}} \quad i \leq j \quad j = 2, 3, \dots, n \quad (4.21b)$$

for  $j = 1$  ;

$$L_{i1} = A_{i1} \quad (4.21c)$$

for  $i = 1$  ;

$$U_{1j} = \frac{A_{1j}}{L_{11}} \quad (4.21d)$$

The components of the right-hand side of Eq.4.19 are modified accordingly and can be found by:

$$F'_1 = \frac{F_1}{L_{11}} \quad (4.22a)$$

$$F'_i = \frac{F_i - \sum_{k=1}^{i-1} L_{ik} F'_k}{L_{ii}} \quad i = 2, 3, \dots, n \quad (4.22b)$$

By back substitution the values of the vector {C} in Eq.4.19 can be found by:

$$C_n = F'_n \quad (4.23a)$$

$$C_j = F'_j - \sum_{k=j+1}^n U_{jk} C_k \quad j = n-1, n-2, \dots, 1 \quad (4.23b)$$

The partial differential equations for two-dimensional fluid flow and charge flux were similarly solved by adopting the procedure explained above. Equations similar to Eq.4.18

were developed from partial differential equations involving transient saturated flow and charge flux (Eqs.3.18 and 3.19). Then, LU decomposition is used to solve the system of equations.

### **4.3 Computer coding of the mathematical model**

A FORTRAN 77 computer code called FENCE was developed in the UNIX environment for the mathematical model described here. The numerical model FENCE is a combination of three sub-models:

1. Solute transport
2. Fluid flow
3. Charge flux

A flow chart for FENCE is given in Fig.4.2. During the time cycle the output from one model is used as an input for the other sub-model. Therefore, based on the input parameters, this combined code can model the movement of contaminants with or without the electrokinetic barrier. The code can handle heterogenous and anisotropic conditions encountered in real field situations. Boundary conditions like constant or flux conditions can be specified. The program can also handle any source or sink terms encountered in the field.

Based on the requirement of individual problems the finite element mesh can either be generated by the computer program or entered manually. For generating the mesh, the number of rows of nodes in the x direction and y direction and the distance between rows in the x and y direction are needed. Based on this information specified in the input file FENCE.DAT the program can generate the finite element mesh, nodal and data

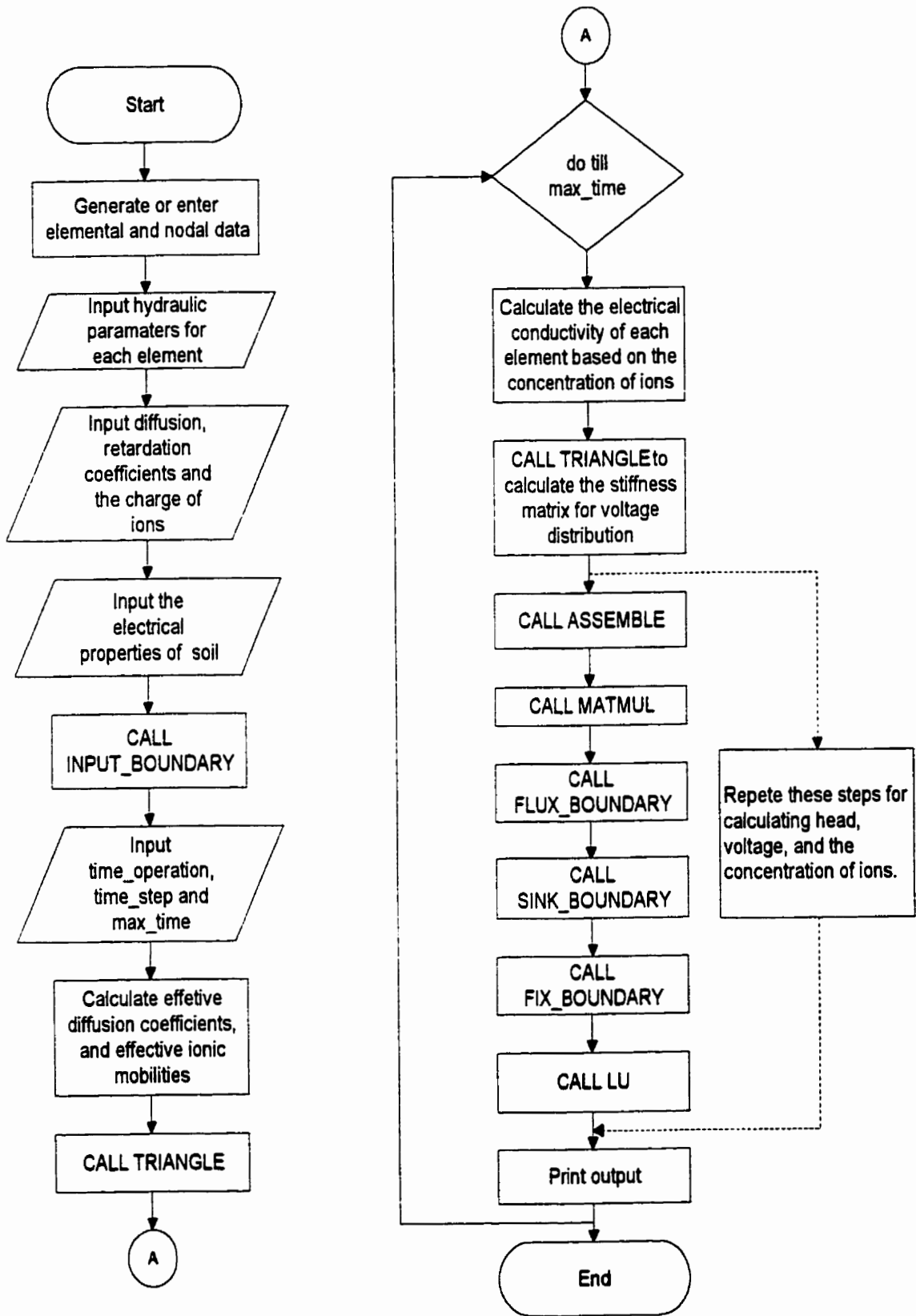


**Figure 4.2** Flow chart for the computer code FENCE.

automatically. Based on the elemental data the program calculates the band width. Then, the material properties of the aquifer, solute transport properties and electrical properties are entered. Based on the information effective diffusion coefficients and ionic mobilities are calculated. Then, subroutine INPUT\_BOUNDARY is called to read the initial and boundary conditions for hydraulic head, voltage, and solute concentration at individual nodes. Fixed boundary conditions, flux boundary conditions, source or sink terms can be specified at individual nodes or elements. Operational parameters like, duration of electrical potential application during a 24h period is specified. Subroutine TRIANGLE is then called to calculate the element stiffness and capacitance matrices. Now the problem enters a time cycle to begin the simulation. Based on the initial concentration of the chemicals present, the program calculates the electrical conductivity of individual elements. Based on this electrical conductivity, the element stiffness and capacitance matrices are calculated using subroutine TRIANGLE. Then, the subroutine ASSEMBLE is called to add the global stiffness matrix and global capacitance matrix. Subroutine MATMUL is called to multiply the global capacitance matrix and the vector quantities (e.g. Concentration) obtained during the previous time step and adds the resultant to the global force matrix. Then subroutine FLUX\_BOUNDARY, SINK\_BOUNDARY and FIX\_BOUNDARY are called to account for the specified boundary conditions. Finally the systems of equations are solved using subroutine LU by LU decomposition. This procedure is repeated to find the hydraulic head, voltage, pH distribution and the distribution of contaminant ions. The voltage distribution is first calculated based on the electrical conductivity of the individual elements. Then, the hydraulic head distribution is calculated based on the voltage distribution. Finally the

concentrations of individual ions are calculated based on the head and voltage distribution. The results of the previous time steps are used as the input for the next time step and the procedure explained above is repeated. The results are stored in a specified format in the output file FENCE.OUT.

#### **4.4 Verification of computer code**

##### **4.4.1 Verification with Ogata-Banks analytical solution**

The computer code FENCE must be verified with existing analytical solutions to make sure that, the model is correct and the computer code is error free. Model verifications by comparison with analytical solutions were made for two different situations.

Without the coupling of the electrokinetic phenomena the model will reduce to a simple advection-dispersion equation. Ogata-Banks (Fetter, 1992) developed an analytical solution for the advection-dispersion equation. The results of the analytical solution were compared with the model results under specified boundary conditions to verify the developed formalism. The one-dimensional advection-dispersion equation is given by:

$$D_x \frac{d^2C}{dx^2} - V_x \frac{dC}{dx} = \frac{\partial C}{\partial t} \quad (4.24)$$

where:

$V_x$  = velocity of the contaminant ( $m \cdot s^{-1}$ ),

$D_x$  = dispersion coefficient of the contaminant ( $m^2 \cdot s^{-1}$ ).

Ogata-Banks solution for advection-dispersion equation of the form 4.24 is given by:

$$C(x, t) = \left( \frac{C_0}{2} \right) \left\{ \operatorname{erfc} \left[ \frac{(x - vt)}{2(D_{dx} t)^{1/2}} \right] + e^{\left( \frac{Vx}{D} \right)} \operatorname{erfc} \left[ \frac{(x + vt)}{2(Dt)^{1/2}} \right] \right\} \quad (4.25)$$

where:

$C_0$  = concentration at  $x = 0$

$V$  = velocity of the water ( $m \cdot s^{-1}$ ),

$D_{dx}$  = dispersion coefficient of the contaminant ( $m^2 \cdot s^{-1}$ ),

$t$  = time (s),

$\operatorname{erfc}()$  = complementary error function,

$x$  = distance (m).

The boundary conditions for this analytical solution are:

$$C(0, t) = C_0 \quad t \geq 0 \quad (4.26b)$$

$$C(x, 0) = 0 \quad x \geq 0 \quad (4.26a)$$

$$C(\infty, t) = 0 \quad t \geq 0 \quad (4.26c)$$

For a hypothetical case, the model results are compared with the analytical solution given by Eq. 4.25. A graphical representation of the comparison is given in Fig.4.3. The model results agreed very well with the analytical solution proving that, the model predicts the advection and dispersion processes of the solute transport accurately.

#### 4.4.2 Verification with Esrig's analytical solution

During the second stage of the model verification, the model results of the pore water pressure variation under an applied electrical potential gradient were compared with the analytical solution derived by Esrig (1968). The model must reduce to a one-dimensional fluid flow equation without the solute transport part in the model. Esrig (1968) derived

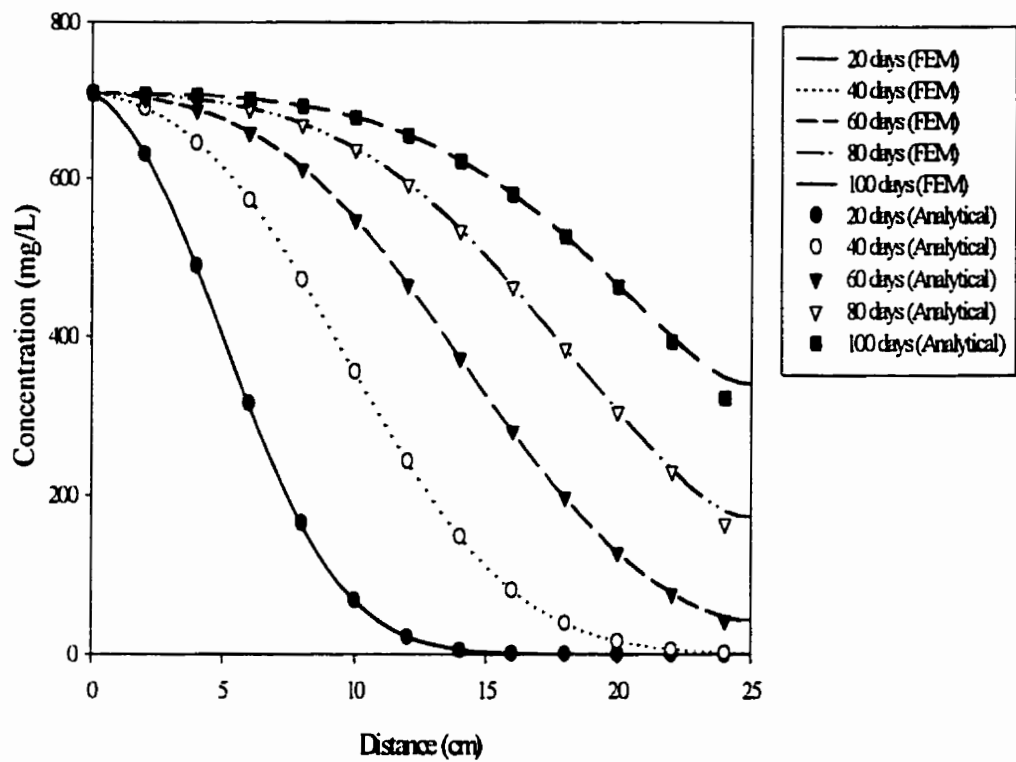


**Figure 4.3** Verification of the FEM solution with Ogata-Banks analytical solution for Advection-Dispersion equation.

an analytical solution to find the changes in pore water pressure distribution under a uniform electrical field in which the voltage remains constant with time. The analytical solution gives the pore water pressure distribution along the soil column under uniform electrical field at different time intervals. The one-dimensional fluid flow equation is given by:

$$\frac{\partial^2 P}{\partial x^2} + \frac{K_e}{K_h} \rho_w \frac{\partial^2 E}{\partial x^2} = \frac{1}{C_v} \frac{\partial P}{\partial t} \quad (4.27)$$

where:

- $K_e$  = electro-osmotic conductivity ( $m^2 \cdot V^{-1} \cdot s^{-1}$ ),  
 $K_h$  = hydraulic conductivity ( $m \cdot s^{-1}$ ),  
 $C_v$  = Terzaghi coefficient of consolidation =  $K_h / (m_v \rho_w)$ ,  
 $m_v$  = coefficient of volume compressibility ( $m^2 \cdot Kg^{-1}$ ),  
 $\rho_w$  = density of water ( $Kg \cdot m^{-3}$ ),  
 $P$  = pore water pressure.

Esrig (1968) derived an analytical solution for Eq.4.27 under a set of boundary conditions. The boundary conditions are:

$$\text{Cathode: } x = 0 ; t = t ; E = 0 ; \quad (4.28a)$$

$$\text{Anode: } x = L ; t = t ; E = E_m ; P = 0 ; \quad (4.28b)$$

$$x = x ; t = 0 ; E = E(x) ; P = 0 ; \quad (4.28c)$$

The solution to Eq.4.27 for these boundary conditions is:

$$P = -\frac{K_e}{K_h} \rho_w (E(x) - E_m) + \frac{2K_e \rho_w E_m}{K_h \pi^2} \sum_{n=0}^{\infty} \left\{ \frac{(-1)^n}{\left(n + \frac{1}{2}\right)^2} \sin \left[ \frac{\left(n + \frac{1}{2}\right) \pi x}{L} \right] e^{-\left(n + \frac{1}{2}\right)^2 \pi^2 T_v} \right\} \quad (4.29)$$

where:

$$T_v = C_v t / L^2.$$

The model results were compared with the analytical solution for a hypothetical case (Fig.4.4). A uniform voltage was applied between the anode and the cathode. Because of the electro-osmotic flow, water flows from the anode towards the cathode. The pore pressure starts to build up near the cathode and its is distributed along the soil column. A good agreement between the model results and the analytical solution proved that, the computer code accurately predicts the change in pore water pressure due to an applied electrical potential gradient.

#### **4.3.3 Mass balance and charge balance calculations**

Additional checks on the model behaviour were performed by the mass balance and charge balance calculations. The mass balance and charge balance were calculated by adopting the procedure suggested by Huyakorn and Pinder (1983). The cumulative mass and charge balance errors were computed within the computer code and were used as indicators of the global accuracy of the numerical solution. Triangular elements were used for the discretization of the domain. For a finite element mesh size of 1.08 cm<sup>2</sup> and a time step of 5 min, under hydraulic, electrical and chemical gradients:

- the mass balance calculations for the fluid flow indicated that 99% of the water in the system was conserved.
- the mass balance calculations for the solute transport indicated that 96% of the solute in the system was conserved.

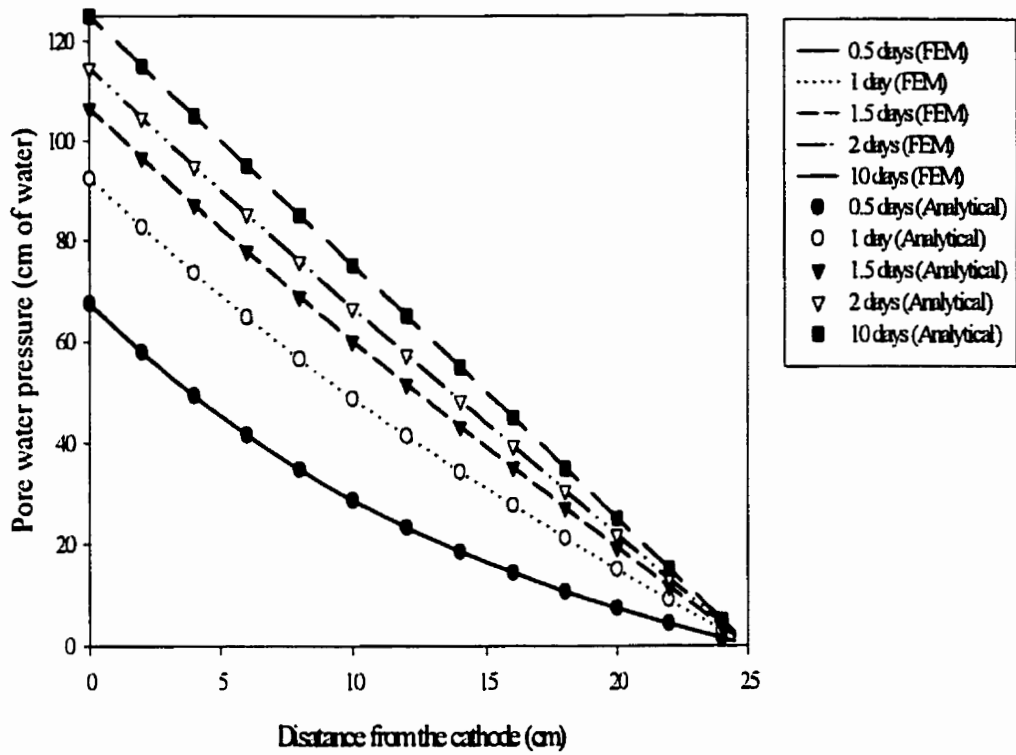


**Figure 4.4** Finite element model verification with the analytical solution derived by Esrig(1968).

- the charge balance calculation for charge flux indicated that 99% of the charge in the system was conserved.

The mass balance and charge balance checks and verification of the computer code with the existing analytical solution proved that, the developed formalism and the computer code are free of errors.

## **5.0 LABORATORY SCALE EXPERIMENTATION**

### **5.1 Objectives**

A laboratory scale experiment was conducted to study the feasibility of using electrokinetic barriers in containing the spread of contaminants in the subsurface. The objectives of the laboratory scale experimental study are:

1. To study the contaminant migration behaviour under hydraulic, electrical and chemical gradients.
2. To evaluate the effectiveness of electrokinetic barriers in containing the spread of contaminants in the soil.
3. To monitor the development of non-linear changes in voltage and hydraulic gradients along the soil column.
4. To study the influence of pH in contaminant migration and the distribution of hydraulic and electrical gradient along the soil column.
5. To validate the numerical model developed in chapter 3 and chapter 4.

### **5.2 Experimental setup**

The laboratory equipment used to study the effectiveness of electrokinetic barriers consisted of:

1. six plexiglass columns
2. a constant head flow device
3. a flow rate measuring system
4. a constant voltage source

5. a data acquisition system consisting of a 24-channel multiplexer for measuring the voltage distribution along the soil column
6. pressure transducers connected to mini tensiometers through manifolds, to measure the pore water pressure distribution along the soil column.

### **5.2.1 Plexiglass soil columns**

The plexiglass columns were used to study the effectiveness of electrokinetic barriers in preventing the migration of contaminants. The length of the column was 30 cm and had a inside diameter of 4.5cm. Three of these columns were used to study the effectiveness of electrokinetic barriers and the other three columns were used as control columns (i.e., only hydraulic treatment). These columns will be referred to as electrical columns and hydraulic columns in this thesis. The electrical columns consisted of ports for installing electrodes and tensiometers, to measure the voltage and pore water pressure distribution along the soil column during the experiment, whereas, the hydraulic columns did not have any ports for measuring the pore water pressure. Since, no electrical potential gradient was applied to the hydraulic columns, it was assumed that, the hydraulic gradient in the hydraulic columns would remain linear during the duration of the experiment. Figure.5.1. shows a typical electrical column used in this experiment.

### **5.2.2 Constant head and Flow rate measuring devices**

A constant head at the up stream end of the sample was provided by the inverted carboy over a cylindrical container. There were six outlets in the cylinder which were connected to the inlet ends of the six soil columns through chemical resistant nylon pipe fittings.

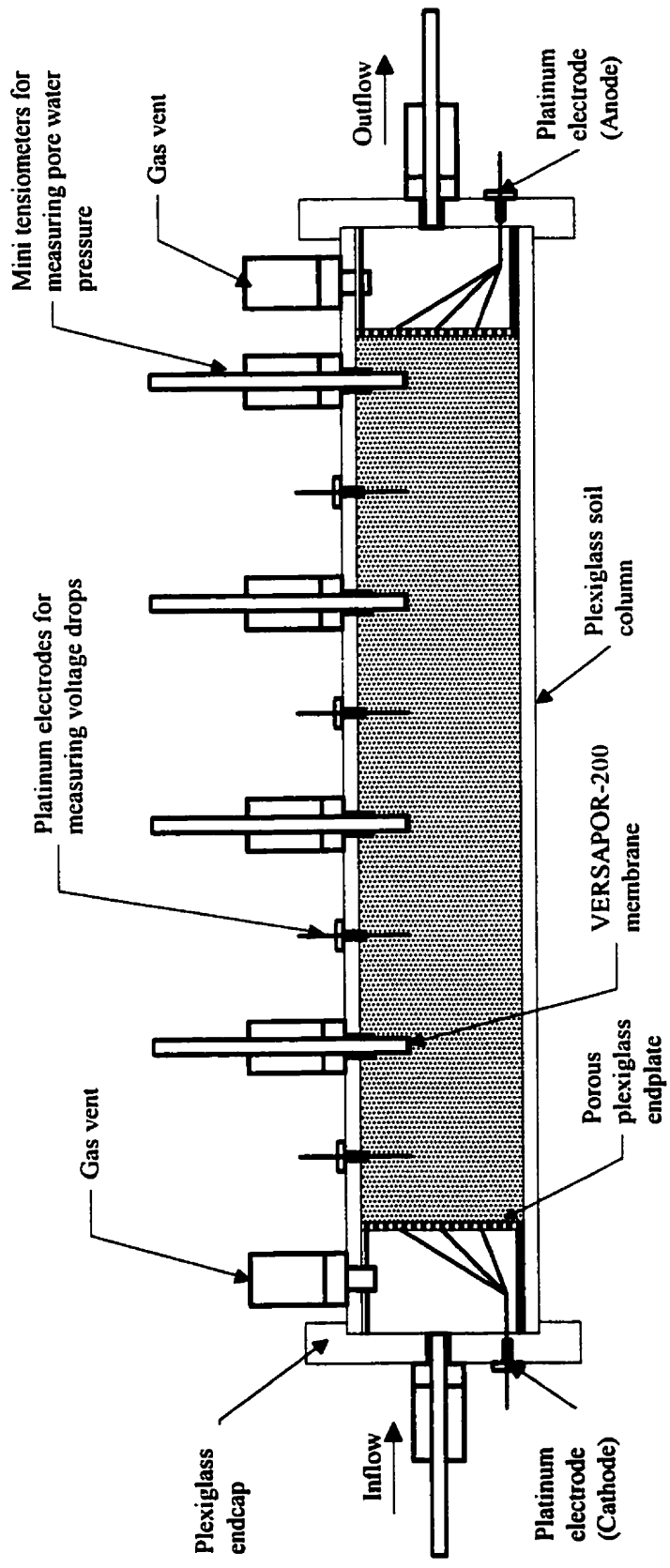


**Figure 5.1** Schematic of the electrical column packed with soil used in the experiment.

The flow rate was measured by the rate of movement of water meniscus through a standard wall glass tubing of 2.4 mm diameter and 1m in length connected to the downstream end of the soil columns. The glass tubes were mounted over a horizontal plywood board pasted with a graduated graph sheet. This arrangement assisted in measuring the flow rate of water flowing through the soil columns and also in maintaining the constant head at the downstream end of the soil column. The small diameter of the glass tubes assisted in accurately measuring hydraulic conductivity and the electro-osmotic conductivity of the soil (Sec.5.6.3 and Sec.5.6.4).

### **5.2.3 Constant voltage source and data acquisition**

The constant voltage across the soil sample was supplied and maintained by BK Precision DC Power Supply 1610. A specially designed 24-channel multiplexer was coupled with the Hewlett Packard multi-meter to measure the current and voltage drops in the samples. A computer controlled data acquisition/control system was used to continuously monitor the voltage distribution along the length of the soil columns and can apply a DC electrical field continuously or in a cycle. Platinum wires (0.51 mm diameter) were used as anode and cathode electrodes. Platinum electrodes were used to avoid the dissolution of electrode material during the process of electrolysis. The voltage potential gradients along the soil sample were also measured using platinum electrodes. The four voltage drop measuring ports were spaced at 6 cm apart starting at 4.5 cm from the upstream end of the soil column.

### **5.2.4 Mini tensiometer and pore water pressure measurement**

Mini tensiometers were made using Nylon tubing of (4.8 mm I.D. and 6.4 mm O.D.) and VERSAPOR 200 membrane. Discs equal in diameter to the outside diameter (6.4mm) of

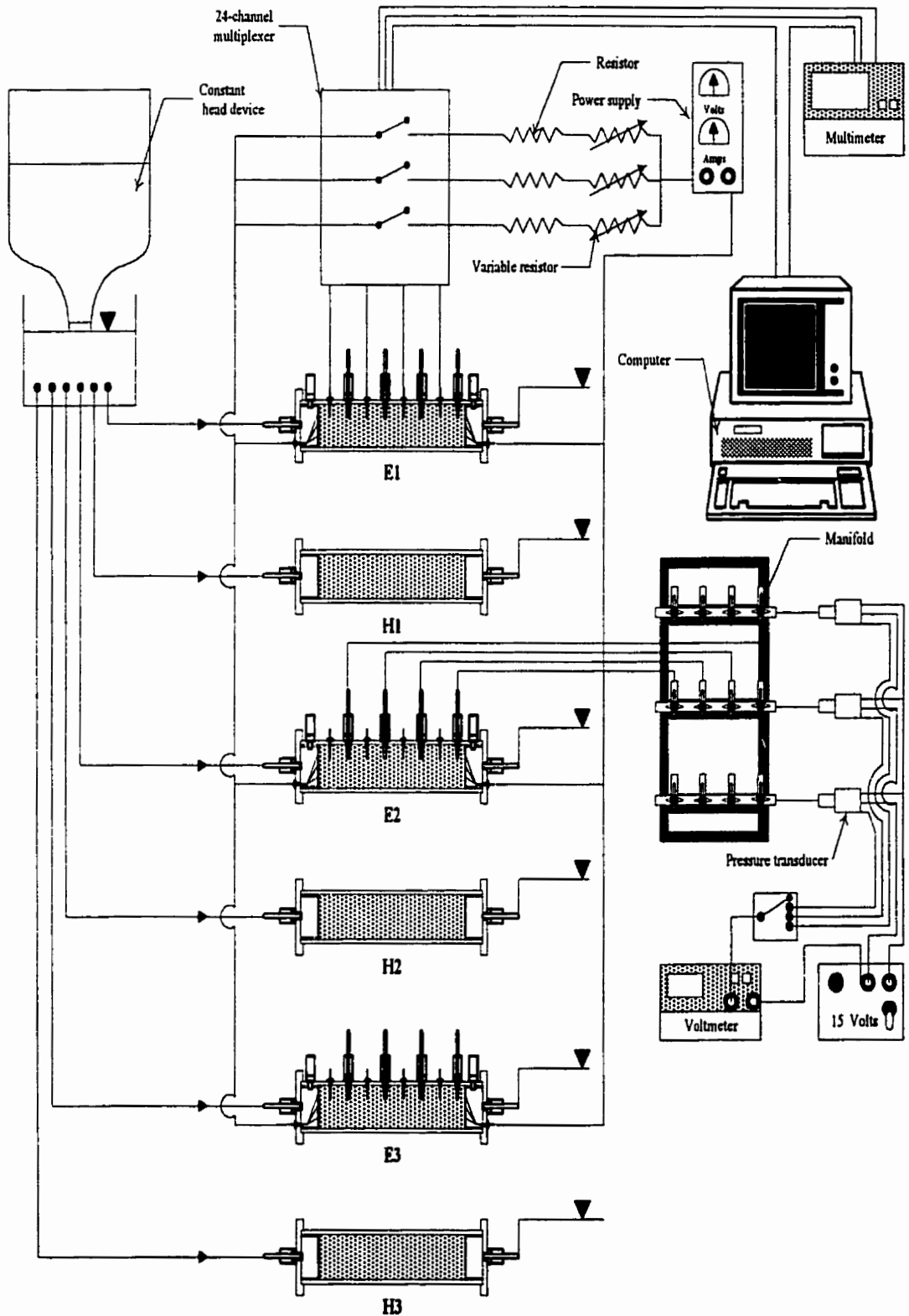


**Figure 5.2** Schematic diagram of the experimental set-up. Columns E1,E2 and E3 are electric columns and columns H1,H2 and H3 are the hydraulic columns.

the Nylon tubing were cut from the VERSAPOR 200 membrane and pasted to the nylon tubes. These tensiometers were then inserted along the length of the soil column spaced at 6 cm apart starting at 7.5 cm from the upstream end of the soil column. The pore water pressure was measured with SENSYM pressure transducers connected to the mini tensiometers through the manifolds. The use of manifolds reduced the number of transducers needed to measure the pore water pressure.

### **5.3 Experimental soil**

The soil used in the experiment was from the Red river series in Manitoba. This soil is predominantly Montmorillonite clay and moderately to strongly calcareous. The soil was collected from 100 cm below the ground surface. The collected soil was air dried and the clods were broken using a roller crusher. The dry soil was then sieved through 2 mm sieve and the soil retained on the 2 mm sieve was discarded. Soil passing through the 2 mm sieve was retained for the electrokinetic experiments. The physical and chemical properties of the soil are described in Sec.5.4.and Sec.5.5.

### **5.4 Physical properties of the soil**

#### **5.4.1 Particle size distribution**

A wet sieve analysis and a hydrometer analysis was performed on the soil particles passing through 2 mm sieve to determine the particle size distribution. A sample of known dry weight was dispersed using sodium hexametaphosphate and washed through No.200 sieve (Canadian Standard Sieve Series). The soil retained on the No.200 sieve was dried in oven and shaken through a series of standard sieves. The percentage by weight of soil

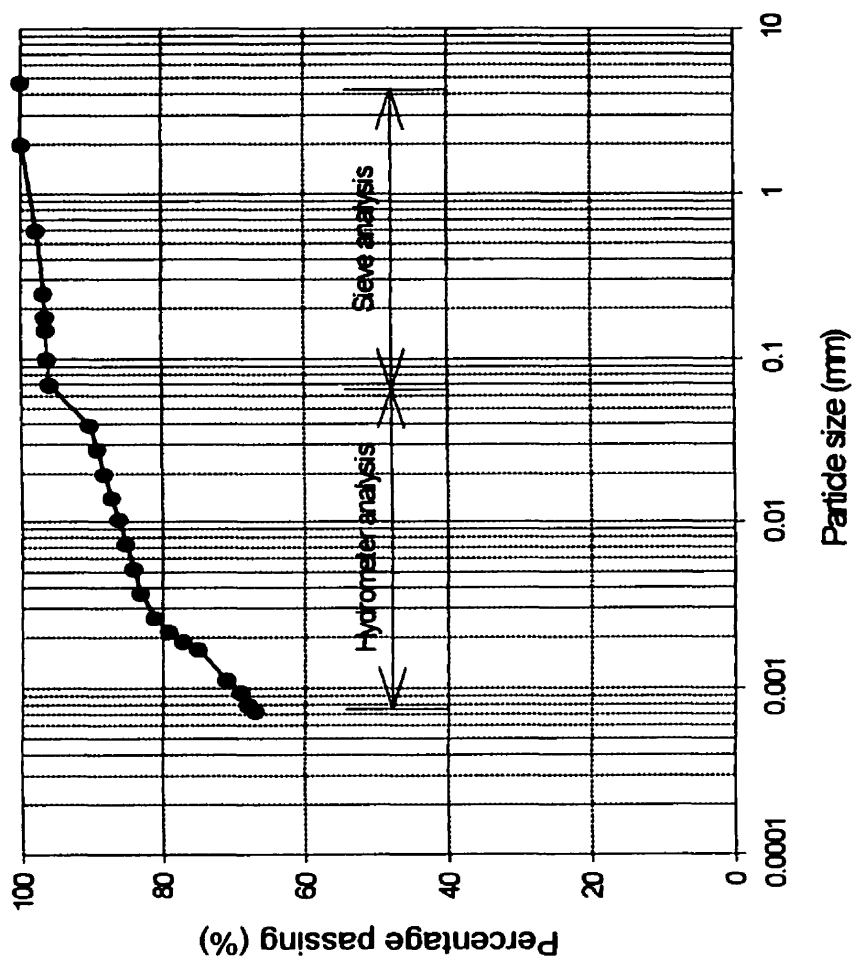


**Figure 5.3** Particle size distribution of Red River clay.

passing through each sieve was calculated by measuring the weight of the soil retained on each sieve. The particle size distribution of the soil passing through No.200 sieve was determined by the hydrometer method (Klute, 1982). Figure.5.3 shows the particle size distribution of the Red River clay. More than 80 % of the soil particle is clay ( $< 2 \mu\text{m}$ ), 15% silt and 5% Sand. From the textural triangle of the USDA classification scheme the Red River soil can be classified as a clayey soil.

#### **5.4.2 Particle density**

The particle density (Specific gravity) of the soil used in the experiments was found by using pycnometer (Klute, 1982). The pycnometer was filled with distilled water at room temperature and weighed with the stopper. Then the pycnometer was partially emptied and a known weight of oven dried soil sample was transferred to the pycnometer. The pycnometer was slightly agitated to release any entrapped air bubble. After allowing the soil to settle, the pycnometer was again filled with water till the water is near the neck. Then with the stopper on, the pycnometer was again weighed. The difference in weight gave the volume of the water displaced by the soil. Adopting this method the particle density of the soil was found to be  $2.65 \text{ g/cm}^3$ .

### **5.5 Chemical properties of the experimental soil**

#### **5.5.1 Soil pH**

Soil pH is a measure of the activity of hydrogen ion in the soil solution. The pH of the soil is indicative of the chemical properties of the soil. Measurement of soil pH in solution of  $\text{CaCl}_2$  is the most satisfactory method (Page, 1982). 15 g of soil was measured out into a

50 mL beaker. 30 mL of 0.01M CaCl<sub>2</sub> was added and the suspension was stirred and the sediment was allowed to settle. The soil was stirred at regular intervals of 30 minutes. The pH of the soil was measured by immersing the pH electrode into the partly settled suspension. The pH of the soil suspension was found to be 7.53.

### **5.5.2 Electrical conductivity**

Electrical conductivity of the soil is used for the determination of total soluble salts present in the soil. 200 g of soil was placed into a 400 mL plastic beaker. Distilled water was added to the soil while stirring until it is nearly saturated. The sample was allowed to stand for one hour to permit the soil to imbibe the water, and then more water was added to achieve a saturated paste. At saturation the soil paste glistens and reflects light, flows slightly when the container is tipped (Page, 1982). The sample was then transferred to a Buchner funnel fitted with a Whatman No. 1 filter paper. Vacuum was applied and the filtrate was collected in a test tube. The electrical conductivity of the filtrate was measured using the YSI Model 32 conductance meter. The electrical conductivity of the soil-water extract was found to be 9.5 dS/m at 25°C.

### **5.5.3 Soluble cations**

The soil pore fluid extract has an electrical conductivity of 9.5 dS/m. This indicates that, the soil has high quantity of soluble cations and anions. To know the base line concentrations of the soluble cations, the soil-water extract was analysed for soluble Ca<sup>2+</sup>, Mg<sup>2+</sup>, Na<sup>+</sup> and K<sup>+</sup>. Concentrations of the soluble cations present in the pore fluid were measured using an atomic absorption spectrometer, by adopting the procedure suggested by Page (1982). The concentration of soluble cations present in the soil is given in Table 5.1.

**Table 5.1** Concentrations of cations and anions present in the experimental soil

<b>Ions</b>	<b>Concentrations (mg/L)</b>
<b>Cations :</b>	
Ca <sup>2+</sup>	1320
Mg <sup>2+</sup>	1120
Na <sup>+</sup>	676
K <sup>+</sup>	78
<b>Anions:</b>	
HCO <sub>3</sub> <sup>-</sup>	305
NO <sub>3</sub> <sup>-</sup>	57
SO <sub>4</sub> <sup>2-</sup>	7656
Cl <sup>-</sup>	880
<b>Exchangeable cations:</b>	
Exchangeable Ca (mEq/100g)	0.65
Exchangeable Mg (mEq/100g)	0.7
Exchangeable Na (mEq/100g)	78.23
Exchangeable K (mEq/100g)	< 0.05
Total exchangeable cations (mEq/100g)	< 79

#### **5.5.4 Soluble anions**

The experimental soil was analysed for the initial concentrations of soluble anions  $\text{CO}_3^{2-}$ ,  $\text{HCO}_3^-$ ,  $\text{Cl}^-$ ,  $\text{SO}_4^{2-}$  and  $\text{NO}_3^-$ . The procedure adopted for finding the concentration of anions is explained by Page (1982). The concentrations of the anions found in the soil are given in Table 5.1.

### **5.6 Experimental procedure**

#### **5.6.1 Soil column preparation**

Specially designed plexi-glass soil columns shown in Fig.5.1 were used for studying the movement of ions under electrical, hydraulic and chemical gradients. The objective is to find the effectiveness of the electrokinetic barriers in preventing contaminant migration in soils. Since, the hydraulic conductivity of the Red river soil was found to be below  $1 \times 10^{-7} \text{ cm} \cdot \text{s}^{-1}$ , 50% UNIMIA industrial scale silica sand was mixed with 50% red river clay by weight to increase the hydraulic conductivity. The prepared sandy clay soil had a hydraulic conductivity in the range of  $5 \times 10^{-7}$  to  $1$  to  $5 \times 10^{-6} \text{ cm} \cdot \text{s}^{-1}$ . This soil was used for packing the soil columns.

Initially, the samples were wet packed which resulted in non-uniform compaction depending on the moisture content and the method of compaction. In addition, the air entrapped within the pores could not be displaced easily during subsequent saturation. These samples were abandoned after three months of preparation. Hence, the soil was dry packed in the soil columns to achieve uniform compaction and bulk density along the length of the soil column. The soil was packed in the columns in 2 cm thick layers (12 layers/column).

The soil was tamped using a tamping device and the inter layers were scarified before pouring another layer of soil. Thin nylon mesh was placed between the perforated end plates and the soil to prevent the soil particles from getting transported with the flowing water. The average bulk density of the soil columns was  $1.47 \text{ g/cm}^3$  for hydraulic columns and  $1.48 \text{ g/cm}^3$  for electrical columns. The bulk densities and the porosities of the electrical columns and the hydraulic columns are given in Table 5.2.

### **5.6.2 Saturation of the soil columns**

The soil columns were saturated using de-ionised and de-aired water. The soil columns were mounted on a specially designed column holder vertically. Application of pressure at the upstream or suction at the down stream to force the water through the column for faster saturation could create channels and preferential pathways in the soil. Therefore, the soil columns were saturated under low gradients (3.75). Water from the constant head device was connected to the bottom of the soil column, and the water was allowed to move upward slowly. Saturating slowly in this manner avoided air entrapment as the saturated front displaced the air which escaped through the outlet at the top. Once the wetting front reached the top (outlet), the orientations of the columns were changed from vertical to horizontal position in the sample holder. The water reached the outlet in about 20 days. After allowing five more days for complete saturation, the mini-tensiometers were installed along the length of the soil columns.

Installing the tensiometers could cause disturbance to the soil column. Therefore, another 5 days was allowed for the sample to reach equilibrium. By adopting this procedure, saturation of the soil column took nearly 1 month before starting the experiment.

**Table 5.2** Bulk density and porosity of the soil columns

<b>Sample No.</b>	<b>Bulk density ( g/cm<sup>3</sup>)</b>	<b>Porosity (%)</b>
Electrical columns :		
E1	1.48	43.07
E2	1.48	43.07
E3	1.49	42.69
Hydraulic columns :		
H1	1.48	43.07
H2	1.47	43.46
H3	1.47	43.46

### 5.6.3 Hydraulic conductivity measurements

After saturating the sample the initial hydraulic conductivities of the soil columns were measured. The rate of movement of the water meniscus in the glass tube was measured for a known time period. Then the hydraulic conductivity of the soil columns was found by:

$$K_h = \frac{a\Delta x}{A\left(\frac{dh}{dx}\right)\Delta t} \quad (5.1)$$

where:

- $K_h$  = hydraulic conductivity ( $\text{cm}\cdot\text{s}^{-1}$ ),
- $\Delta x$  = distance moved by the water meniscus (cm),
- $a$  = cross-sectional area of the glass tube ( $\text{cm}^2$ ),
- $A$  = cross-sectional area of the soil column ( $\text{cm}^2$ ),
- $dh/dx$  = hydraulic gradient,
- $\Delta t$  = time (s).

The hydraulic conductivities of the hydraulic and the electrical columns were monitored throughout the duration of the experiment ( 32 days ).

### 5.6.4 Electro-osmotic conductivity measurements

The flow of water due to hydraulic gradient will induce the contaminant introduced at the upstream end of the soil columns to migrate. The objective of this experiment is to prevent the contaminant from migrating along the soil columns by creating a counter flow by electro-osmosis. To create this opposite flow, the anode was placed at the down stream end and the cathode at the upstream end. This arrangement of electrodes will create an electro-osmotic flow opposite in direction to the flow caused by the hydraulic gradient.

Measurement of electro-osmotic conductivity is a challenging task, because of the presence of flow due to the hydraulic gradient as well as the electrical potential gradient. In addition, application of the electrical potential gradient along the soil columns produces gases at the electrodes due to the electrolysis reaction as explained in chapter 2. Formation of gas bubbles at the electrodes and accumulation of the bubbles near the plexiglass endplate affected the measurement of electro-osmotic conductivities. This is because the gas bubbles that formed during electrolysis sticks to the plexi-glass surface due to surface tension instead of escaping out freely through the gas vent. The gas bubble formation displaces the water meniscus affecting the measurement of electro-osmotic conductivity. To avoid the gas formation from affecting the electro-osmotic conductivity readings, the position of the water meniscus before the application of electrical potential gradient was noted down and the outlet from the column to the glass tube was closed. During the period of application of electrical potential gradient, water depletes at the anode end and the gas bubble accumulates in the inside surface of the glass column and the endplates. After the application of the electrical potential gradient, the gas bubbles attached to the surface of the endplates were disturbed by agitating the water in the chamber with a syringe. This effectively dislodged the gas bubbles. After dislodging the air bubbles, the outlet to the glass tube was opened and the water meniscus was allowed to recede. The electro-osmotic conductivity of the sample was found by:

$$K_e = \frac{(a\Delta x) - K_h \left( \frac{dh}{dx} \right) A \Delta t}{A \left( \frac{dE}{dx} \right) \Delta t} \quad (5.2)$$

where:

$K_e$  = electro-osmotic conductivity ( $\text{cm}^2 \cdot \text{V}^{-1} \cdot \text{s}^{-1}$ ),

$dE/dx$  = electrical gradient ( $\text{V} \cdot \text{cm}^{-1}$ ).

Applying electrical potential gradient along the soil column could cause consolidation due to the electro-osmosis of water. Consolidation of soil could alter the hydraulic conductivity of the soil in the column during the course of the experiment. To get a better estimate of the electro-osmotic conductivity, the hydraulic conductivity was measured before measuring the electro-osmotic conductivity. It is this hydraulic conductivity that was used in Eq.5.2 to calculate the electro-osmotic conductivities of the electrical columns.

#### **5.6.5 Pore water pressure measurements**

The pore water pressure of the soil was measured using the mini-tensiometers attached along the length of the soil column (Sec.5.2.4.). Manifolds were used to reduce the number of pressure transducers needed in measuring the pore water pressure. Three transducers were used in the experiment and were connected to three manifolds. Each of these three manifolds was in turn connected to four mini-tensiometers placed along the length of each electrical column. To measure the pore water pressure, the manifold was opened so that, only one tensiometer was connected to the transducer at a time. After opening the manifold, some time (15 min) was allowed for the tensiometer and the transducer to equilibrate until a steady reading was given by the pressure transducer. Pore water pressures of other tensiometers were measured by adopting the same procedure.

### **5.6.6 Voltage drop measurements**

The voltage drops along the length of the soil column and the current flowing through the soil sample were measured by using the computer controlled data acquisition system (Sec.5.2.3.). The potential drop along the soil sample was measured using the current passing through the sample. A 100  $\Omega$  resistor connected in series to the electrical columns was used as a reference resistor to measure the current passing through the sample. The current passing through the sample was determined by measuring the voltage drop across the 100  $\Omega$  resistor by using Ohm's law. With the help of the data acquisition program the electrical potential gradient can be applied intermittently or continuously based on the experimental needs.

During the present experimental study the electrical potential gradient was applied intermittently. The developed finite element model was used to decide on the duration of application of the electrical potential along the soil column. The measured values of  $K_h$ ,  $K_e$  and the applied hydraulic gradient were used as the input for the model. Several combinations of electrical gradient and duration of power supply were used in the model. Model studies suggested that, an electrical potential gradient of 1  $V \cdot cm^{-1}$  applied for 2 hours per day (2 h ON - 22 h OFF cycle) along the soil column could effectively control contaminant migration. A constant voltage was applied along the three electrical columns for the first two hours in a 24-hour cycle. The power supply was automatically switched off during the rest of the 22 h. After the end of 24 h the power was again automatically switched ON and the cycle was repeated for 32 days. When the power supply was switched ON, the

voltage drops along the length of the column were monitored for every ten minutes and stored in three separate files for the three electrical columns.

#### **5.6.7 Contaminant simulation**

After the samples were saturated, the de-ionized water was replaced with 0.02M KCl solution as a permeant at the upstream end. The  $K^+$  ion was used as a tracer to simulate the contaminant migration under coupled hydraulic-electrical-chemical gradients as it was found in lesser quantity in the experimental soil (78 mg/L). Chloride cannot be used as a tracer as it was present in large quantity in the experimental soil (880 mg/L). After introducing the KCl solution at the upstream end, the data acquisition system was activated.

A hydraulic gradient of 3.75 was applied along the soil column. To stop the contaminant from migrating under the existing hydraulic gradient, a counter gradient (Electrokinetic barrier) of  $1 V cm^{-1}$  was applied along the soil column so that, the flow caused by electro-osmosis is opposite in direction to that of the flow due to the hydraulic gradient. This will stop the water flow due to the hydraulic gradient or even reverse the flow depending on the electro-osmotic conductivity, and the hydraulic conductivity of the soil and the applied voltage and hydraulic gradient. As explained in Sec.5.6.6, a scheme of intermittent application of electrical potential was continued for a 32 day period.

#### **5.6.8 Soil column sectioning and sampling**

The concentration profile of the contaminant ions can be found either by extracting pore fluid along the length of the sample at regular intervals or by sectioning the samples at regular intervals. However, destructive analysis of the sample was chosen over extraction of pore fluid because it was very difficult to extract adequate volume of pore fluid for conducting

chemical analysis. After permeating the soil columns with the contaminant (KCl) and intermittently applying a constant voltage, the samples were sectioned at regular intervals (12 days) to chemically analyse the soil sections, to study the contaminant migration under coupled hydraulic, electrical and chemical gradients.

Since, the contaminant has been introduced at the cathode end, the section starting from the cathode will have higher concentration of contaminants. Hence, the sample was gently pushed from the cathode end, to avoid the contamination of the less contaminated soil section. Using a thin nylon thread, the soil column was sectioned into approximately ten equal sections. New nylon threads were used to cut each section to avoid any cross contamination of the sample. Each sample section was again divided into three parts. A small portion of the sample was used to find the moisture content of the sample, the second portion was used to find the pH of the section and a major portion of the sample section was retained to measure the contaminant ( $K^+$  and  $Cl^-$ ) concentration. These samples were stored in the refrigerator at 4 °C before extracting the pore fluid for conducting the chemical analysis. The samples were transferred to 250 mL beakers and 15 mL of de-ionised water was added to the samples and mixed to prepare the soil paste. After allowing the samples to stand for 4 hours the pore fluid was extracted using the procedure explained in Sec.5.5.2. The addition of water for extracting the salts will reduce the actual concentration of the salts present in the soil. Hence, a dilution factor had to be used to calculate the actual concentration of the salt. The dilution factor was found by:

$$DF = \frac{V_w + V_p}{V_p} \quad (5.3)$$

where:

DF = dilution factor,

$V_w$  = volume of water added,

$V_p$  = volume of pore fluid present in the soil.

The volume of the pore fluid present in the soil section was found from the soil moisture and the weight of the soil section used for pore fluid extraction, using the formula:

$$V_p = \frac{\theta_m}{(100 + \theta_m)} \frac{M_s}{\rho_w} \quad (5.4)$$

where:

$\theta_m$  = dry basis moisture content of the soil,

$M_s$  = mass of the wet soil section,

$\rho_w$  = density of the water.

For accurate determination of the concentrations of  $K^+$  and  $Cl^-$  the extracted pore fluid was triplicated before the chemical analysis was done. The measured concentrations were multiplied by the respective dilution factor of the sections to find the actual pore water concentrations.

### 5.6.9 Chemical analysis for potassium

An atomic absorption spectrometer (Model IL-257) was used for measuring the potassium concentration in the pore fluid. The samples were diluted to bring the concentration of  $K^+$  within the working range of the spectrometer. The procedure adopted is explained below:

1. Standard solutions of potassium were prepared by dissolving appropriate quantities of the reagent-grade potassium chloride in distilled water for calibrating the spectrometer.
2. 1 mL of the pore fluid extract was pipetted out into a 50 mL volumetric flask.
3. 2 mL of 5% Lanthanum oxide was added to the samples and the standards to control the interferences of other ions, for accurate determination of  $K^+$  concentration.
4. The samples were diluted by adding deionised water to 50 mL mark in the volumetric flasks.
5. After calibrating the atomic absorption spectrometer using the standard solutions according to the instructions specified in the equipments operation manual, the concentration of the  $K^+$  present in the pore fluid was measured.
6. Finally, the measured concentrations were multiplied by the appropriate dilution factors to obtain the actual concentrations of  $K^+$  in the soil sections.

#### **5.6.10 Chemical analysis for chloride**

The chloride electrode (ion-selective electrode) and the OAKTON (Mode No.2500) ion meter were used for the determination of chloride concentration in the pore fluid. The samples were diluted to bring the concentrations within the linear working range of the equipment. The procedure adopted for the determination of chloride concentration is explained below:

1. Standard solutions of chloride were prepared by dissolving appropriate quantities of reagent-grade sodium chloride in distilled water for calibrating the ion-meter.
2. 1mL of the pore fluid extract was pipetted into a 50 mL beaker.

3. 0.2 mL of ionic strength adjuster (5M NaNO<sub>3</sub>) was added to the standards and the samples to reduce the interferences of other ions.
4. The sample was diluted 10 times by adding 9 mL of distilled water.
5. After calibrating the ion-meter using the standard solutions according to the instructions specified in the equipments operation manual, the concentration of the Cl<sup>-</sup> present in the pore fluid was measured.
6. Finally the measured concentrations were multiplied by the appropriate dilution
7. factors to obtain the actual concentrations of Cl<sup>-</sup> in the soil sections.

## **6.0 RESULTS AND DISCUSSION**

### **6.1 Introduction**

A one-dimensional column experiment was conducted for 32 days to find the effectiveness of the electrokinetic barrier in containing the spread of contaminants. Using the data acquisition system controlled by a computer program a constant voltage of 24V was applied only for 2 h in a 24 h cycle. During the experiment, the hydraulic conductivity, electro-osmotic conductivity, voltage distribution and the pore water pressure distribution were monitored regularly by adopting the procedures explained in chapter 5. Two soil columns, one each from hydraulic and electrical columns were sectioned after 8, 20 and 32 days. Pore fluids of the sections were extracted and analysed for potassium and chloride ions. A finite element model was developed to understand the migration of ions under hydraulic, electrical and the chemical gradients (Chapter 3 and Chapter 4). The experimental results were compared with the model predictions to determine the validity of the model. The experimental results and the model predictions of the electro-kinetic barriers are discussed in this chapter.

### **6.2 Hydraulic and electro-osmotic conductivities**

The hydraulic conductivities remained constant at  $1 \times 10^{-6}$  cm/s for the hydraulic columns and  $0.8 \times 10^{-6}$  for the electrical columns (Fig 6.1 and Fig 6.2). The electro-osmotic conductivity of the electrical columns also remained constant at  $5 \times 10^{-6}$   $\text{cm}^2 \cdot \text{V}^{-1} \cdot \text{s}^{-1}$  (Fig.6.2). The electro-osmotic conductivity is approximately five times higher than that of the

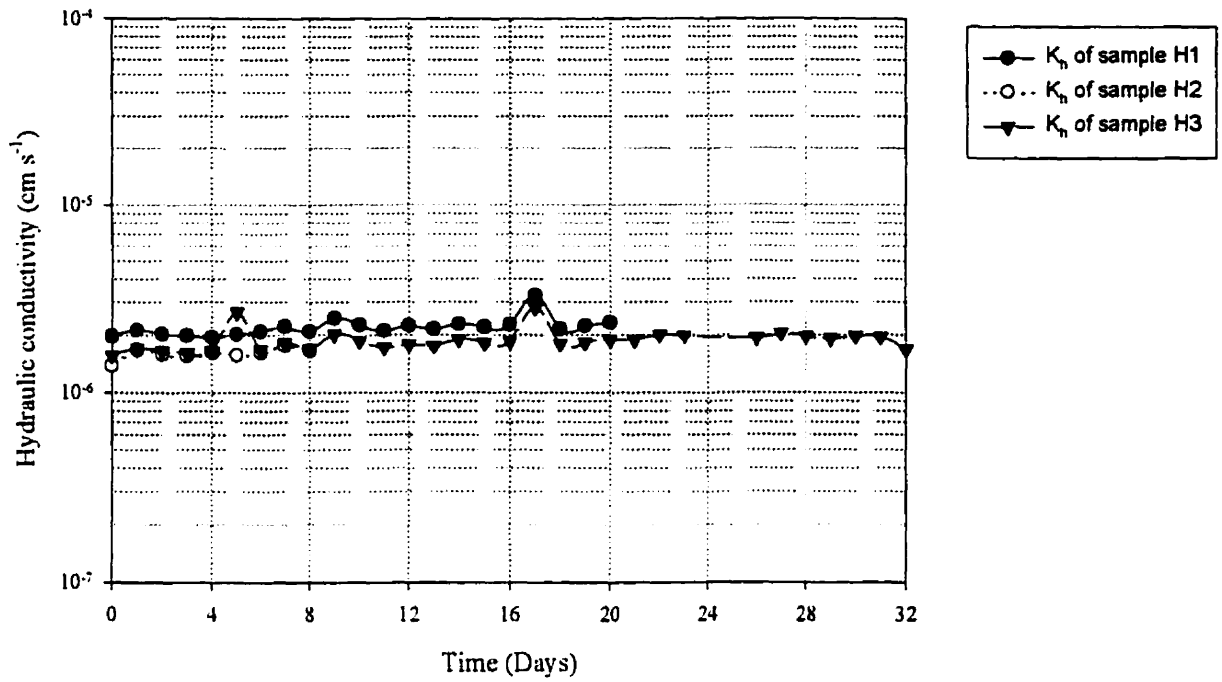


**Figure 6.1** Hydraulic conductivity of the hydraulic columns.

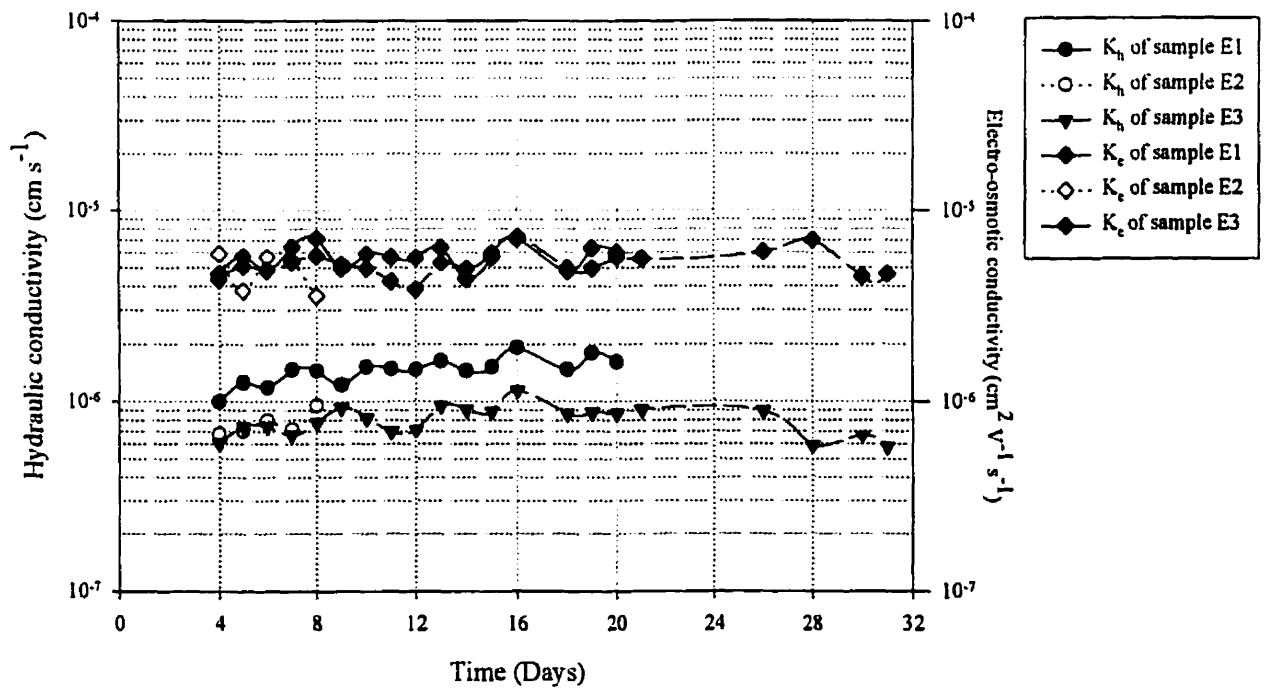


**Figure 6.2** Hydraulic and electro-osmotic conductivities of the electrical columns.

hydraulic conductivity. According to Mitchell (1993), the electro-osmotic conductivities of most of the soils ranges between  $10^{-4}$  to  $10^{-5} \text{ cm}^2 \cdot \text{V}^{-1} \cdot \text{s}^{-1}$ . There could be two reasons for the lower electro-osmotic conductivity of the soil used in the experiment:

1. the higher percentage of sand (>50%) in the soil
2. the higher concentration of salts present in the soil ( EC =  $9.5 \text{ dS} \cdot \text{m}^{-1}$ ).

According to Kruyt (1952) an increase in ionic concentration will affect the zeta potential and reduces the electro-osmotic conductivity of the soil (Eq.2.5).

### **6.3 Electrical conductivity**

The experimental soil contained large quantities of natural soluble salts (Table 5.1). Hence, during saturation with distilled water, these salts are being washed from the upstream end of the soil. However, the salts were not completely washed out of the column during saturation. Due to the change in the ionic concentration, there is a wide variation in the distribution of the electrical conductivities of both the hydraulic and the electrical columns. The electrical conductivity is lower ( $\approx 2 \text{ dS} \cdot \text{m}^{-1}$ ) near the upstream end and higher ( $\approx 8 \text{ dS} \cdot \text{m}^{-1}$ ) at the downstream end of the soil column (Figs.6.3 and 6.4). During the course of the experiment the salts were getting washed out of the hydraulic columns. Hence, the electrical conductivity was continuously decreasing with time (Fig.6.3). However, in the electrical columns the salts which accumulated near the downstream end during saturation never got washed out of the columns. This is because the electro-osmotic counter gradient stopped the migration of water and salts in the electrical columns (Fig.6.4). The changes in the electrical conductivity profile indicate that, the bulk rate of movement of ions in the

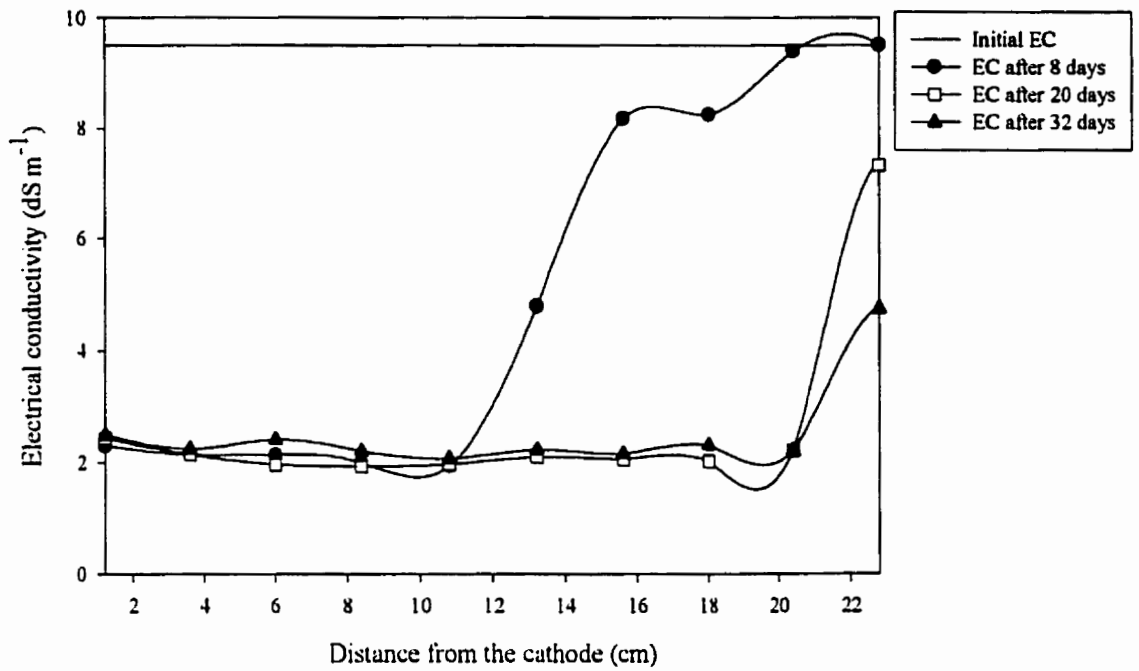


**Figure 6.3** Electrical conductivity distribution in the hydraulic columns.

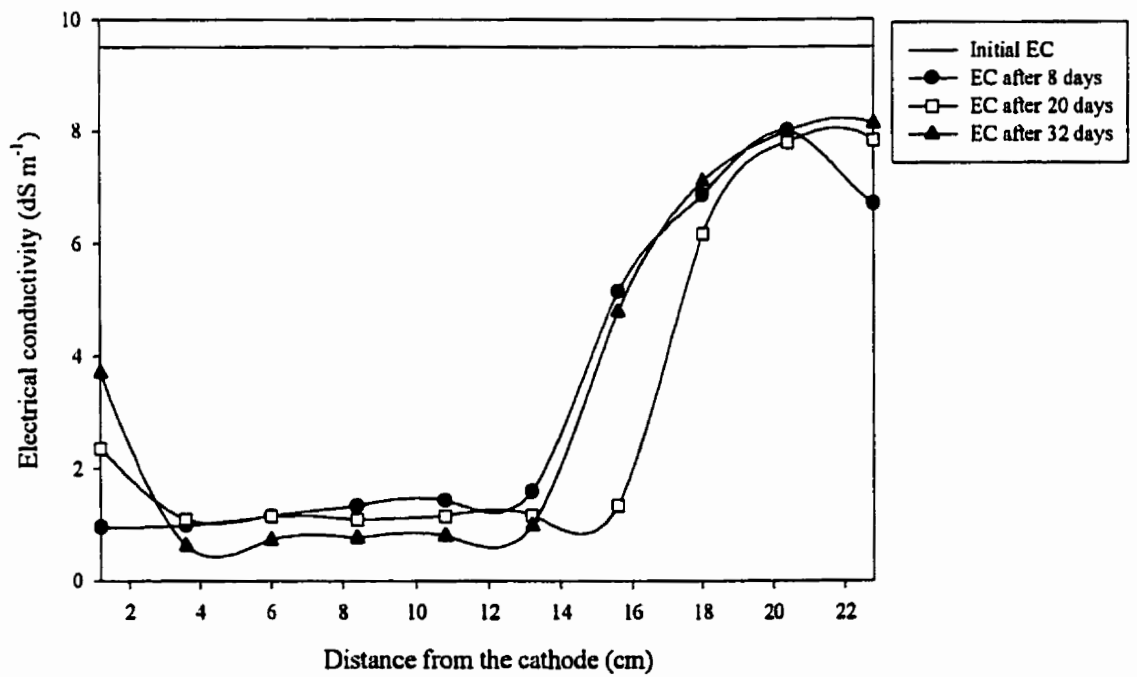


**Figure 6.4** Electrical conductivity distribution in the electrical columns.

electrical columns, was more than 7 mm/day, whereas, in the electrical columns, the bulk movement of ions was completely stopped by the electro-osmotic counter gradient. This clearly indicates that, the electro-osmotic counter gradient (electrokinetic barriers) could be effectively used to prevent the migration of the contaminants in the sub-surface.

#### **6.4 Experimental results and model predictions**

A two-dimensional finite element model was developed to simulate the contaminant migration under the influence of electrokinetic barriers. Triangular elements were used for the discretization of the domain (soil column) (Fig.6.5). The domain was divided into 100 elements of equal size and shape. The model was calibrated using the concentration measurements and the pH measurements obtained from the experiment after 8 days. The values of the model parameters (retardation coefficients) were adjusted by trial and error method until the concentration profiles matched the values obtained from the experiment after 8 days. These values were then used in the model to predict the changes in pore water pressure distribution, voltage distribution and concentration profiles of pH,  $K^+$  and  $Cl^-$  for the subsequent times. The parameters measured from the experiments, model calibration and literatures are presented in Table 6.1. The experimental results are compared with the model predictions in this section.

##### **6.4.1 pH distribution**

The initial pH of the soil used in the experiment was 7.5. In the hydraulic columns the pH remained constant during the experiment. Due to the production of  $H^+$  ions at the anode and the  $OH^-$  ions at the cathode in the electrical columns, the pH dropped to  $\approx 2$  at the anode

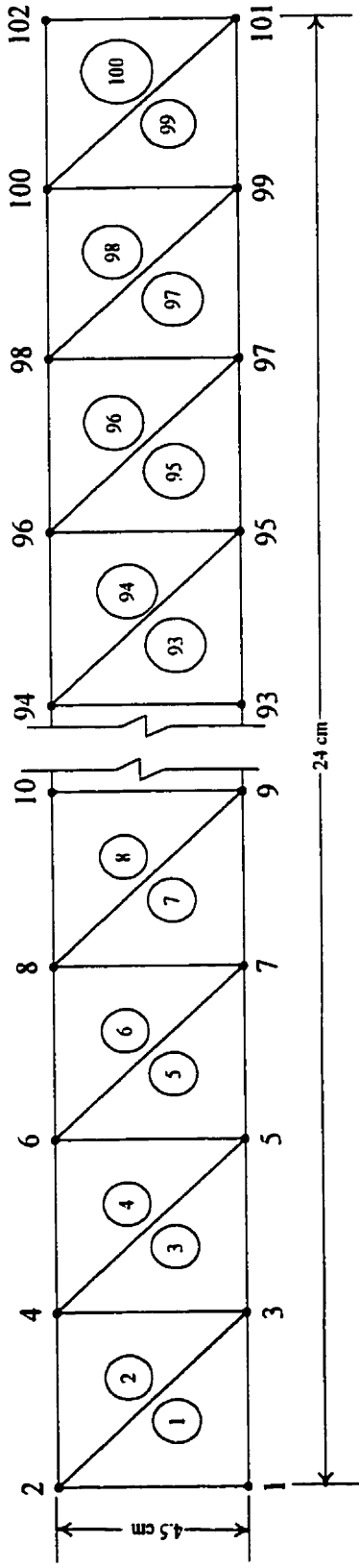


**Figure 6.5** Finite element discretization of the soil column used in the experiment.

**Table 6.1** Modelling parameters used in the computer model

<b>Modelling parameter</b>	<b>Value</b>
Diffusion coefficient of K <sup>+</sup>	19.6×10 <sup>-6</sup> cm <sup>2</sup> •s <sup>-1</sup> (Mitchell, 1993)
Diffusion coefficient of Cl <sup>-</sup>	20.3×10 <sup>-6</sup> cm <sup>2</sup> •s <sup>-1</sup> (Mitchell, 1993)
Diffusion coefficient of H <sup>+</sup>	93.1×10 <sup>-6</sup> cm <sup>2</sup> •s <sup>-1</sup> (Mitchell, 1993)
Diffusion coefficient of OH <sup>-</sup>	52.8×10 <sup>-6</sup> cm <sup>2</sup> •s <sup>-1</sup> (Mitchell, 1993)
Retardation coefficient of K <sup>+</sup>	5 (model calibration)
Retardation coefficient of Cl <sup>-</sup>	1 (model calibration)
Retardation coefficient of H <sup>+</sup>	200 (model calibration)
Retardation coefficient of OH <sup>-</sup>	100 (model calibration)
Hydraulic conductivity	1×10 <sup>-6</sup> cm <sup>-1</sup> •s <sup>-1</sup> (measured)
Electro-osmotic conductivity	5×10 <sup>-6</sup> cm <sup>-2</sup> •V <sup>-1</sup> •s <sup>-1</sup> (measured)
Porosity	0.44 (measured)
Storativity	0.002 cm <sup>-1</sup> (Istok, 1989)
Length of the soil column	24 cm (measured)
Width of the soil column	4.5 cm (measured)
Initial concentration of K <sup>+</sup>	78 mg/L (measured)
Initial concentration of Cl <sup>-</sup>	880 mg/L (measured)
Initial pH	7.5 (measured)
Electrical capacitance of the soil	0.0 Farad•cm <sup>-3</sup> (Alshwabkeh and Acar, 1996)

compartment and increased to  $\approx 12$  at the cathode compartment within 2 days of processing. Migration of the pH front could affect the transport of contaminants in the electrical columns. Considering a target pH of 5, the acid front from the anode end was migrating at a rate of 0.5 mm/day and for a target pH of 9, the base front from the cathode was migrating at a rate of 1 mm/day. Even though the ionic mobilities of  $H^+$  ion is higher than that of the  $OH^-$  ions, the  $H^+$  ions migrated at a lesser rate due to the high cation-exchange capacity of the soil (Table.5.1.).

Since, the experimental soil had high amount of exchangeable cations, the migration of pH front is retarded to a great extent (Fig.6.6). Acar and Alshawabkeh (1996) reported that, the acid front migrated at a rate of 10 to 18mm/day. Eykholt and Daniel (1994) reported that, the acid front from the anode compartment swept through the soil column. The acid front was migrating at a much faster rate in their experiments. This might have been due to the lower buffering capacity of the Kaolinite clay used in their experiments.

For modelling the pH migration, constant boundary conditions were assumed at the anode and the cathode compartments. A constant pH of 2 at the anode and a pH of 12 at the cathode were assumed. Model calibrations with the experimental results for 8 days showed that, a high retardation factor of 200 for the  $H^+$  ions and 100 for the  $OH^-$  ions matched the experimental values of the soil pH. These retardation factors were used to predict the pH profiles for 20 and 32 days. The model predictions and the experimental results are presented in Fig.6.6. The model predictions closely matched the measured pH values of the electrical columns.

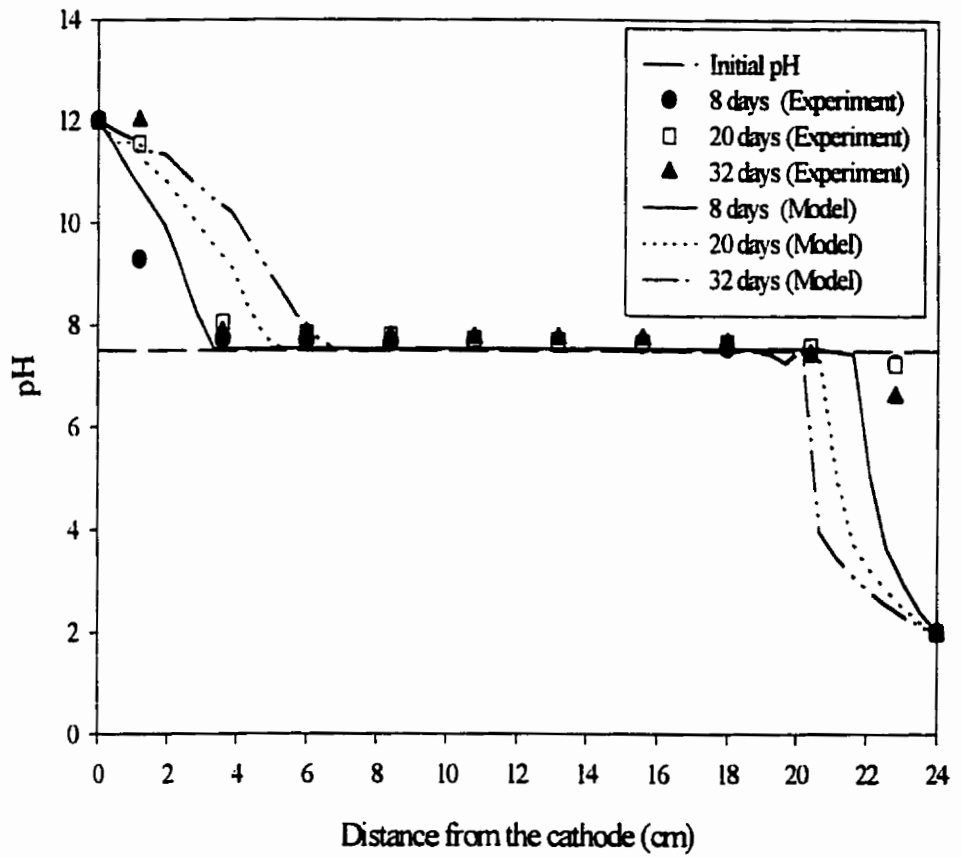


**Figure 6.6** pH distribution in the electrical columns.

#### **6.4.2 Voltage distribution**

The voltage distribution along the soil column remained linear during the duration of the experiment (Fig.6.7). A highly non-linear distribution of voltage gradient was reported by Alshawabkeh and Acar (1996) and Eykholt and Daniel (1994). Due to the non-uniform distribution of the electrical conductivity along the length of the soil column (Fig.6.4), non-linear distribution of the electrical potential gradient was expected. However, this could have been masked by the increase in resistance at the anode and the cathode, caused by the production of gases, which resulted in the linear distribution of the voltage. For modelling the voltage distribution, a uniform distribution of ions at the beginning of the experiment was assumed. The non-uniform distribution of ions caused by the massive migration of ions brought about by the hydraulic flow during the saturation was not taken into account in the model. Hence, the model also predicted a linear distribution of voltage along the soil column (Fig.6.7).

#### **6.4.3 Hydraulic head distribution**

As the voltage gradient remained linear with time, a linear distribution of hydraulic head along the soil column was expected. However, the hydraulic head distribution did not remain linear. The hydraulic head was changing with time (Fig.6.8). This could have been due to the variation in the electro-osmotic conductivity along the length of the soil column brought about by the accumulation of salts at the down stream end during saturation. As explained in Sec.6.2 this variation in ionic concentration could have changed the zeta potential and created a non-uniform distribution of electro-osmotic conductivity along the soil column. This variation in the electro-osmotic conductivity could have caused a

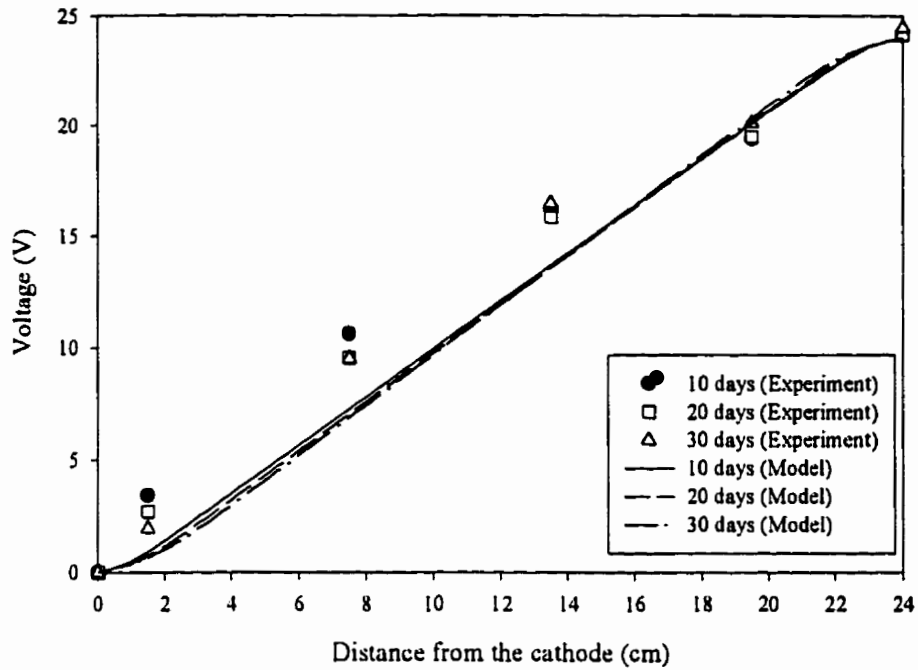


**Figure 6.7** Voltage distribution along the electrical columns.

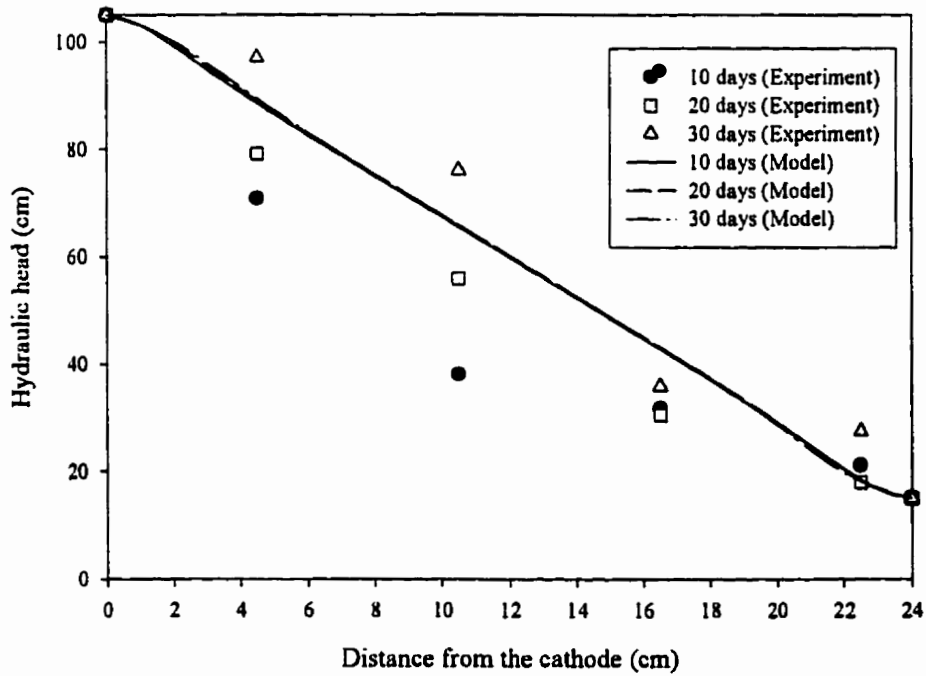


**Figure 6.8** Hydraulic head distribution along the electrical columns.

non-uniform electro-osmotic flow and lead to the non-linear hydraulic head distribution along the soil column. The computer model predicted a linear distribution of the hydraulic head as a uniform electro-osmotic conductivity was assumed for the electrical columns (Fig.6.8).

#### **6.4.4 Distribution of potassium**

A 0.02M potassium chloride was used as a tracer to monitor the contaminant migration in the hydraulic columns and the electrical columns. The migration rate of potassium could demonstrate the effectiveness of the electro-kinetic barrier in preventing the contaminant migration. The concentration of  $K^+$  ions present in the cathode compartment is continuously increasing with time in the electrical columns. The positively charged cations ( $K^+$ ) present in the solution may have been attracted towards the cathode and negatively charged anions being repulsed from the cathode. The distribution of potassium in the hydraulic and the electrical columns after 8, 10 and 32 days are presented in the Figs.6.9, 6.11 and 6.13. The concentration profiles of potassium in the hydraulic and the electrical columns indicate that, the migration of potassium is controlled effectively in the electrical columns. Considering a target value of 200 mg/L, in the hydraulic columns, the concentration profile of  $K^+$  was migrating at a rate of 2.0mm/day, whereas, in the electrical columns, the concentration profile of  $K^+$  ion was migrating at a rate less than 0.1 mm/day. The migration rate of  $K^+$  ions was reduced more than 20 times by the electrokinetic barriers. This clearly demonstrates that, the electrokinetic barrier could be effectively used to prevent the contaminant migration in the sub-surface.

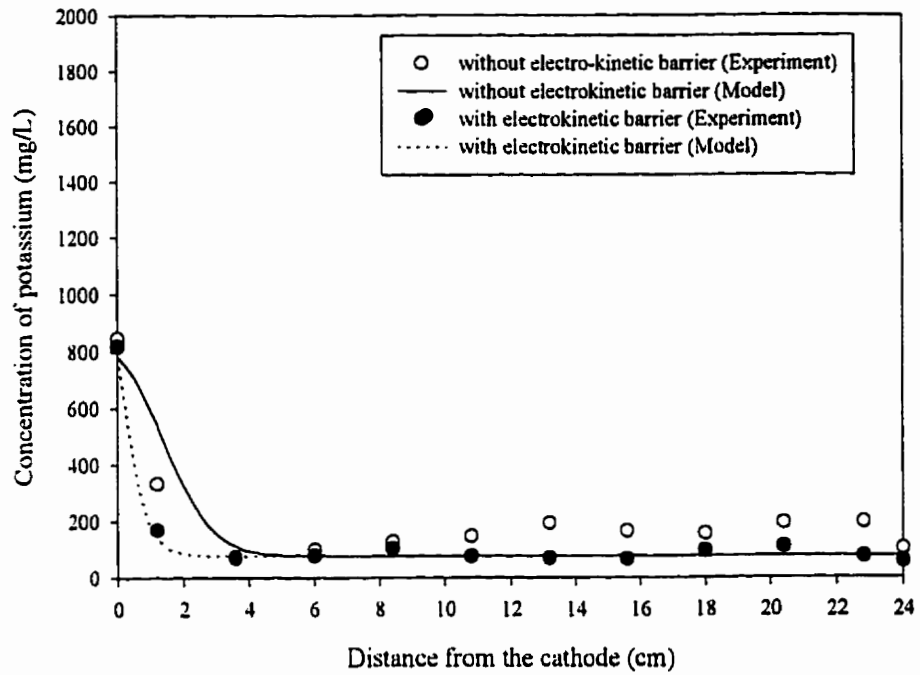


**Figure 6.9** Distribution of potassium ions after 8 days.

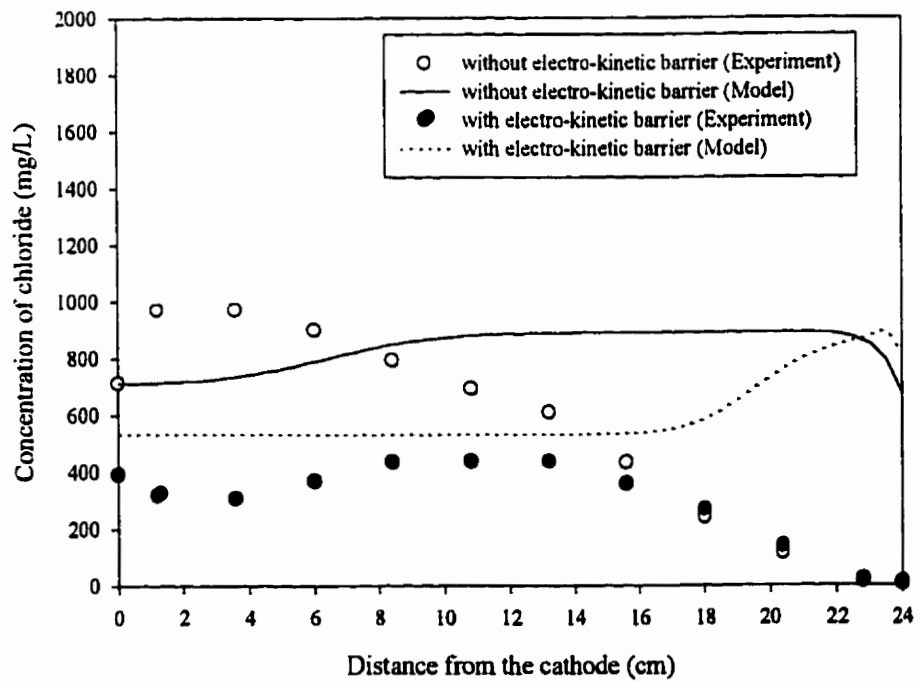


**Figure 6.10** Distribution of chloride ions after 8 days.

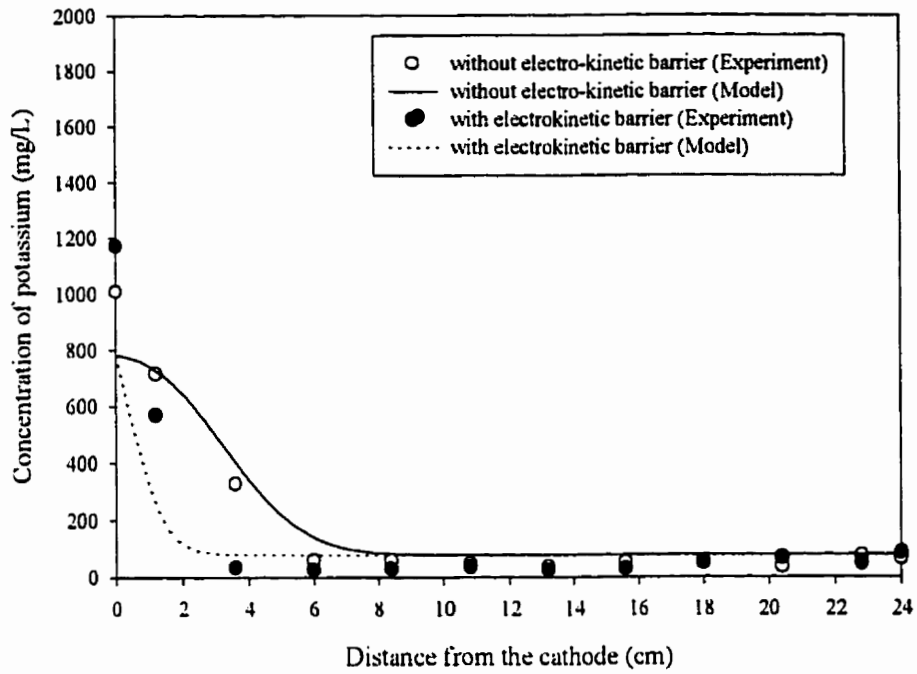


**Figure 6.11** Distribution of potassium ions after 20 days.

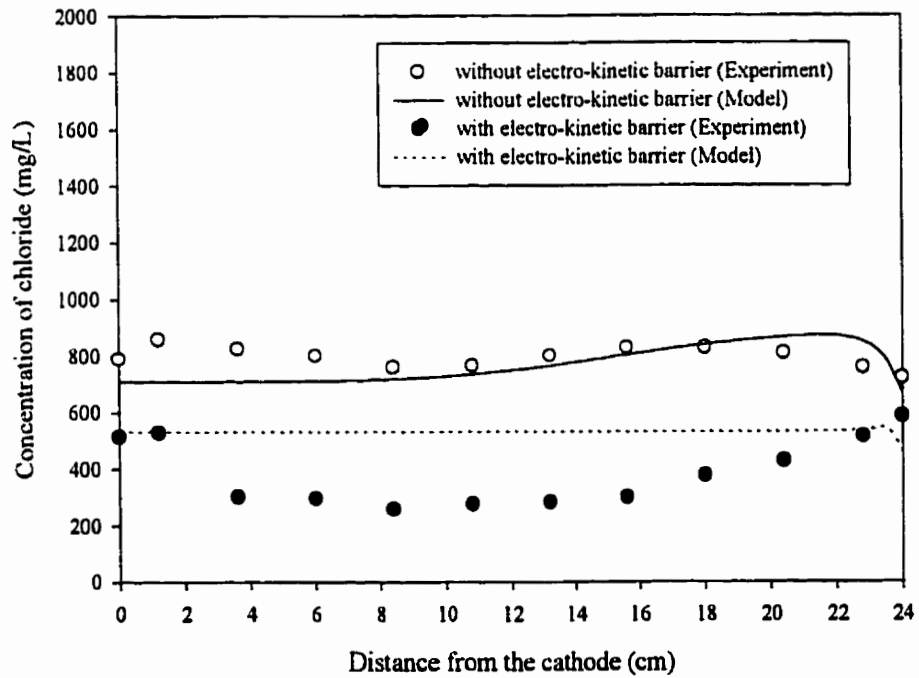


**Figure 6.12** Distribution of chloride ions after 20 days.

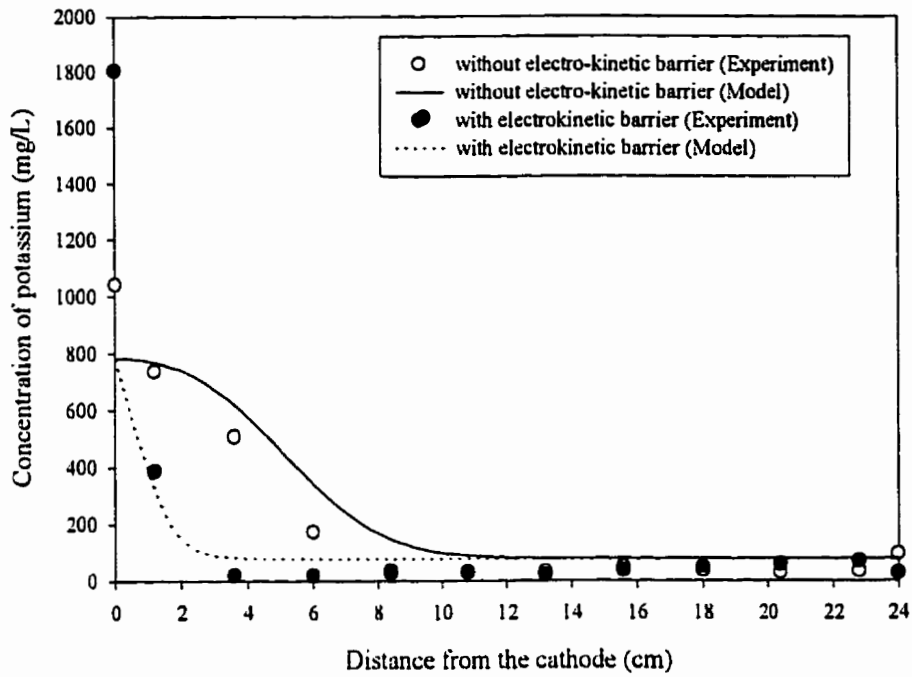


**Figure 6.13** Distribution of potassium ions after 32 days.

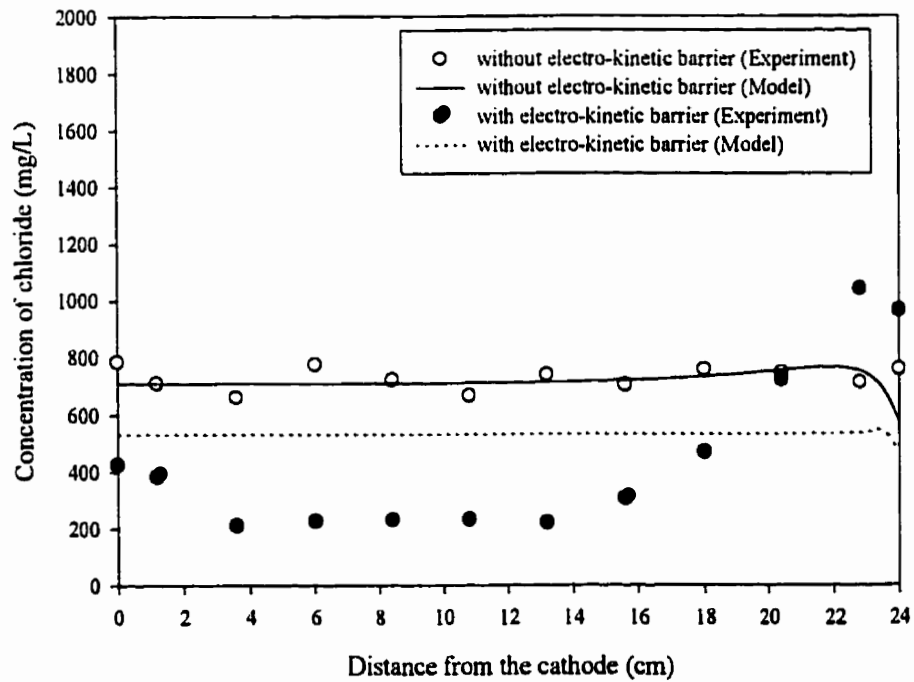


**Figure 6.14** Distribution of chloride ions after 32 days.

Model calibrations with the experimental results obtained after 8 days showed that, a retardation factor of 5 for potassium matched well with the experimental results. The migration of potassium was slightly retarded in the electrical and hydraulic columns since the potassium is replacing the exchangeable sodium present in the soil (Table. 5.1). A constant concentration of 782 mg/L of potassium (0.02M) was used as the boundary condition at the upstream end. The model predictions closely matched the measured concentration values of potassium in the electrical and the hydraulic columns (Figs.6.9,6.11 and 6.13). The model predictions, and the experimental results demonstrate the effectiveness of electrokinetic barriers in preventing the migration of contaminants.

#### **6.4.5 Distribution of chloride**

The initial concentration of chloride present in the soil pore fluid was 880 mg/L. However, the chloride concentration of the solution flowing from the up stream end of the column was only 709mg/L. Hence, the distribution of chloride would not give a better estimate of the contaminant migration. The chloride concentration at the cathode almost reduced to half during the experiment. The cathode may be repulsing the negatively charged chloride ions present in the cathode compartment. The concentration of the chloride ion at the cathode compartment reduced from 709 mg/L to 500 mg/L. This made the direct comparison of the concentration profiles between the hydraulic and the electrical columns difficult. The distributions of Cl<sup>-</sup> ion in the soil after 8,20 and 32 days are presented in Figs.6.10, 6.12 and 6.14. Figure 6.10 indicates that, after 8 days, the chloride concentration at the downstream end reduced below 880 mg/L in both the hydraulic and the electrical columns. As explained before the natural chloride present in the soil could have been washed away from the soil

during saturation and during the process of the experiment. However, the chloride concentration increased with time in both the hydraulic and the electrical columns. After 20 days the chloride almost reaches the downstream end of the soil column. However, in the electrical columns the concentration of chloride increases continuously near the anode end (Fig.6.14). The anode may have attracted the negatively charged chloride ions and is not letting it pass through the anode compartment.

For modelling the migration of chloride ions, constant concentration boundary condition is assumed at the upstream end (709 mg/L for the hydraulic columns and 500 mg/L for the electrical columns). Since, a uniform initial concentration of chloride was assumed, without taking into account the non-uniform distribution of Cl<sup>-</sup> brought about by the washing away of salt present in the soil during saturation, the model predictions did not match well with the measured values. The model reasonably predicted the distribution of chloride in the hydraulic columns after 20 days. However, the drop in concentration of the percolating solution at the cathode and the accumulation of chloride ions at the anode compartment brought a greater deviation between the model predictions and the measured values in the electrical columns.

## **7.0 FIELD APPLICATION SCENARIOS**

### **7.1 Introduction**

A two-dimensional numerical model has been developed by using the finite element method. The model was used to evaluate the effect of various schemes of electrode arrangement for possible field applications. The effect of various aquifer parameters, boundary conditions and electrode arrangements were simulated. A similar kind of model study was done by Renaud and Probstein (1987) to find the effect of electro-osmotic flow to divert the groundwater from passing through a hypothetical hazardous waste land fill. The aim of this model study was to evaluate the effectiveness of electrokinetic barriers for improving the efficiency of contaminated site clean-up technologies like vapour-extraction and pump-and-treat techniques. The steady-state model results of two such electrode arrangements as an aid for site clean-up techniques are presented here. The aquifer properties used for the model simulations are:

Hydraulic conductivity :  $5 \times 10^{-9} \text{ m} \cdot \text{s}^{-1}$

Electro-osmotic conductivity :  $2 \times 10^{-9} \text{ m}^2 \cdot \text{V}^{-1} \cdot \text{s}^{-1}$

### **7.2 Electrokinetic barriers for vapour-extraction system**

Leakage of hydrocarbon contaminants from the underground storage tanks is a major source of groundwater contamination (Domenico and Schwartz, 1990). As most of the hydrocarbon contaminants are highly volatile, vapour extraction method is widely used for remediating such contaminated soils and groundwater (Fetter, 1992). If the water table in the region is

above the contaminated zone, vapour-extraction procedure will not be effective, as all the pore spaces are saturated with water. For fine textured soils like silt and clay having a low hydraulic conductivity, it is very difficult to pump the water out of the aquifer and lower the water table below the contaminated zone. As electro-osmosis is very effective in moving water in fine grained soils, the electrodes can be installed upstream of the contaminated zone in such a way that, the electro-osmotic flow is opposite in direction to that of the flow due to the hydraulic gradient (Fig.7.1). This electrode arrangement will reduce the influx of water through the contaminated zone and will also drain the zone downstream of the electrodes to lower the water table below the contaminated zone. As the water table is lowered below the contaminated zone, most of the pore spaces will be free for the air to pass through. This will increase the efficiency of the vapour-extraction system in cleaning up the volatile hydrocarbon contaminants.

An electrical potential gradient of  $25 \text{ V}\cdot\text{m}^{-1}$  was applied continuously to achieve the steady-state distribution of hydraulic head. A constant head of 26 m was assumed at one end and 14 m at the other end. The steady-state simulation results are presented in Figs.7.2 and 7.3. From the distribution of hydraulic head shown in Figs.7.2a and 7.2b, it is evident that, the water table could be lowered below the contaminated zone. Assuming a linear distribution of hydraulic head to begin with, the steady-state model results showed a reduction of 5 m (reduced from 18 m to 13 m) in the hydraulic head at a distance of 10 m downstream from the centre of the electrokinetic barriers. Figures.7.3a and 7.3b indicate the electrical potential distribution. The electro-osmotic flow will be perpendicular to the electrical equi-potential lines. The electrical potential distribution also indicates that,

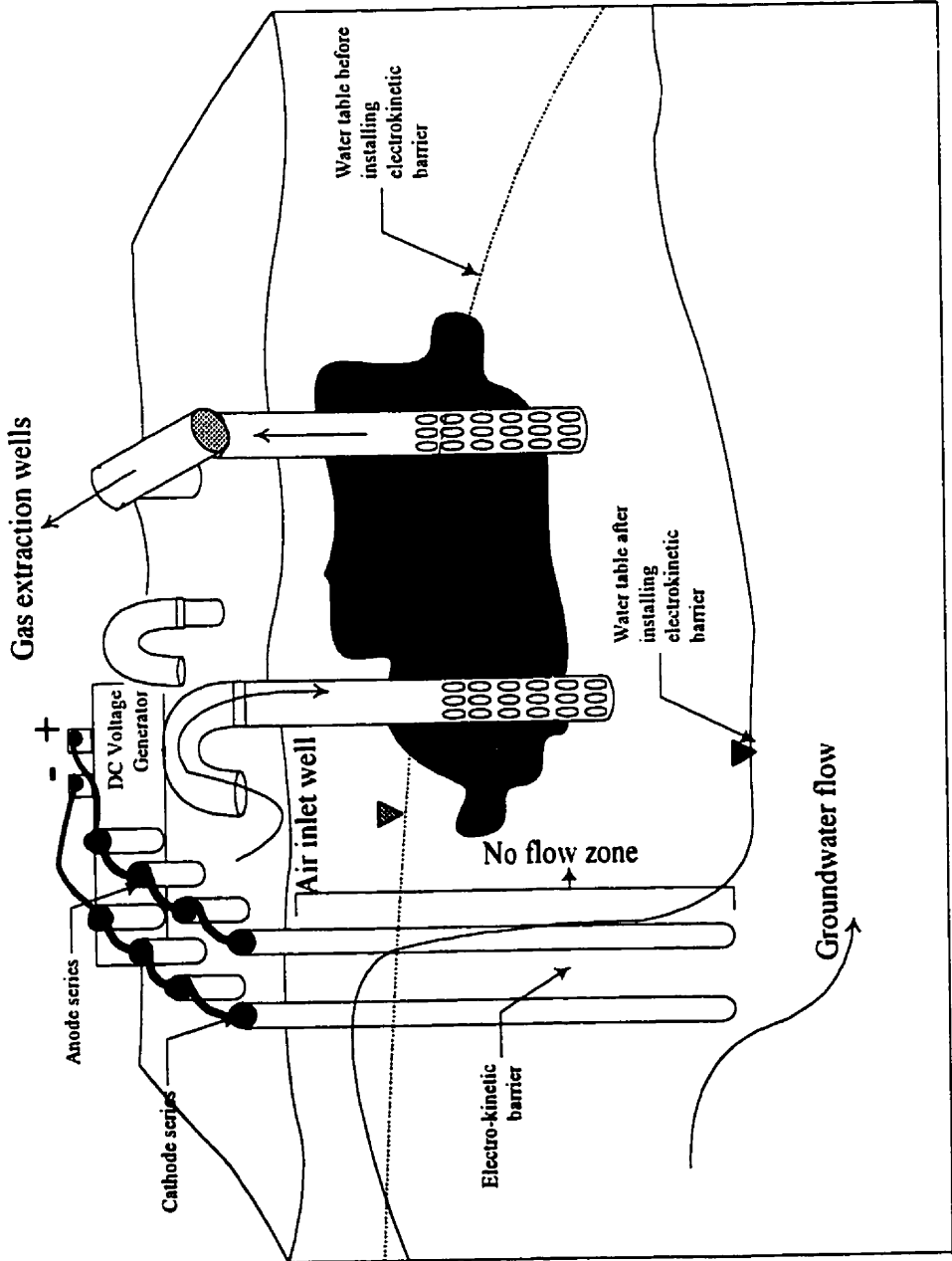


**Figure 7.1** Hydrodynamic control of water table using electro-kinetic barriers for increasing the efficiency of vacuum extraction technique in removing volatile contaminants.

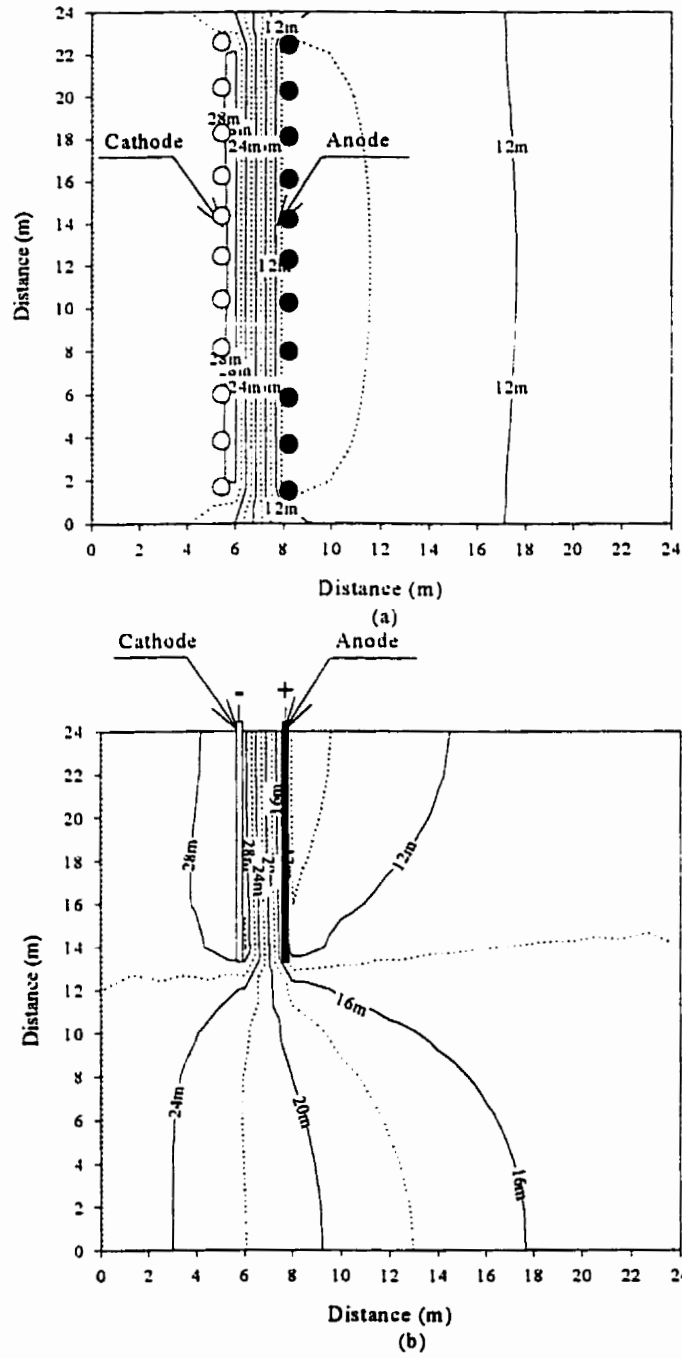


**Figure 7.2** Simulation results of constant hydraulic head lines for a proposed electrokinetic barrier arrangement with the vapour-extraction system (a) plan view (b) side view.

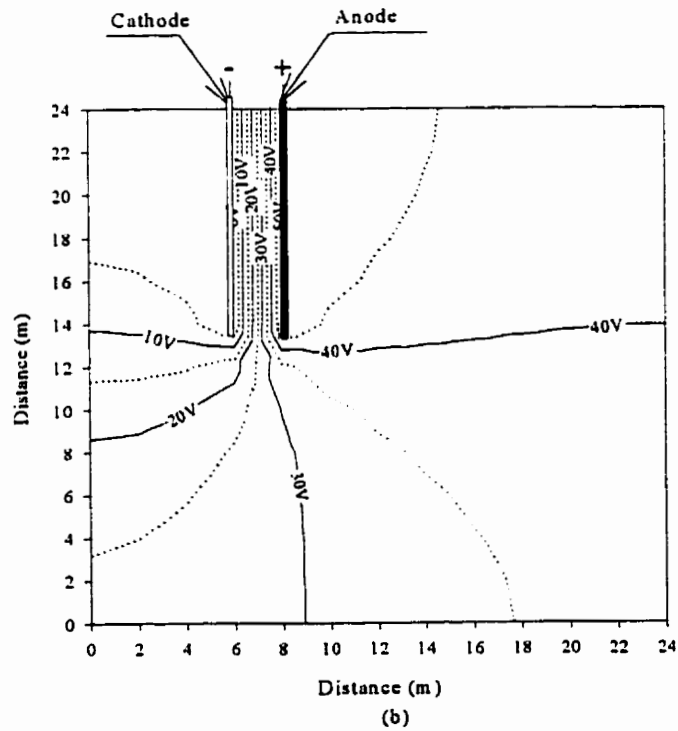
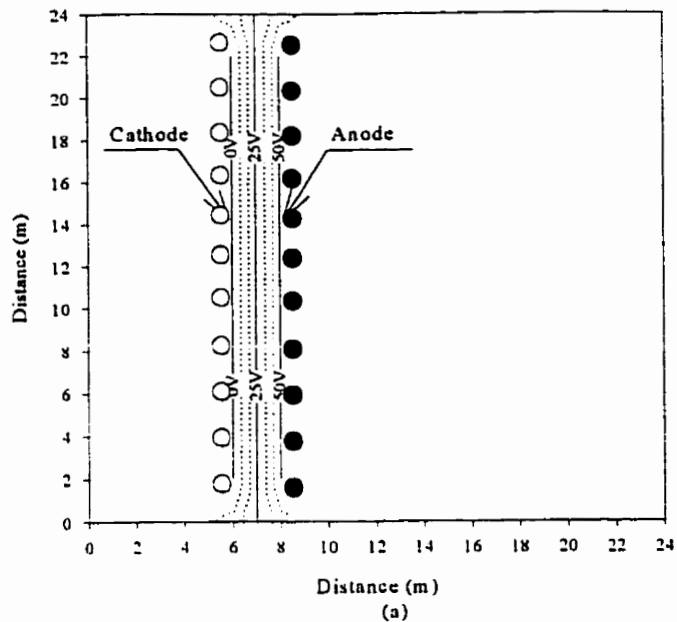


**Figure 7.3** Simulation results of constant voltage lines for a proposed electrokinetic barrier arrangement with the vapour-extraction system (a) plan view (b) side view.

the electro-osmotic flow could lower the water table, downstream of the electrodes, well below the contaminated zone.

### **7.3 Electrokinetic barriers for pump-and-treat system**

For this simulation, the same aquifer parameters have been used except, it was assumed that, the contaminant present is not highly volatile. Therefore, the vapour-extraction method will be less efficient for cleaning up the contaminated site. The pump-and-treat technique might be a viable option for the clean-up. However, the aquifer contains fine-grained soil with low hydraulic conductivity causing the yield of the well to be very low. As the flow due to electro-osmosis is effective in fine grained soils, the well yield can be augmented by the use of an electrical potential gradient. The electrode arrangement as shown in Fig.7.4 can be used in conjunction with pump-and-treat technique for increasing the yield of the well and also for containing the spread of the contaminants. Electrodes are installed in such a way that, the electro-osmotic flow is directed towards the contaminated zone and the well. Increasing the well yield will increase the efficiency of the pump-and-treat technique in remediating the contaminated soil.

An electrical potential gradient of  $12.5 \text{ V}\cdot\text{m}^{-1}$  was applied continuously to achieve the steady-state distribution of hydraulic head. A constant head of 26 m was assumed at one end and 14 m at the other end. The steady-state simulation results are presented in Figs.7.5 and 7.6. Assuming a linear distribution of hydraulic head to begin with, the steady-state model results showed a head build up of 8 m (increased from 20 m to 28 m) in the hydraulic head at a distance of 7 m from the centre of the electrokinetic barriers on either side. The

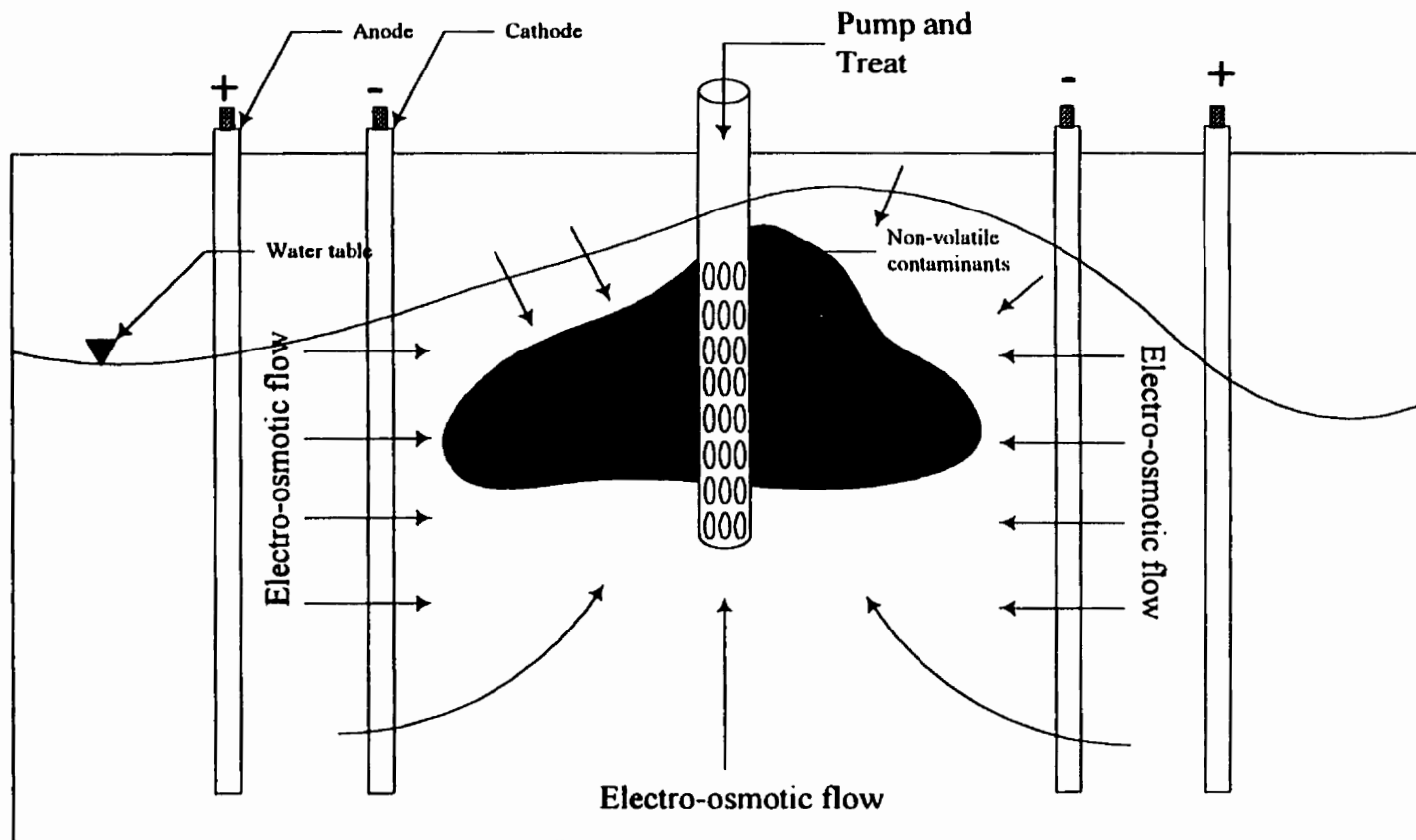


**Figure 7.4** Control of contaminant plume by electro-osmotic flow using electro-kinetic barriers. This setup can also improve the contaminant flushing using pump-and-treat technique.

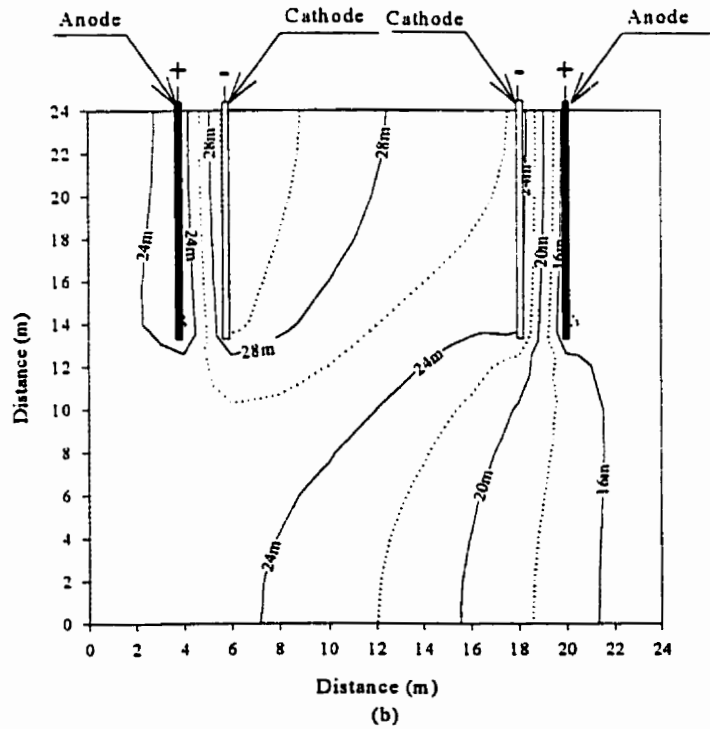
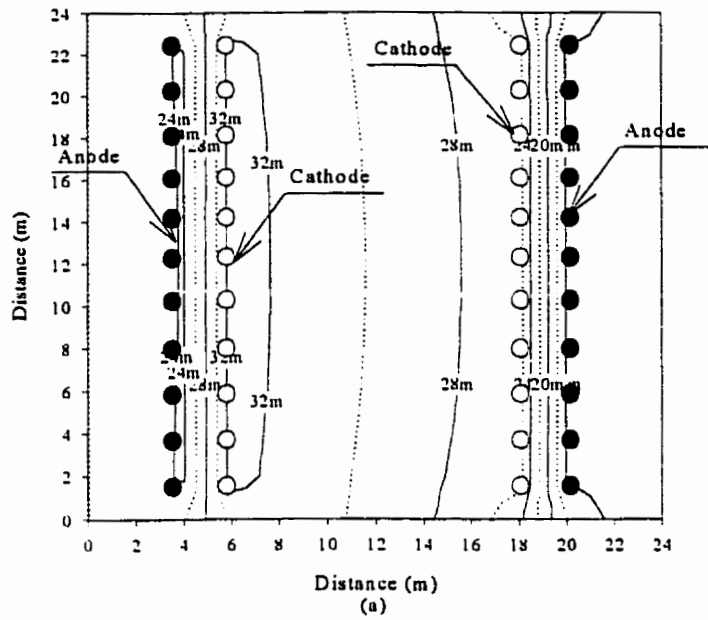


**Figure 7.5** Simulation results of constant hydraulic head lines for a proposed electrokinetic barrier arrangement with the pump-and-treat system (a) plan view (b) side view.

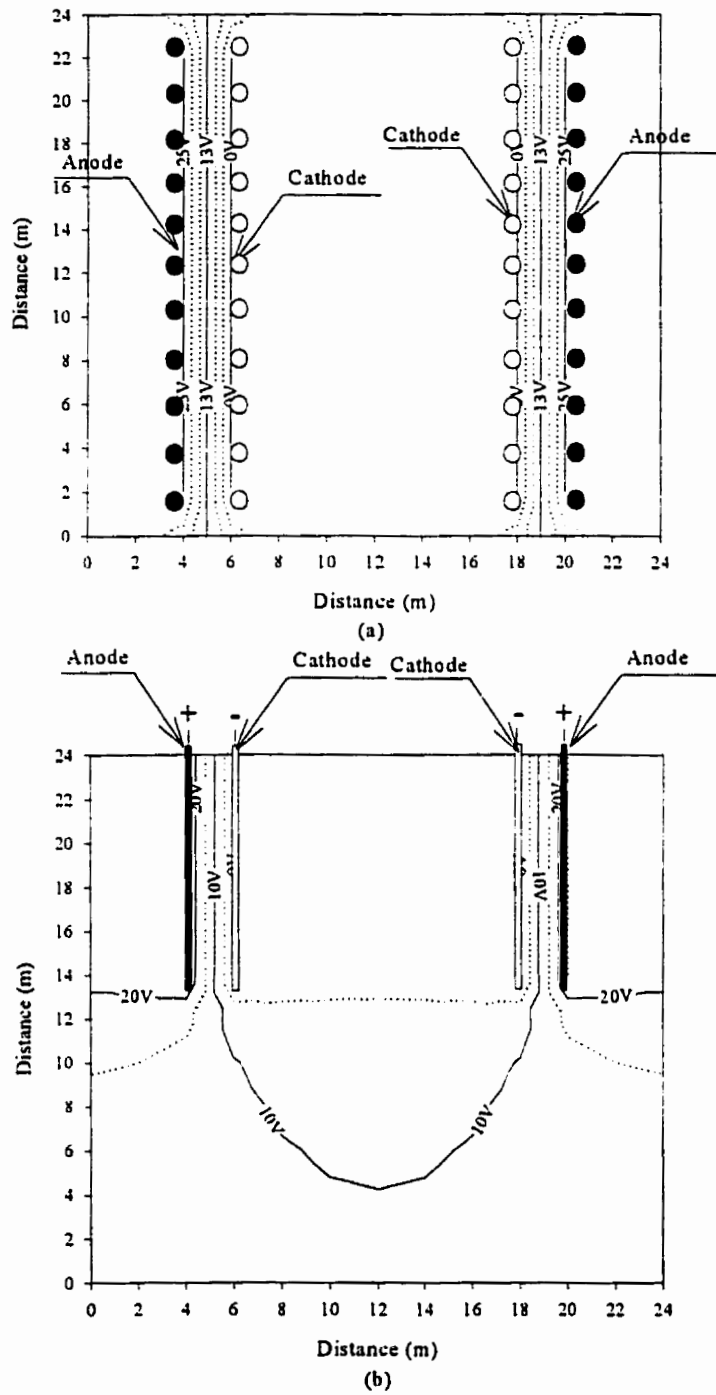


**Figure 7.6** Simulation results of constant voltage lines for a proposed electrokinetic barrier arrangement with the pump-and-treat system (a) plan view (b) side view.

constant head lines from Figs.7.5a and 7.5b shows that, a groundwater mound could be created near the contaminated zone and the pumping well. The electrical potential distribution in Figs.7.6a and 7.6b also indicates that, the electro-osmotic flow could create a groundwater mound within the contaminated zone thereby augmenting the well yield and the rate of contaminant removal.

## **8.0 CONCLUSIONS AND RECOMMENDATIONS**

### **Summary**

The Electrokinetic barrier is an emerging technique for preventing groundwater contamination. One of the main objectives of this study was to conduct laboratory experiments to investigate the feasibility of using electrokinetic principle in creating subsurface barriers for contaminant migration.

- The laboratory experiments proved that, the electrokinetic barriers can be effectively used for containing the spread of contaminants. The concentration profile of  $K^+$ , in hydraulic columns was migrating at a rate of 2 mm/day, whereas, in the electrical columns, the concentration profile of  $K^+$  ion was migrating at a rate of less than 0.1 mm/day. The rate migration of  $K^+$  ion was reduced approximately 20 times by the electrokinetic barriers.
- The distribution of electrical conductivity also proved that, the electrokinetic barriers are effective in mitigating contaminant migration in the subsurface. In the hydraulic columns, the electrical conductivity profile (bulk movement of ions) was moving out of the column at a rate of 7 mm/day, whereas, in the electrical columns, the electrical conductivity profile did not change appreciably with time. This indicates that, the electro-osmotic counter gradient in the electrical columns prevented the bulk movement of ions out of the electrical columns.

The second objective of this study was to investigate the changes in electrical and hydraulic potential gradients and the development of pH front during the creation of electrokinetic barriers.

- Regular monitoring of the experimental columns showed that, the voltage gradient remained linear. Since, the electrical conductivity distribution was not uniform, a non-linear distribution of electrical potential gradient was expected. However, this could have been masked by the increase in resistance at the anode and the cathode caused by the production of gases which resulted in the linear distribution of the voltage.
- The hydraulic gradient remained non-linear due to the non-uniform distribution of electro-osmotic conductivity brought about by the wide variation in ionic concentration along the soil column.
- The pH front was migrating at a much lower rate due to the high buffering capacity of the soil. Due to a high buffering capacity of the soil, the development of pH front, might not affect the functioning of electrokinetic barriers in the Red river soil.

The third objective was to develop a two dimensional model for contaminant transport under coupled hydraulic, electrical and chemical gradients.

- A two-dimensional finite element model was developed based on the established theory of electrokinetics (Chapter 3 and Chapter 4). The model is capable of handling heterogenous and anisotropic formations of the aquifers.
- Migration of a pH front due to the electrolysis reactions at the anode and the cathode and development of non-linear hydraulic and electrical potential gradients brought about by the changes in electrical properties could be simulated by the developed model.

The final objective was to evaluate the model predictions by comparing it with the experimental results.

- The developed model closely predicted the migration of potassium under coupled hydraulic, electrical and chemical gradients. It also proved that, the transport of contaminants could be effectively controlled by the combined effects of electro-osmosis and electro-migration.
- The developed model can be used as a tool for designing the field installations of the electrokinetic barriers. The model predictions showed that, the electrokinetic barriers can be used in conjunction with conventional remediation techniques like pump and treat system and vapour extraction systems for preventing contaminant migration. It will also increase the efficiency of the system in removing the contaminants.

#### **Recommendations for future research**

- Laboratory experiments proved that, electrokinetic barrier is effective in preventing the spread of the cationic contaminants and accelerates the spread of anionic contaminants. Experiments should be conducted to see if a three-row electrode configuration cathode-anode-cathode will be effective in preventing the spread of both anionic and cationic contaminants.
- Pilot scale studies should be conducted to verify the effectiveness of electrokinetic barriers in preventing the spread of hydrocarbon contaminants like gasoline from underground storage tanks and migration of leachates from landfills.
- The efficiency of electrokinetic barriers under unsaturated conditions has to be investigated.

- Economics of the application of electrokinetic barrier and the best electrode material for field applications have to be studied.

## REFERENCES

- Acar, Y.B. 1992. Electrokinetic Cleanups. *Civil Engineering*. pp. 58-60.
- Acar, Y.B. and A.N. Alshawabkeh. 1993. Principles of Electrokinetic Remediation. *Environmental Science and Technology* 27(13):2638-2647.
- Acar, Y.B., A.N. Alshawabkeh and R.J. Gale. 1993. Fundamentals of Extracting Species from Soils by Electrokinetics. *Waste Management* 13:141-151.
- Acar, Y.B. and A.N. Alshawabkeh. 1996. Electrokinetic remediation. I: Pilot-scale test with lead-spiked kaolinite. *Journal of Geotechnical Engineering* 122(3):173-185.
- Acar, Y.B., R.J. Gale, J. Hamed and G. Putnam. 1990. Acid/Base Distributions in Electrokinetic Soil Processing. *Bulletin of Transportation Research, Record No 1288, "Soils, Geology, and Foundations"* pp. 23-34.
- Acar, Y.B., R.J. Gale, G.A. Putnam, J. Hamed and R.L. Wong. 1990. Electrochemical Processing of Soils: Theory of pH Gradient Development by Diffusion, Migration, and Linear Convection. *Journal of Environmental Science and Health, Part (a): Environmental Science and Engineering* 25(6):687-714.
- Acar, Y.B., H. Li and R.J. Gale. 1992. Phenol Removal from Kaolinite by Electrokinetics. *Journal of Geotechnical Engineering* 118(11):1837-1852.
- Acar, Y.B., E.E. Ozsu, A.N. Alshawabkeh, M.F. Rabbi and R.J. Gale. 1996. Enhance soil bioremediation with electric fields. *Chemtech* 26(4):40-44.
- Ahmad, E., A.R. Jones and T.D. Hinsely. 1997. Electromelioration of a sodic horizon from an Illinois Natraqualf. *Soil Science Society of America* 61(6):1761-1765.
- Alshawabkeh, A.N. and Y.B. Acar. 1992. Removal of Contaminants from Soils by Electrokinetics: A Theoretical Treatise. *Journal of Environmental Science and Health, Part (a): Environmental Science and Engineering* 27(7):1835-1861.
- Alshawabkeh, A.N. and Y.B. Acar. 1996. Electrokinetic remediation. II: Theoretical model. *Journal of Geotechnical Engineering* 122(3):186-196.
- Bear, J. and A. Verruijt. 1987. *Modelling groundwater flow and pollution*. D. Reidel Publishing Co. Dordrecht, Holland pp. 414.

- Bruell, C.J., B.A. Segall and M.T. Walsh. 1992. Electroosmotic Removal of Gasoline Hydrocarbons and TCE from Clay. *Journal of Environmental Engineering* 118(1):68-83.
- Casagrande, L. 1949. Electroosmosis in soils. *Geotechnique* 1(3):159-177.
- Corapcioglu, M.Y. 1991. Formulation of electro-osmotic processes in soils. *Transport in porous media* 6(4):435-444.
- Domenico, P.A. and F.W. Schwartz. 1990. *Physical and Chemical Hydrogeology*. John Wiley & Sons, Inc.
- Elsawaby, M.S. 1981. Electromelioration of soda-saline soils of Egypt. II. Improvement of physical properties of Ferash soil. *Agricultural Research Review* pp. 185-197.
- Environment Canada. 1996. Summary report. National Pollutant Release Inventory.
- Esrig, M.I. 1968. Pore pressures, consolidation and electrokinetics. *Journal of Soil Mechanics and Foundation Division, Proc ASCE* 94(SM4):899 - 921.
- Esrig, M.I. and S. Majtenyi. 1965. A new equation for electroosmotic flow and its implications for porous media. HRB Publication 1331.
- Evans, J.C., E.D. Stahl and E. Drooff. 1987. Plastic concrete cutoff walls. In *Geotechnical practice for waste disposal '87*, R. D. Woods 13:462-472. New York: Americal Society of Civil Engineers.
- Eykholt, G.R. and D.E. Daniel. 1991. Electrokinetic decontamination of soils. *Journal of Hazardous Materials* 28(1-2):208-209.
- Eykholt, G.R. and D.E. Daniel. 1994. Impact of System Chemistry of Electroosmosis in Contaminated Soil. *Journal of Geotechnical Engineering* 120(5):797-815.
- Fetter, C.W. 1992. *Contaminant Hydrogeology*. Toronto: Maxwell Macmillan Canada.
- Hamed, J., Y.B. Acar and R.J. Gale. 1991. Pb(II) Removal from Kaolinite by Electrokinetics. *Journal of Geotechnical Engineering* 117(2):241-271.
- Hannesin, S.F. and R.W. Gillham. 1998. Long-term performance of an insitu iron-wall for remediation of VOC's. *Ground Water* 36(1):164-170.
- Hess, P.J. 1986. Ground-water use in Canada, 1981. National hydrology research institute.

- Hillel, D. 1982. *Introduction to soil physics*. New York: Academic Press.
- Huyakorn, P.S. and G.F. Pinder. 1983. *Computational methods in subsurface flow*. New York: Academic Press.
- Istok, J. 1989. *Groundwater modelling by the finite element method*. Washington: American Geophysical Union.
- Javandel, I., C. Doughty and C.F. Tsang. 1995. *Groundwater transport: Handbook of mathematical models*. Washington, DC: American Geophysical Union.
- Kitahara, A. and A. Watanabe. 1984. Electrical phenomena at interfaces. Surfactant science series. Marcel Dekker, Inc. No. 15 pp. 463.
- Klute, A. 1982. *Methods of soil analysis*. Second. Madison, WI: American society of Agronomy, Inc. Soil Science Society of America, Inc.
- Koryta, J. 1982. *Ions, Electrodes, and Membranes*. New York: John Wiley and Sons.
- Koryta, J. and J. Dvorak. 1987. *Principles of Electrochemistry*. New York: John Wiley and Sons.
- Kruyt, H.R. 1952. *Colloid Science(I): Irreversible Systems*. Amsterdam: Elsevier Publishing.
- Lageman, R., W. Pool and G. Seffinga. 1989. *Electro-Reclamation: Theory and Practice*. Chemistry & Industry. pp. 585-590.
- Lewis, R.W. 1973. Numerical Analysis of Electro-Osmotic Flow in Soils. *Journal of the Soil Mechanics and Foundations Division* 99(SM8):603-616.
- Lewis, R.W. and R.W. Garner. 1972. A finite element solution of coupled electrokinetic and hydrodynamic flow in porous media. *International journal for numerical methods in engineering* 5(1):41-55.
- Lorenz, P.B. 1969. Surface conductance and electrokinetic properties of kaolinite beds. *Clay and Clay Minerals* 17:223-231.
- Mise, T. 1961. Electro-osmotic dewatering of soil and distribution of the pore water pressure. In *Proceedings of 5th International Conference on Soil Mechanics and Foundation Engineering*, 1: 255-257.
- Mitchell, J.K. 1991. Conduction phenomena: from theory to geotechnical practice. *Geotechnique* 41(3):299-340.

- Mitchell, J.K. 1993. *Fundamentals of Soil Behaviour*. 2. New York, NY: John Wiley & Sons, Inc.
- National Round Table on the Environment and the Economy. 1997. *Removing Barriers: Redeveloping Contaminated Sites for Housing*. Canada Mortgage and Housing Corporation.
- Page, A.L. 1982. *Methods of soil analysis*. Second. Madison, WI: American society of Agronomy, Inc.
- Pamucku, S. and J.K. Wittle. 1992. Electrokinetic Removal of Selected Heavy Metals from Soil. *Environmental Progress* 11(3):241-250.
- Probstein, R.F. and R.E. Hicks. 1993. Removal of contaminants from soils by electric fields. *Science* 260:498-503.
- Putnam, G.A. 1988. Determination of pH Gradients in the Electrochemical Processing of Koalinite. *Civil Engineering*. Louisiana State University. p. 255.
- Qian, Y. 1998. Effect of cationic surfactant (CTAB) in the electrokinetic remediation of diesel contaminated soils. Department of Biosystems Engineering. University of Manitoba. p. 158.
- Renaud, P.C. and R.F. Probstein. 1987. Electroosmotic control of hazardous wastes. *PCH PhysicoChemical Hydrodynamics* 9(1/2):345-360.
- Rogoszewski, P., H. Bryson and Wagner.K. 1983. *Remediation action technology for waste disposal sites*. Park Ridge, NJ: Noyes data corporation.
- Ryan, C.R. 1987. Vertical barriers in soil for pollution containment. In *Geotechnical practice for waste disposal '87*, R. D. Woods 13:p. pp. 182-204. New York: Americal Society of Civil Engineers.
- Segall, B.A. and C.J. Bruell. 1992. Electroosmotic Contaminant-Removal Processes. *Journal of Environmental Engineering* 118(1):84-100.
- Seegerlind, L.J. 1984. *Applied finite element analysis*. second edition. New York: John Wiley and Sons.
- Shapiro, A.P. and R.F. Probstein. 1993. Removal of Contaminants from Saturated Clay by Electroosmosis. *Environmental Science and Technology* 27(2):283-291.

- Thomas, S.P. 1996. Surfactant-enhanced electrokinetic remediation of hydrocarbon-contaminated soils. Unpublished M.Sc. Thesis, Department of Biosystems Engineering, University of Manitoba. pp. 260.
- Wang, H.F. and M.P. Anderson. 1982. *Introduction to groundwater modeling: Finite difference and finite element methods*. San Francisco: W.H.Freeman and Company.
- Yeung, A.T. 1990. Coupled Flow Equations for Water, Electricity and Ionic Contaminants through Clayey Soils under Hydraulic, Electrical and Chemical Gradients. *Journal of Non-Equilibrium Thermodynamics* 15(3):247-267.
- Yeung, A.T. 1994. Electrokinetic flow processes in porous media and their applications. *Advances in Porous Media*. Elsevier. No. 2, pp. 309-395.
- Yeung, A.T. and J.K. Mitchell. 1993. Coupled fluid, electrical and chemical flows in soil. *Geotechnique* 43(1):121-134.